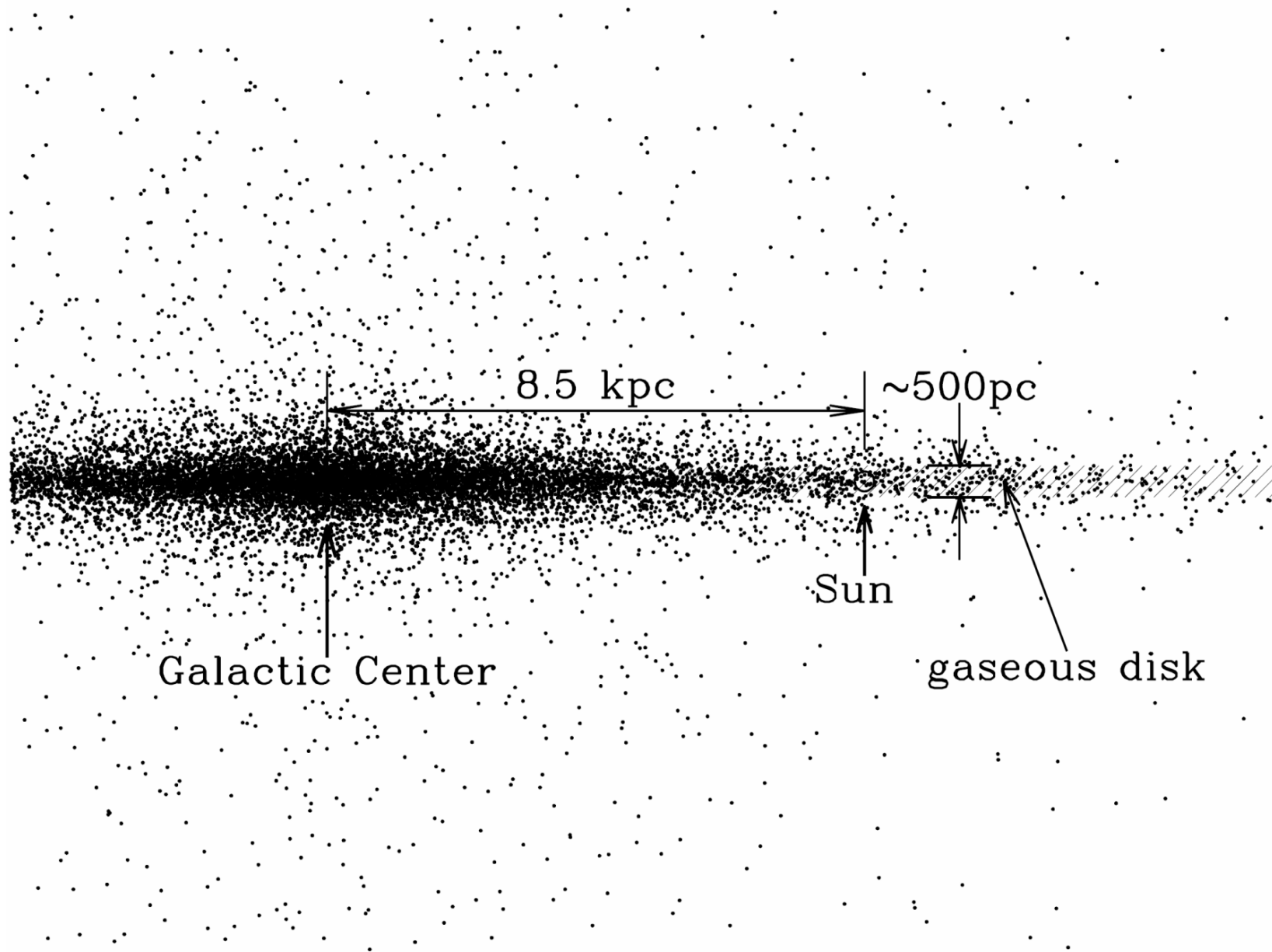


Molecular Clouds and Star Formation

Stars are formed in molecular cloud cores,
whereas planets are formed,
contemporaneously, in young circumstellar disks.

<http://www.astro.ncu.edu.tw/~wchen/Courses/Stars/Lada1995summerschool.pdf>



A THEORY OF THE INTERSTELLAR MEDIUM: THREE COMPONENTS REGULATED BY SUPERNOVA EXPLOSIONS IN AN INHOMOGENEOUS SUBSTRATE

CHRISTOPHER F. McKEE

Departments of Physics and Astronomy, University of California, Berkeley

AND

JEREMIAH P. OSTRIKER

Princeton University Observatory

Received 1977 February 3; accepted 1977 May 2

ABSTRACT

Supernova explosions in a cloudy interstellar medium produce a three-component medium in which a large fraction of the volume is filled with hot, tenuous gas. In the disk of the galaxy the evolution of supernova remnants is altered by evaporation of cool clouds embedded in the hot medium. Radiative losses are enhanced by the resulting increase in density and by radiation from the conductive interfaces between clouds and hot gas. Mass balance (cloud evaporation rate = dense shell formation rate) and energy balance (supernova shock input = radiation loss) determine the density and temperature of the hot medium with $(n, T) = (10^{-2.5}, 10^{5.7})$ being representative values. Very small clouds will be rapidly evaporated or swept up. The outer edges of "standard" clouds ionized by the diffuse UV and soft X-ray backgrounds provide the warm ($\sim 10^4$ K) ionized and neutral components. A self-consistent model of the interstellar medium developed herein accounts for the observed pressure of interstellar clouds, the galactic soft X-ray background, the O VI absorption line observations, the ionization and heating of much of the interstellar medium, and the motions of the clouds. In the halo of the galaxy, where the clouds are relatively unimportant, we estimate $(n, T) = (10^{-3.3}, 10^{6.0})$ below one pressure scale height. Energy input from halo supernovae is probably adequate to drive a galactic wind.

Interstellar Medium (ISM)

- Gas, dust + radiation, magnetic fields, cosmic rays (i.e., charged particles)
- Very sparse ---
$$\frac{[\text{star-star distance}]}{[\text{stellar diameter}]} \sim 1 \text{ pc} / 10^{11} \text{ cm} \sim 3 \times 10^7 : 1$$

or $\sim 1 : 10^{22}$ in terms of volume (space)
- Mass: 99% mass in gas, 1% in dust \sim 15% of total MW visible matter
- Of the gas, 90%, H; 10% He
- Hydrogen: **mainly H I (atomic), H II (ionized), and H₂ (molecular)**
- Studies of ISM ---
 - Beginning of evolution of baryonic matter “recombination”
 - Stars form out of ISM
 - Important ingredient of a galaxy

Material Constituents of the ISM

Component	T (K)	n (cm ⁻³)	Properties
Hot, intercloud and coronal gas	10 ⁶	10 ⁻⁴	
Warm intercloud gas	10 ⁴	0.1	
Diffuse cloud (H I)	10 ²	0.1	Mostly H I; n _e /n ₀ =10 ⁻⁴
H II regions	10 ⁴	>10	
Dark Molecular Clouds	10	> 10 ³	Mostly H ₂ mol. and dust
Supernova Remnants	10 ⁴ ~10 ⁷	>1	
Planetary Nebulae			

Energy Density in the Local ISM

Component	u (eV/cm ³)	Properties
Cosmic microwave background	0.265	
FIR radiation from dust	0.31	
Starlight	0.54	
Thermal kinetic energy	0.49	
Turbulent kinetic energy	0.22	
Magnetic field	0.89	
Cosmic rays	1.39	

There seems to be equi-partition between these energies. Why?
Read Draine's book, page 10

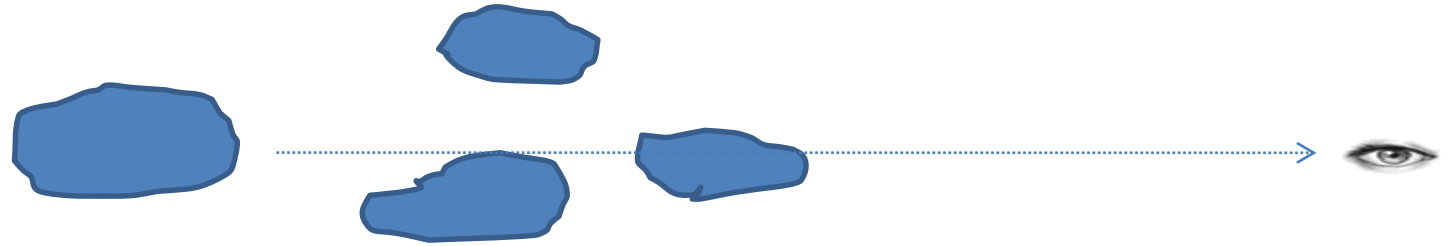
A “standard” HI cloud

$$D \sim 5 \text{ pc}$$

$$M \sim 50 M_{\odot};$$

$$d_{\text{intercloud}} \sim 100 \text{ pc}$$

$$V_{\text{cloud}} \sim 10 \text{ km s}^{-1}$$



Clouds are patchy \rightarrow extinction depends greatly on the sightline

Extinction = absorption + scattering

Extinction versus reddening

$A_v=30$ toward the Galactic center

In the Galactic plane, $A_v \sim 0.7-1 \text{ mag kpc}^{-1}$

Extinction \leftrightarrow amounts of dust grains along the line of sight

Reddening \leftrightarrow grain properties (size, shape, composition, structure)

Different clouds along the line of sight ...

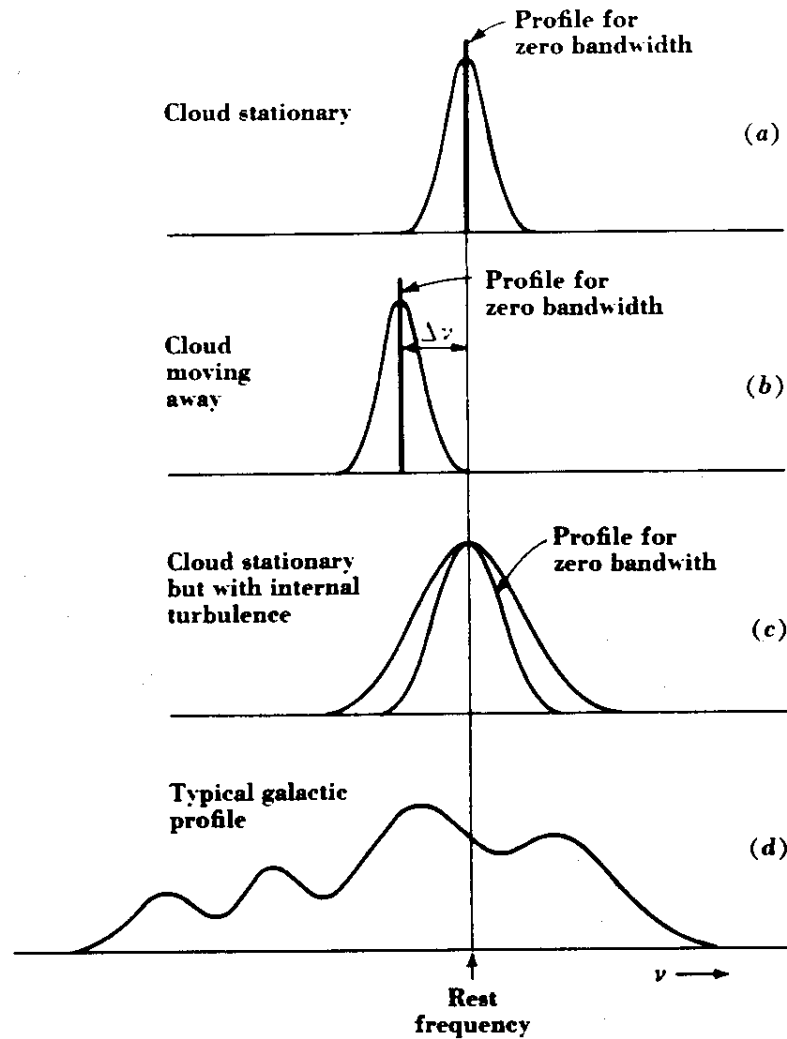


Fig. 8-59. Idealized hydrogen-line profiles.

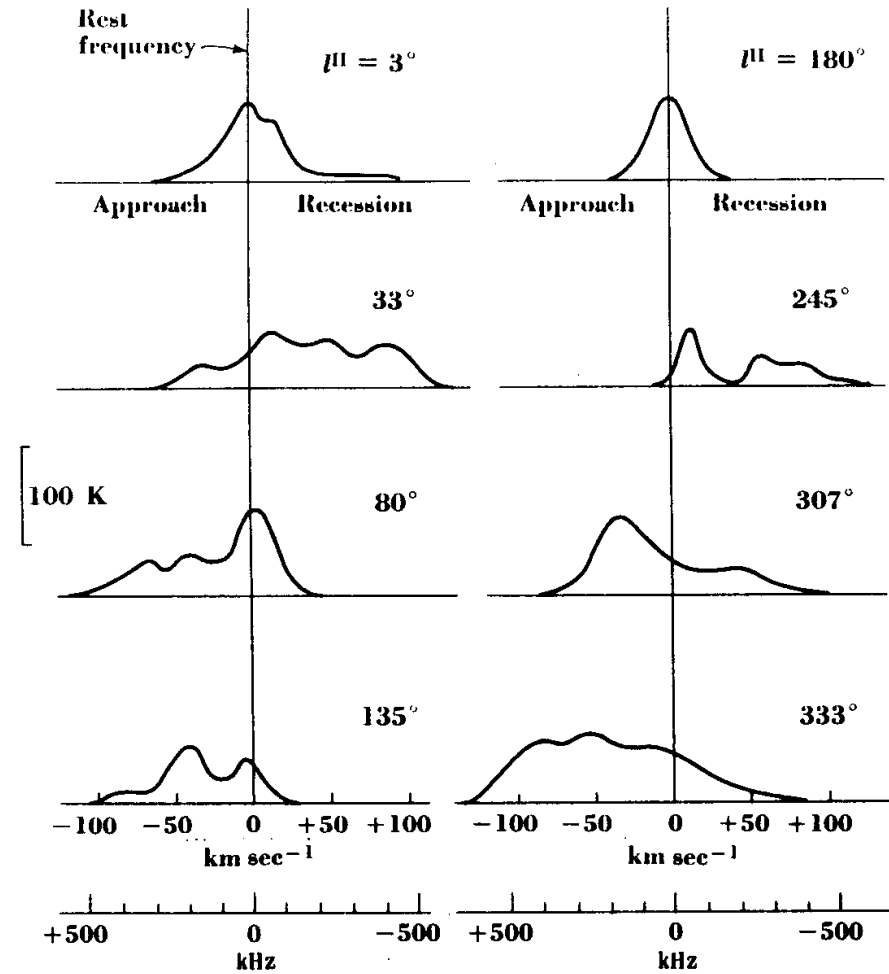
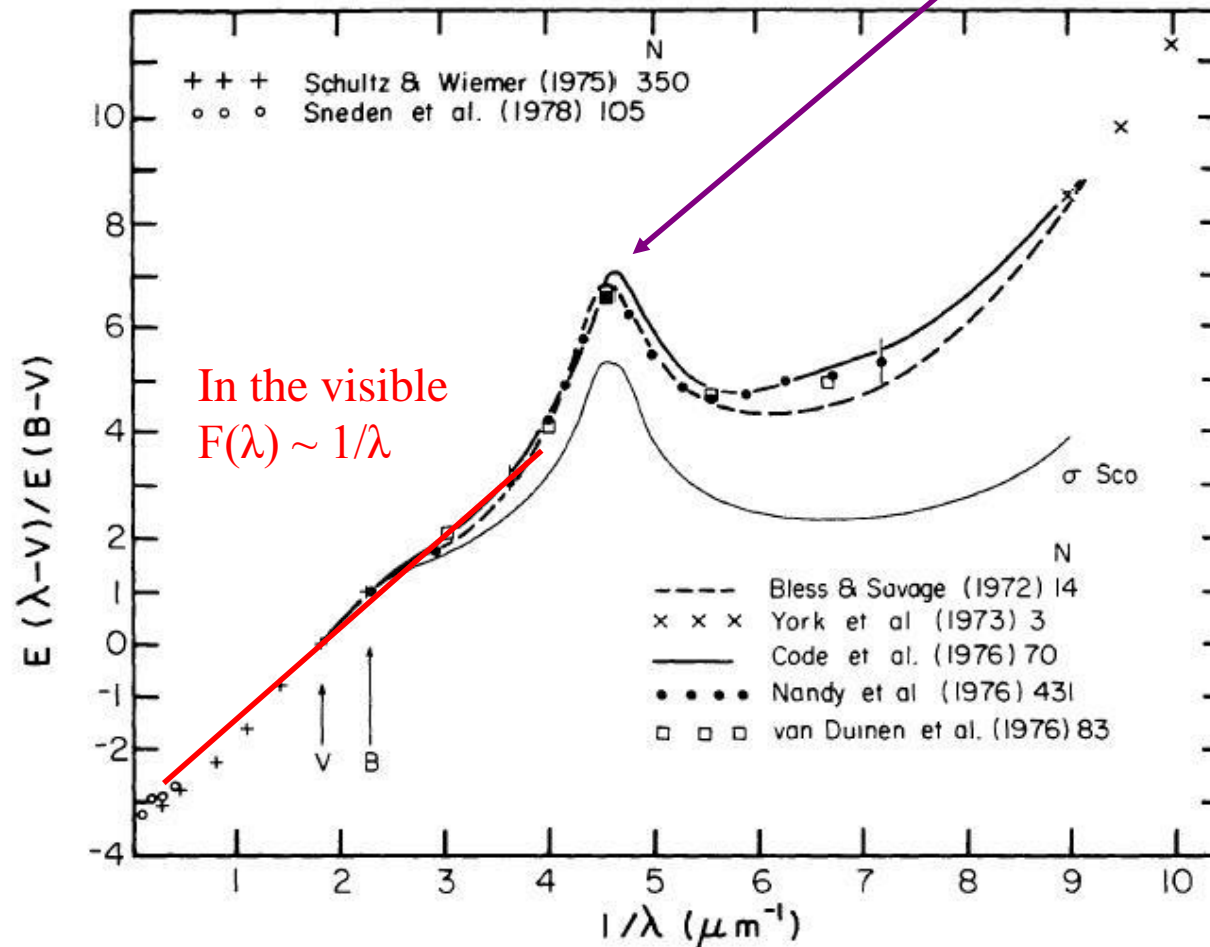


Fig. 8-60. Hydrogen-line profiles at different longitudes in the plane of our galaxy. (After Kerr and Westerhout, 1964).

The 'normalized' extinction (extinction law)

$$F(\lambda) = \frac{A_\lambda - A_V}{A_B - A_V} = \frac{E_{\lambda-V}}{E_{B-V}}$$

The UV 'bump'
 $1/\lambda \sim 4.6 \rightarrow \lambda \sim 2200\text{\AA}$



$F(V) = 0$

$F(B) = +1$

Find

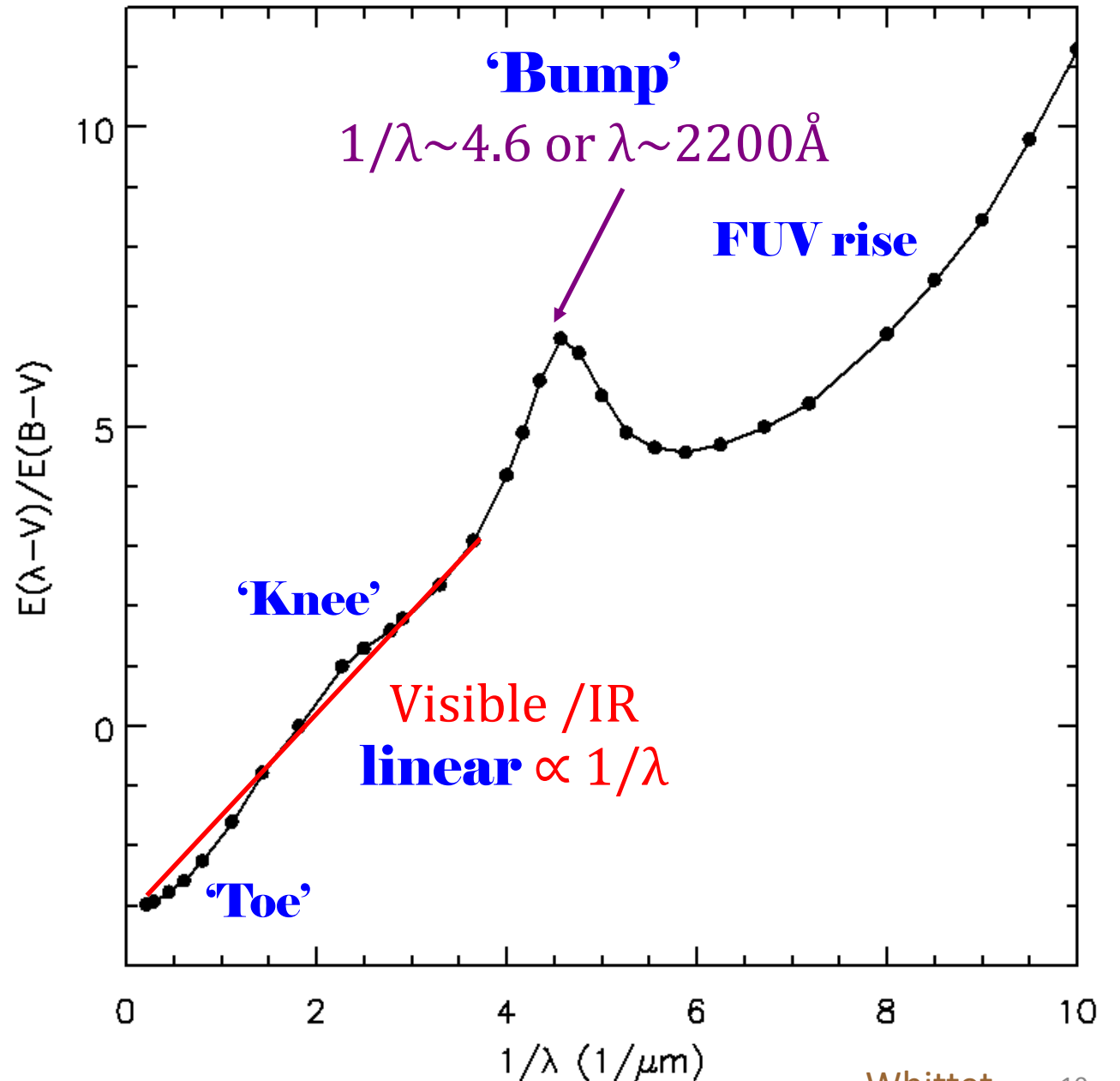
$A_B/A_V = ?$

The 'normalized' extinction (extinction law)

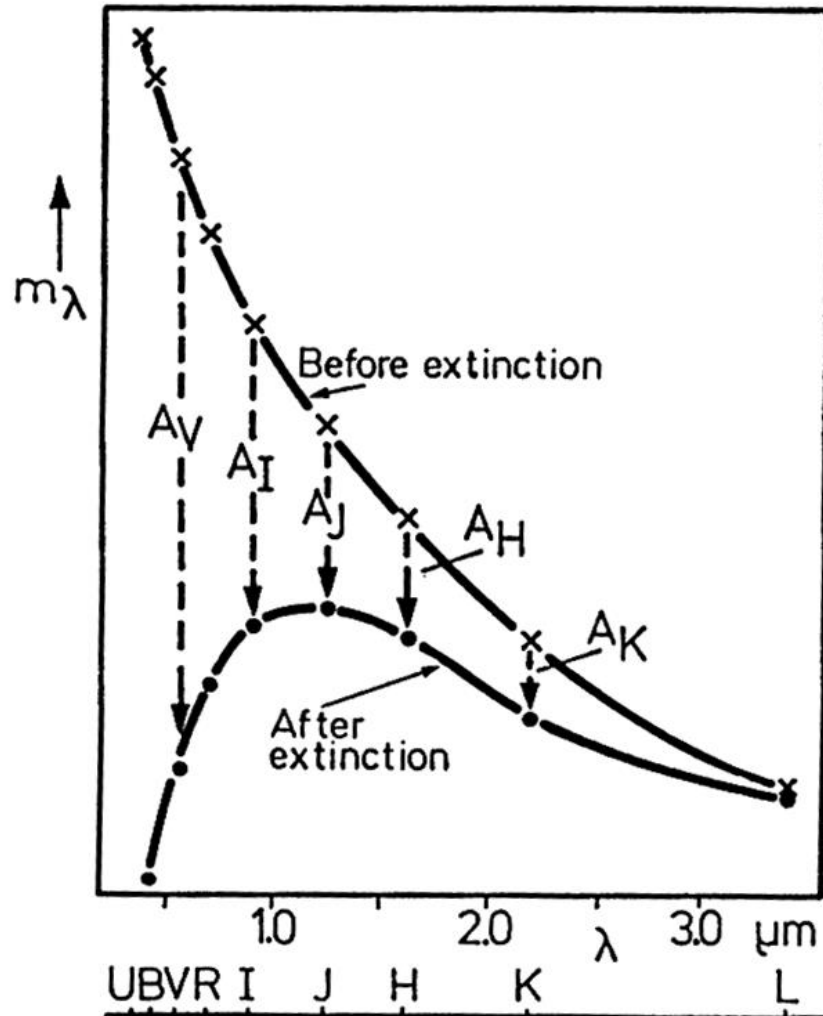
$$F(\lambda) = \frac{A_\lambda - A_V}{A_B - A_V} = \frac{E_{\lambda-V}}{E_{B-V}}$$

$$F(V) = 0$$

$$F(B) = +1$$



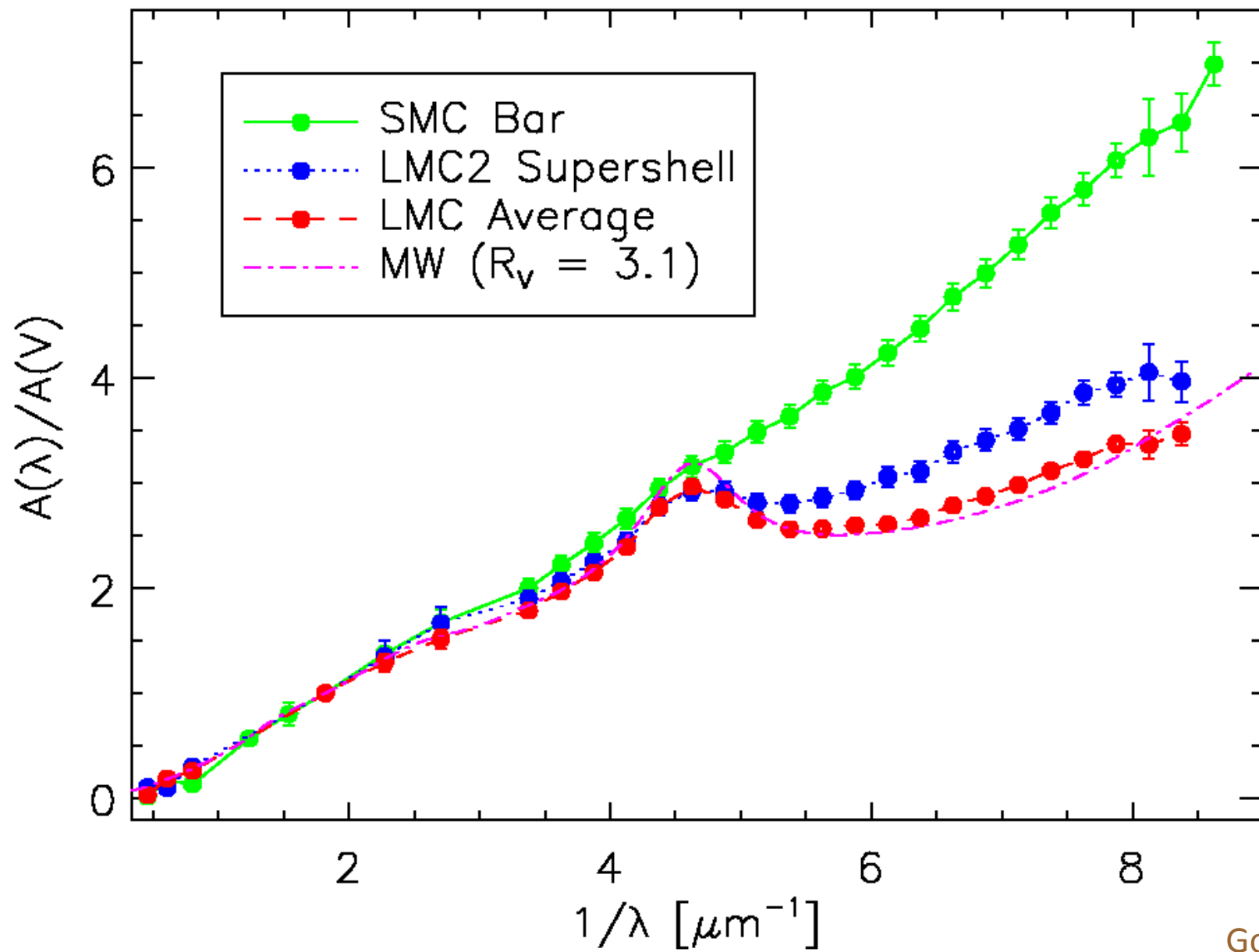
$$A_\lambda = -2.5 \log(e^{-\tau_\lambda}) \equiv 1.086 \tau_\lambda \equiv 1.086 N_d \sigma_\lambda Q_{ext}$$



Filter	A_λ / A_V
<i>V</i>	1.531
<i>B</i>	1.324
<i>V</i>	1.000
<i>R</i>	0.748
<i>I</i>	0.482
<i>J</i>	0.282
<i>H</i>	0.175
<i>K</i>	0.112
<i>L</i>	0.058
<i>M</i>	0.023
<i>N</i>	0.052

$$A_K \approx 0.1 A_V$$

Rieke & Lebofsky (1985)



Gordon et al (2003)

EXTINCTION IN THE DIFFUSE INTERSTELLAR MEDIUM

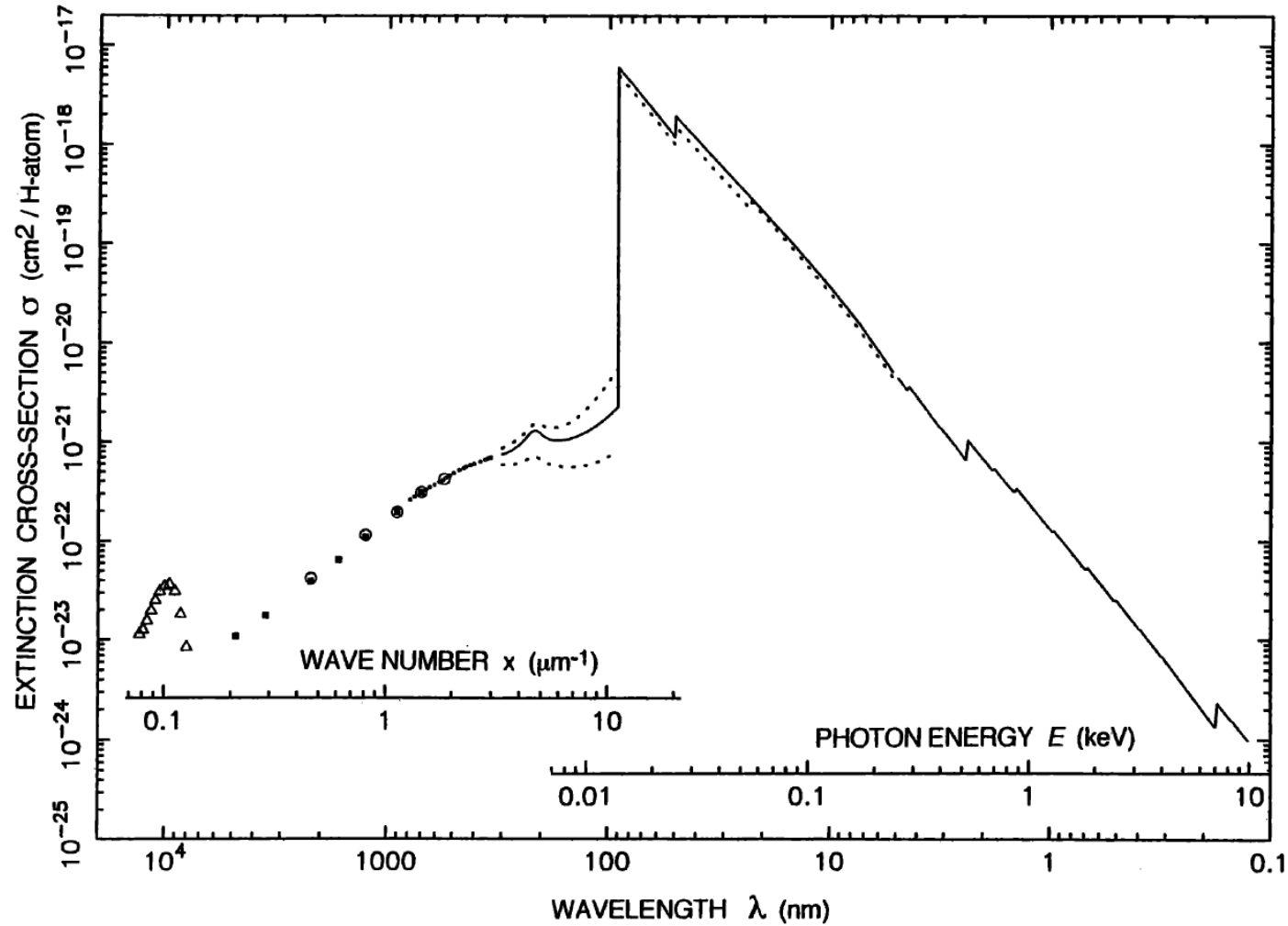
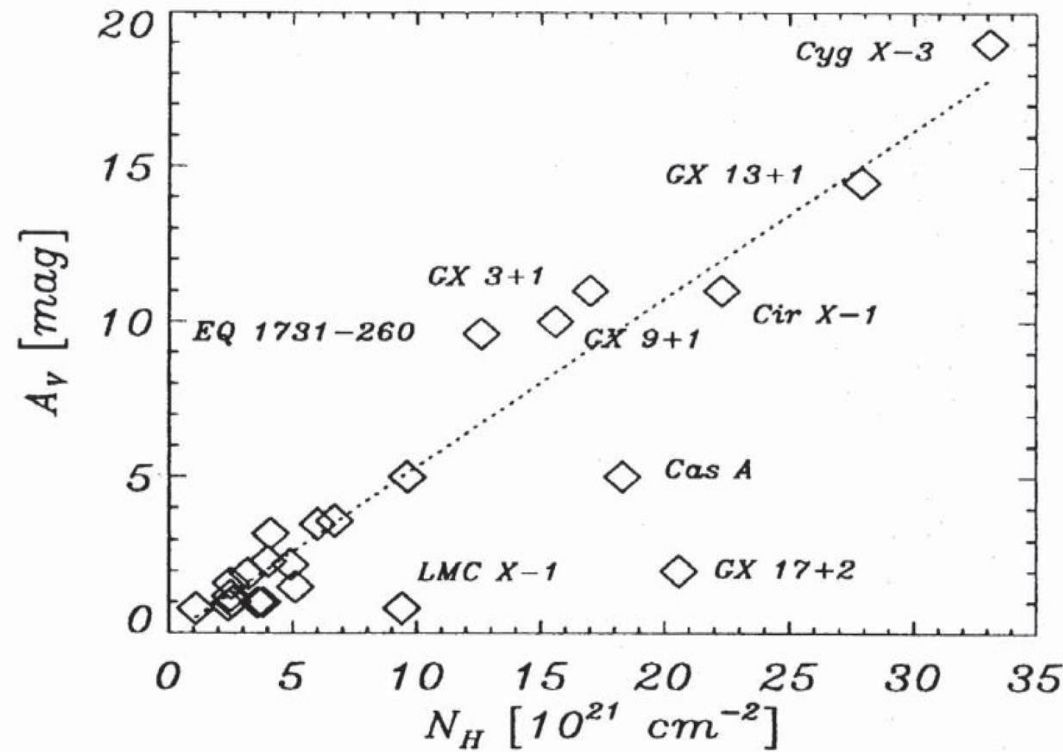


Figure 1. Solid line: The extinction cross-section normalized per H-atom of the diffuse neutral (95% HI, 5% HII, 10% HeI) interstellar medium from the far-infrared to the X-rays. Dotted lines: The UV extinction on the lines of sight in two extreme cases, HD 204827 (upper curve) and HD 37023 (θ_1 -Orionis D, lower curve). Shortward of the Lyman limit, the dotted line corresponds to the ionization state of the solar neighbourhood (80% HI, 20% HII, 5% HeI, 5% HeII). The sources of the data are given in the text.

Ryter (1996)

Gas and dust coexist.



A gas-to-dust ratio ~ 100
(by mass) seems
universal.

Fig. 3. Visual extinction vs. equivalent hydrogen column density. The fit (dotted line) does not contain GX 17+2 and LMC X-1. It yields $N_H = 1.79 \pm 0.03 A_V [\text{mag}] \times 10^{21} [\text{cm}^{-2}]$

$$\frac{N_H}{A_V} \approx 1.8 \times 10^{21} \text{ atoms cm}^{-2} \text{ mag}^{-1}$$

Exercise

1. The star Vega is used to define the zeroth magnitude in all the classical (Vega) photometric systems, e.g., Johnson.
2. Plot its spectral energy distribution (SED) from UV to IR.
3. What is the spectral type of Vega? What is its effective temperature?
4. Compare this in a plot with a blackbody curve of the temperature.
5. It was surprising hence when *IRAS* data revealed IR excess of Vega. What are the flux densities observed by *IRAS*? Given the age of Vega, why is this discovery significant?

<http://www.astro.utoronto.ca/~patton/astro/mags.html#conversions>

Band	lambda_c	dlambda/lambda	Flux at m=0	Reference
	um		Jy	
U	0.36	0.15	1810	Bessel (1979)
B	0.44	0.22	4260	Bessel (1979)
V	0.55	0.16	3640	Bessel (1979)
R	0.64	0.23	3080	Bessel (1979)
I	0.79	0.19	2550	Bessel (1979)
J	1.26	0.16	1600	Campins, Reike, & Lebovsky (1985)
H	1.60	0.23	1080	Campins, Reike, & Lebovsky (1985)
K	2.22	0.23	670	Campins, Reike, & Lebovsky (1985)

Astronomical Magnitude Systems.pdf

Stars are formed in groups → seen as star clusters if gravitationally bound

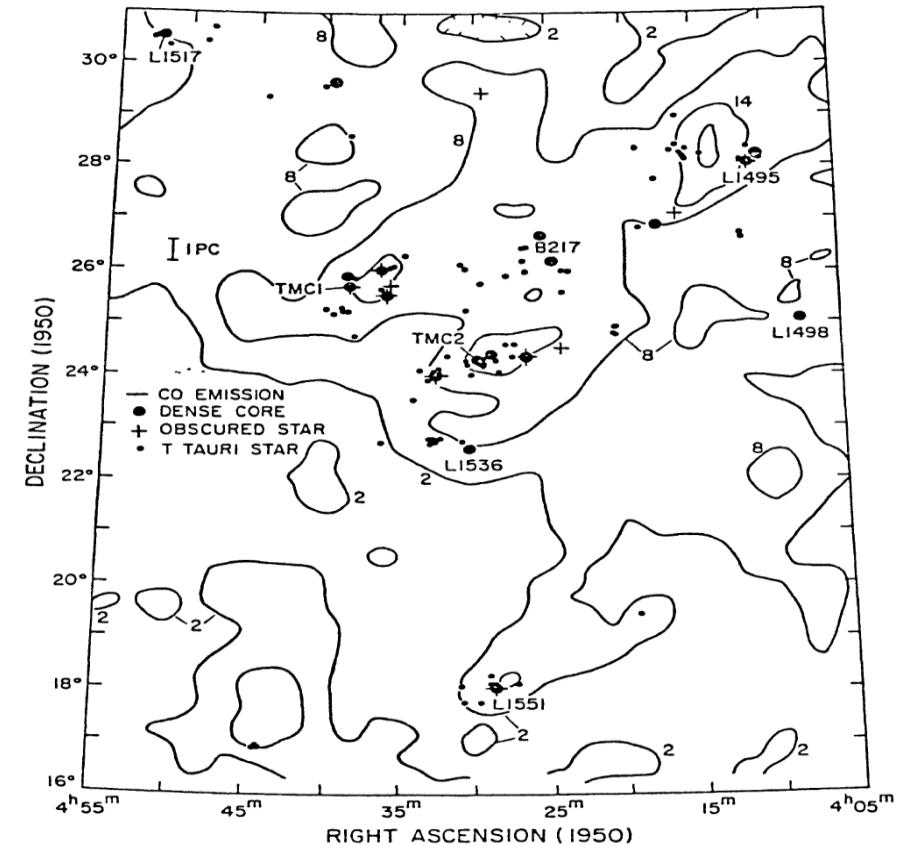
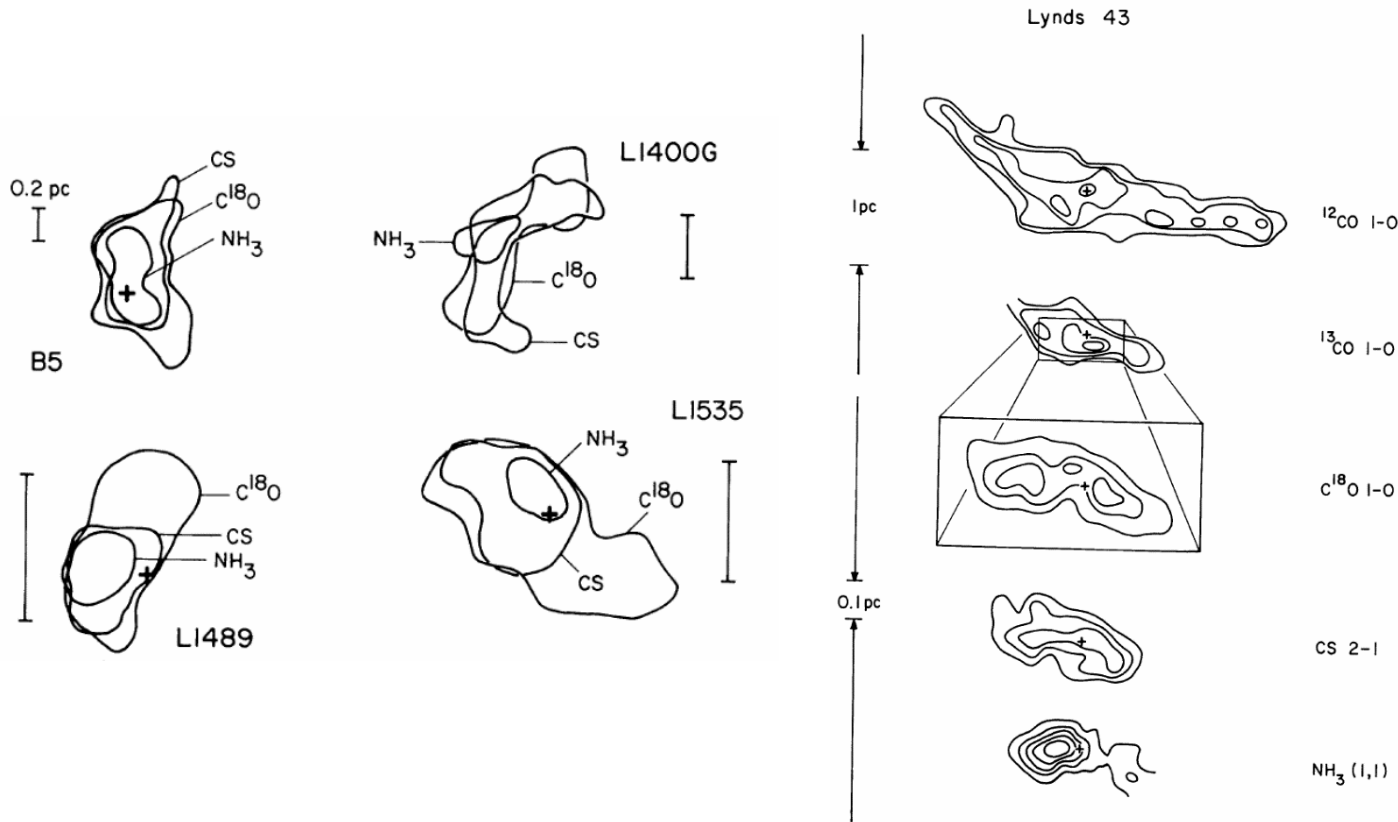
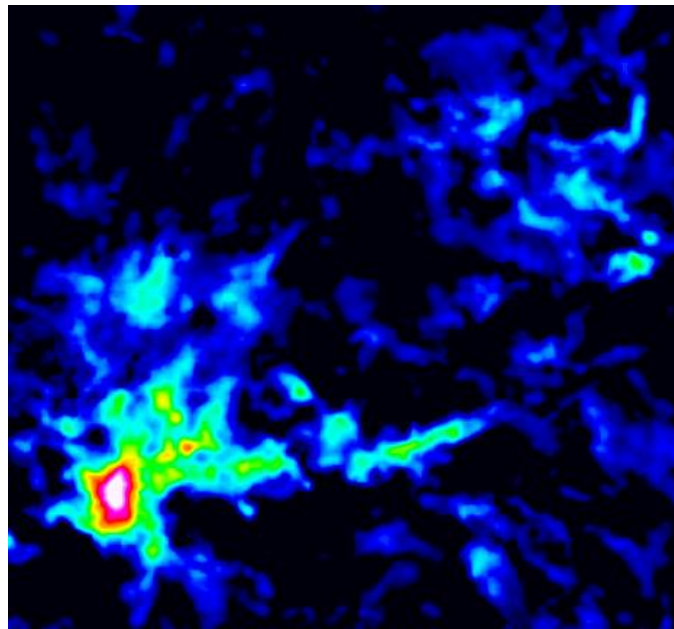
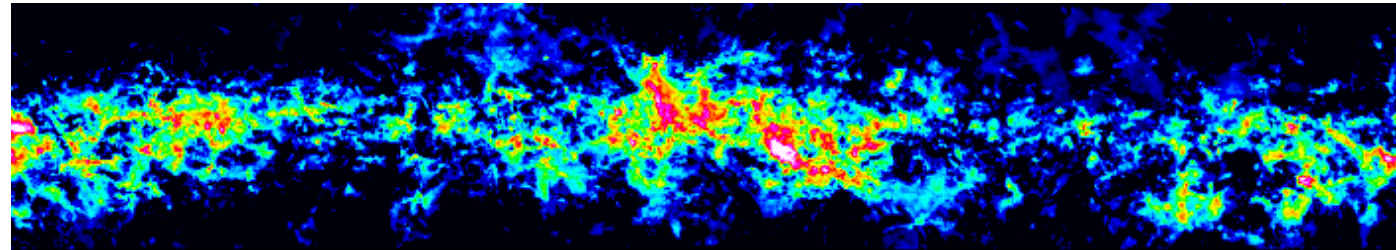
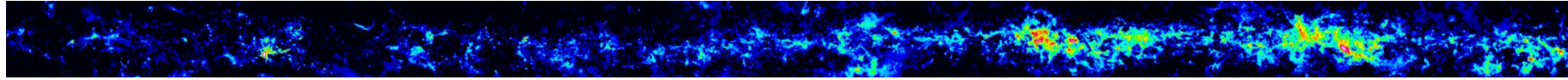


Figure 2 CO contour map of the Taurus molecular cloud with positions of dense NH₃ cores, embedded infrared sources, and visible T Tauri stars (from Myers 1986).

Molecular clouds observed by different tracers ...

Taurus molecular cloud

Filamentary Molecular Clouds



Molecular clumps/ clouds/condensations

$$n \sim 10^3 \text{ cm}^{-3}, D \sim 5 \text{ pc},$$
$$M \sim 10^3 M_{\odot}$$

Dense molecular cores

$$n \geq 10^4 \text{ cm}^{-3}, D \sim 0.1 \text{ pc},$$
$$M \sim 1-2 M_{\odot}$$

Giant Molecular Clouds

$$D = 20 \sim 100 \text{ pc}$$

$$\mathcal{M} = 10^5 \sim 10^6 M_{\odot}$$

$$\rho \approx 10 \sim 300 \text{ cm}^{-3}$$

$$T \approx 10 \sim 30 \text{ K}$$

$$\Delta v \approx 5 \sim 15 \text{ km}^{-1}$$

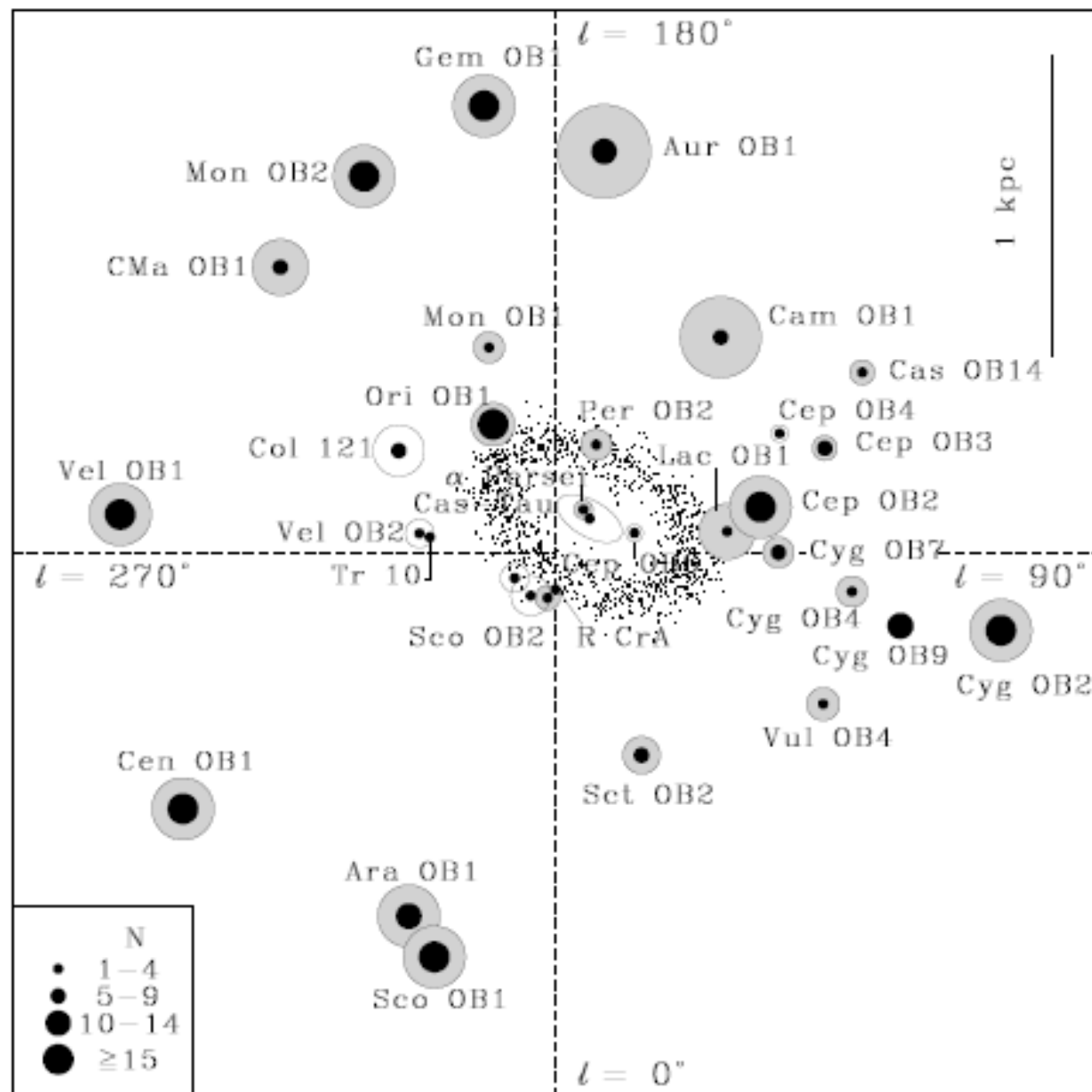
Nearby Examples

Massive Star-Forming Region

- *Per OB2* (350 pc)
- *Orion OB Association* (350-400 pc) ... rich

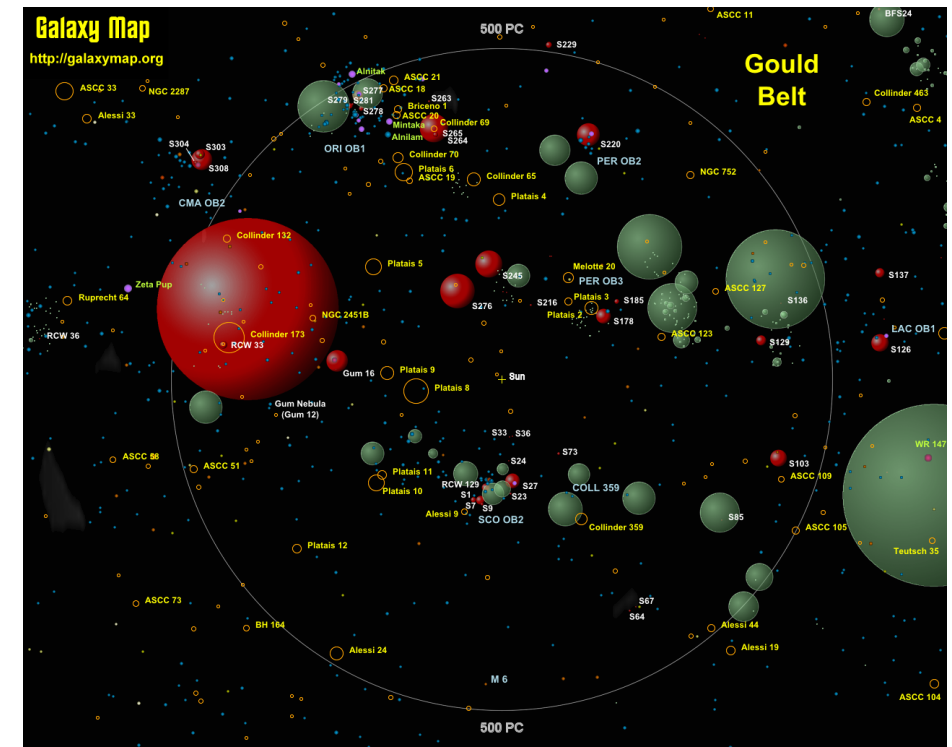
Low-Mass Star-Forming Regions

- *Taurus Molecular Cloud (TMC-1)* (140 pc)
 - *Rho Ophiuchi cloud* (130 pc)
 - *Lupus* (140 pc)
 - *Chamaeleon* (160 pc)
 - *Corona Australis* (130 pc)
- } 4/5 in the southern sky ... why?

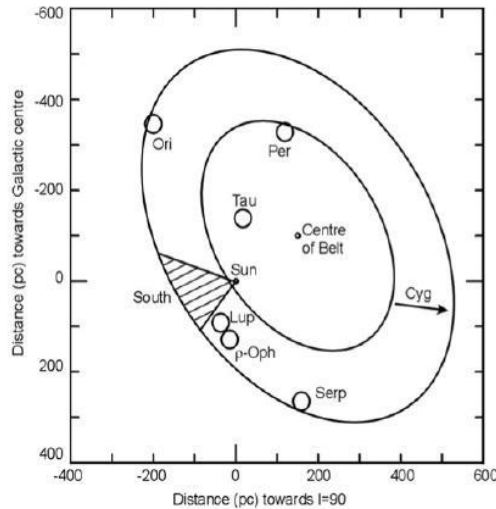


The **Gould Belt**, a (partial) ring in the sky, ~1 kpc across, centered on a point 100 pc from the Sun and tilted about 20 deg to the Galactic plane, containing star-forming molecular clouds and OB stars = local spiral arm

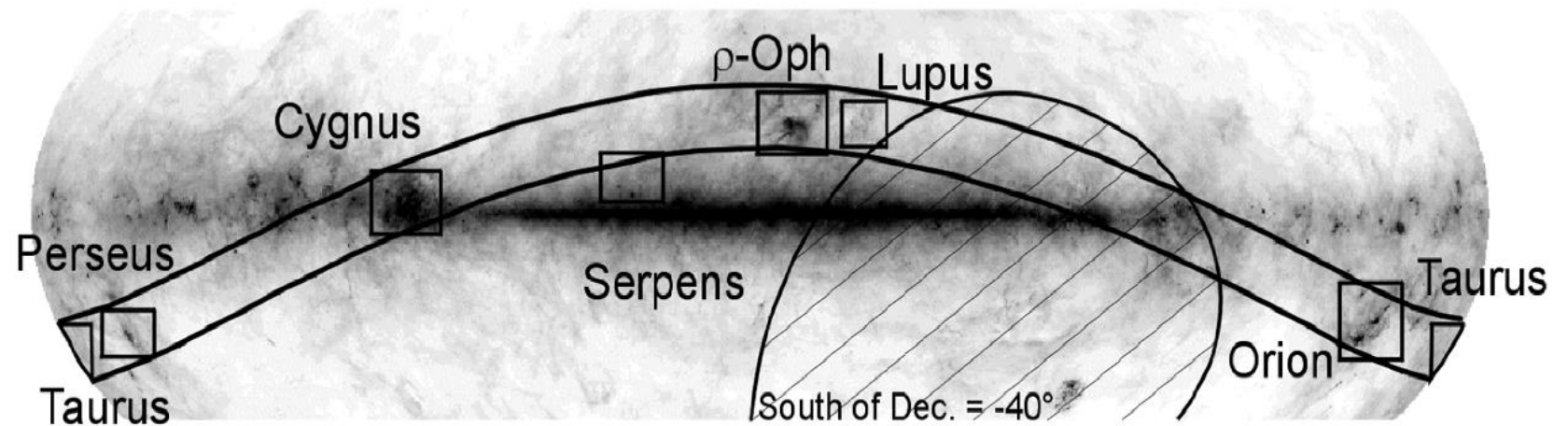
Origin unknown (dark matter induced star formation?)



http://galaxymap.org/detail_maps/download_maps/gould.png



<http://www.jach.hawaii.edu/JCMT/surveys/gb/>

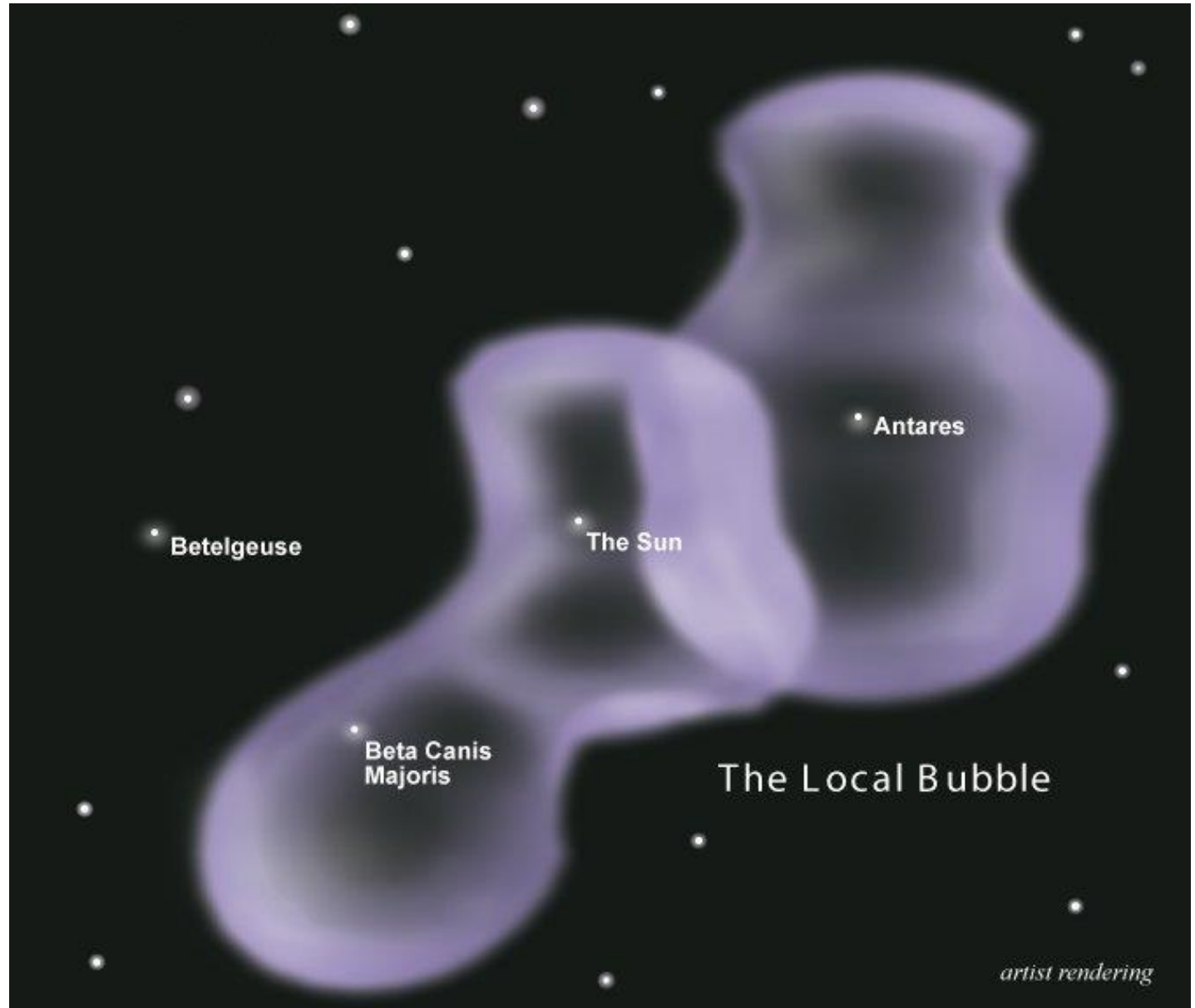


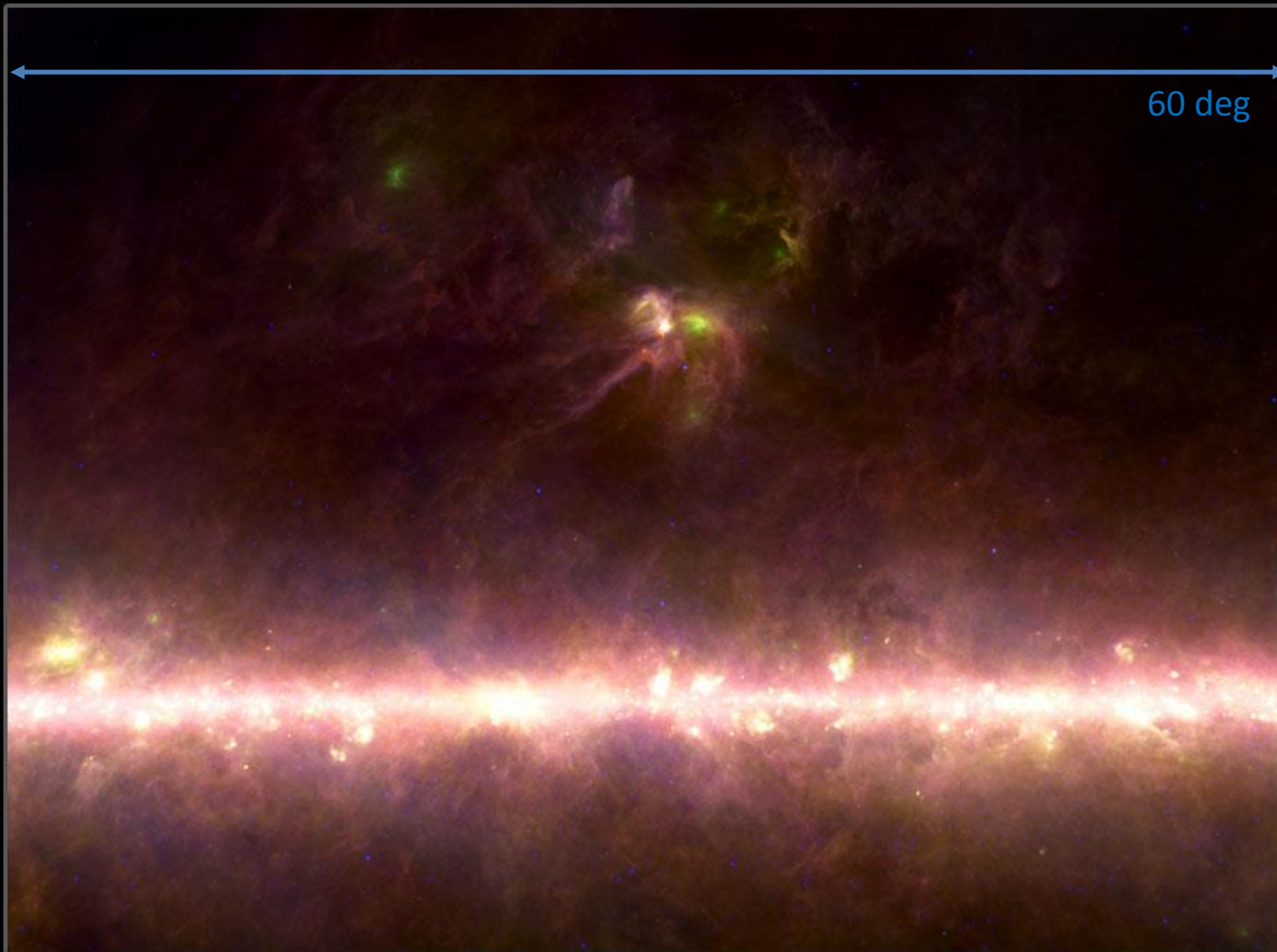
Gould's Belt superimposed on to an IRAS 100 micron emission map

The **Local Bubble**, a cavity of sparse, hot gas, ~ 100 pc across, in the interstellar medium, with H density of 0.05 cm^{-3} , an order less than typical in the Milky Way.

Likely caused by a (or multiple) supernova explosion (10-30 Myr ago).

Where is the supernova (remnant)?
Check out the Orion-Eridanus Superbubble





Rho Oph & The Galactic Center
IRAS



Blue , green and red = 12, 60, and 100 micron

Barnard 72 in Ophiuchus

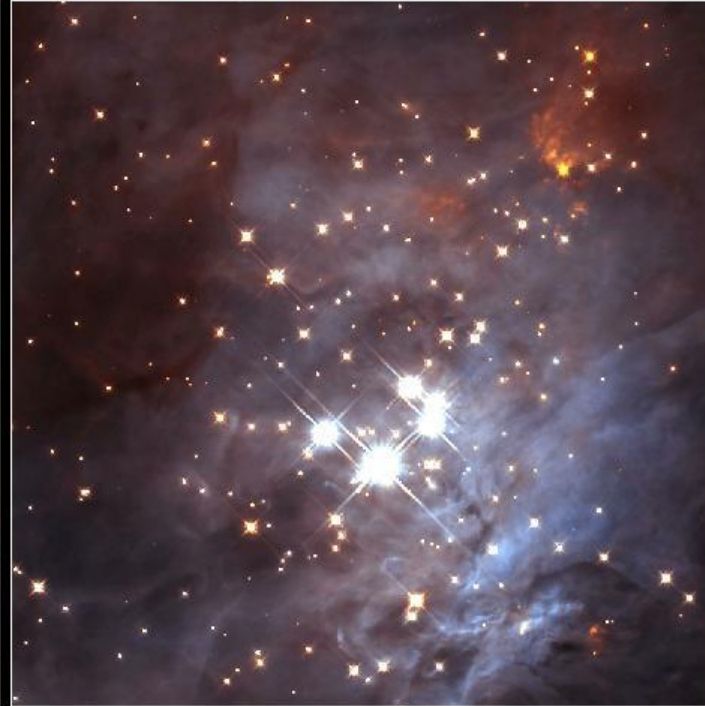


Massive Star-Forming Regions ---- OB associations

Visible • WFPC2



Infrared • NICMOS



Trapezium Cluster • Orion Nebula
WFPC2 • Hubble Space Telescope • NICMOS

NASA and K. Luhman (Harvard-Smithsonian Center for Astrophysics) • STScI-PRC00-19

(Bok) Globules silhouetted against emission nebulosity



© Anglo-Australian Observatory Photograph by David Malin

A dark cloud core seen against a star field

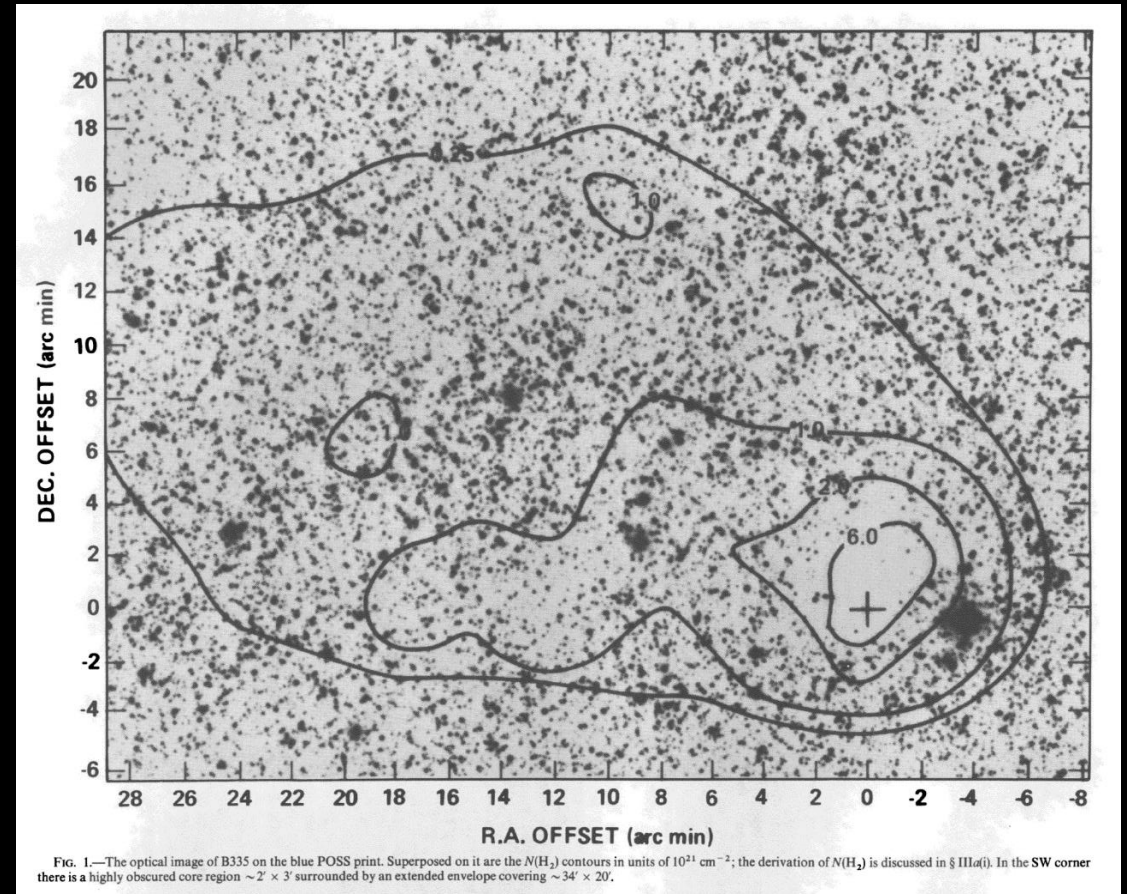


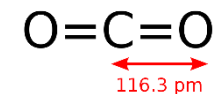
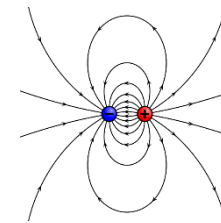
FIG. 1.—The optical image of B335 on the blue POSS print. Superposed on it are the $M(\text{H}_2)$ contours in units of 10^{21} cm^{-2} ; the derivation of $M(\text{H}_2)$ is discussed in § IIIa(i). In the SW corner there is a highly obscured core region $\sim 2' \times 3'$ surrounded by an extended envelope covering $\sim 34' \times 20'$.

Frerking et al. (1987)

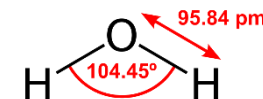
Molecules in space

H₂ molecules

- the main constituent of cold clouds, but lacking a permanent electric dipole moment, so is very difficult to detect. A rotationally excited molecule would radiate through a relatively slow electric quadrupole transition.
- Only in a hot medium, where stellar radiation or stellar wind excites vibrational and electronic states which then decay relatively quickly.



Zero electric dipole moment



Dipole moment = 1.85 Debyes

Refer to the slides for WPC's ISM course

<http://www.astro.ncu.edu.tw/~wchen/Courses/ISM/index.htm>

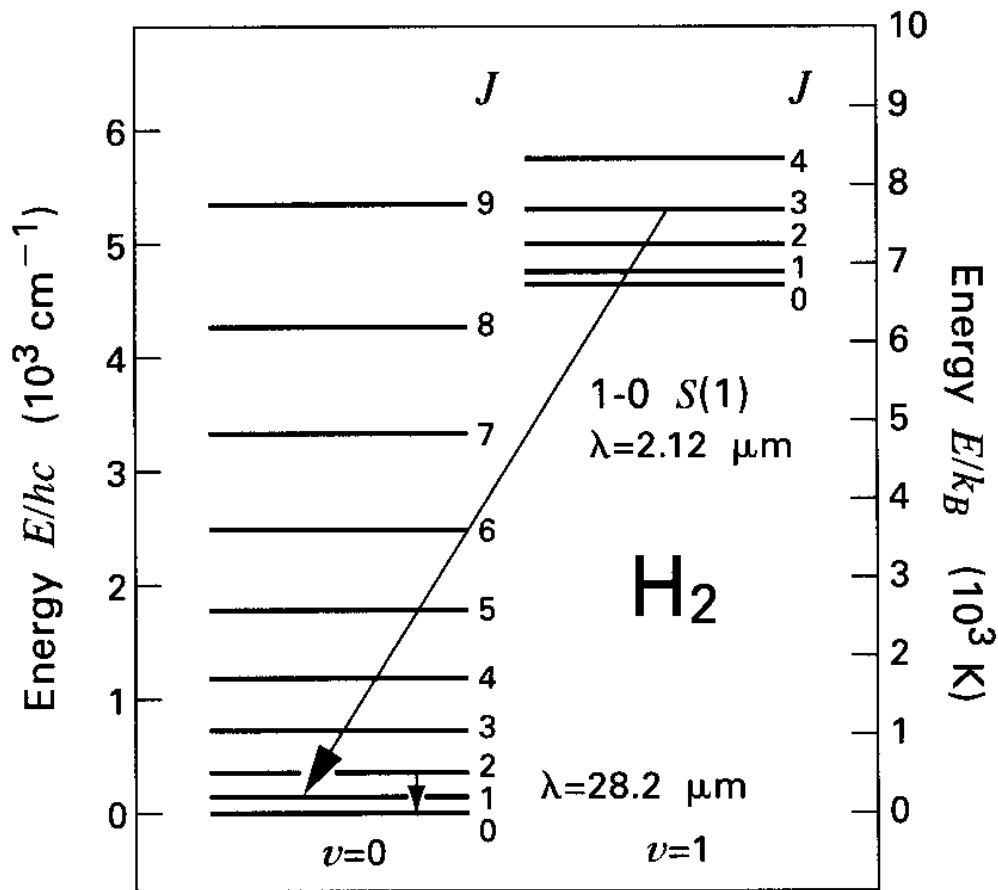
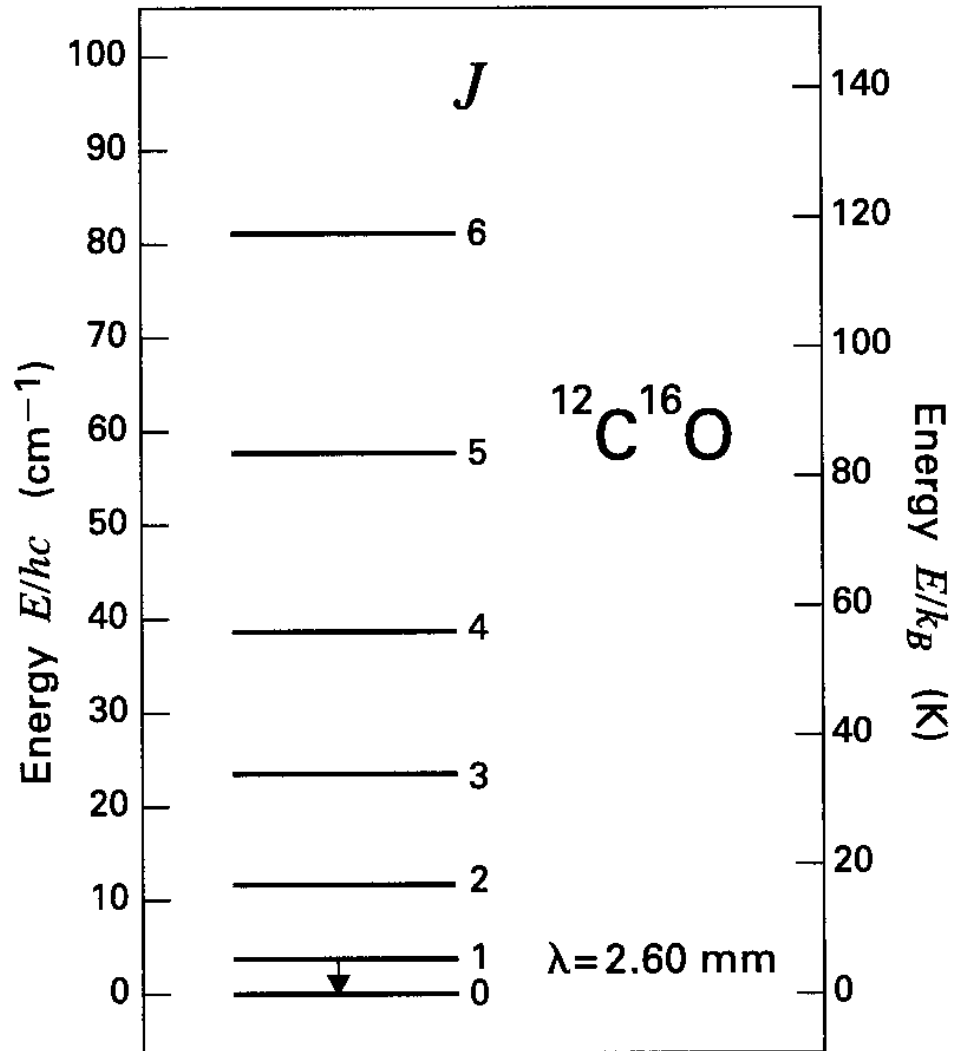


Figure 5.4 Rotational levels of H₂ for the first two vibrational states. Within the $v = 0$ state, the $J = 2 \rightarrow 0$ transition at 28.2 μm is displayed. Also shown is the transition giving the 1-0 S(1) rovibrational line at 2.12 μm . Note that two different energy scales are used.

CO molecules

- simple and abundant. Strong binding energy $E=11.1$ eV self-shielding against UV field
- with a permanent electric dipole moment; radiating strongly at radio frequencies.
- $^{12}\text{C}^{16}\text{O}$ easiest to detect; isotopes $^{13}\text{C}^{16}\text{O}$, $^{12}\text{C}^{18}\text{O}$, $^{12}\text{C}^{17}\text{O}$, $^{13}\text{C}^{18}\text{O}$ also useful
- Excitation of CO to the $J=1$ level mainly through collisions with ambient H_2 $X_{\text{CO}} = 2 \times 10^{20} \text{ cm}^{-2} [\text{K km/s}]^{-1}$ (Bolatto et al. 2013, ARAA)
- At low densities, each excitation is followed by emission of a photon. At high densities, the excited CO transfers the energy by collision to another H_2 molecule; $n_{\text{crit}} \approx 3 \times 10^3 \text{ cm}^{-3}$. Low critical density \rightarrow CO to study large-scale distribution of clouds, as a tracer of H_2
- $^{12}\text{C}^{16}\text{O}$ almost always optical thick; same line from other rare isotopes usually not. $N_{\text{H}} = 10^6 N_{^{13}\text{CO}}$



2.6 mm = 115 GHz

Only 5 K above the ground level ... can be excited by collisions with ambient molecules or CMB photons

Figure 5.6 Rotational levels of $^{12}\text{C}^{16}\text{O}$ within the ground ($v = 0$) vibrational state. The astrophysically important $J = 1 \rightarrow 0$ transition at 2.60 mm is shown.

CO band heads in the Becklin-Neugebauer (BN) object --- an infrared-emitting, embedded, massive protostar

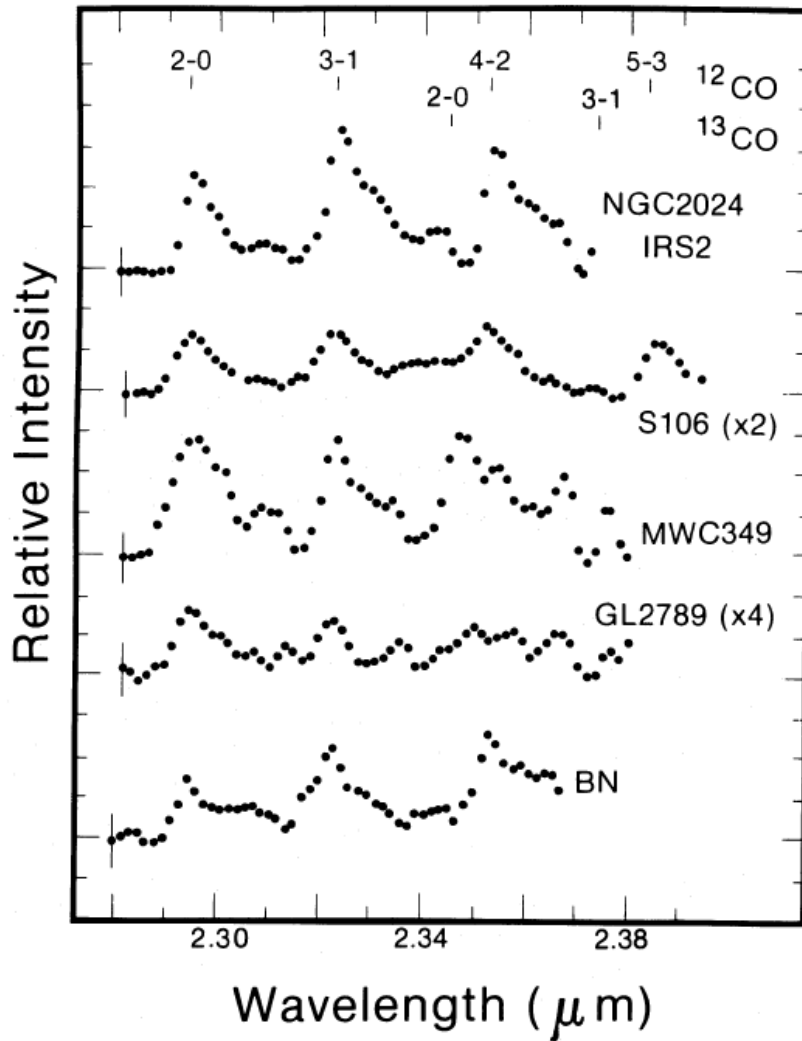


FIG. 2.—Spectra of those sources in which CO band head emission was detected. Linear baselines have been subtracted from each spectrum. The positions of the band heads are indicated at the top of the figure. Vertical scale marks are separated by $2 \times 10^{-17} \text{ W cm}^{-2} \mu\text{m}^{-1}$. Noise levels are indicated on the short wavelength data points.

Gaballe & Persson (1987)

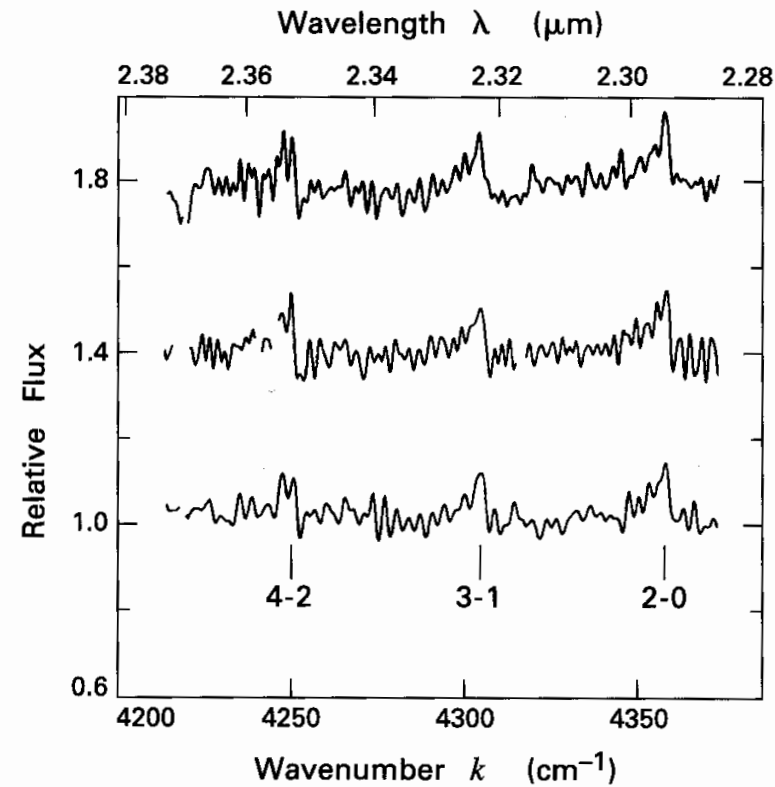
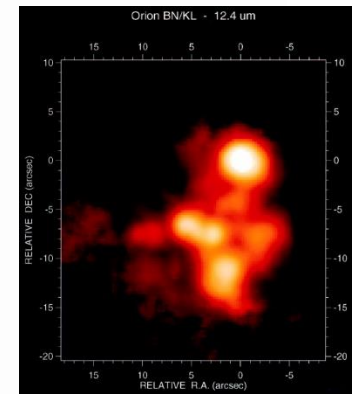
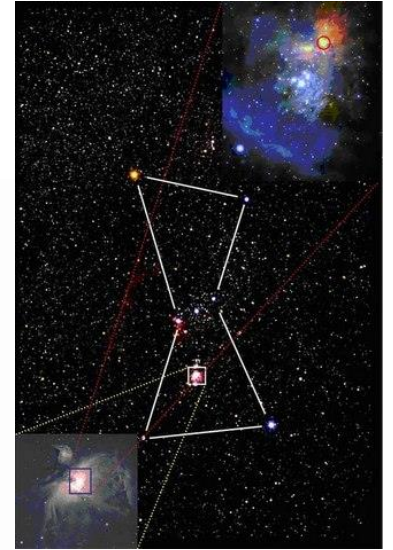


Figure 5.8 Near-infrared spectrum of the BN object in Orion, shown at three different observing times. The relative flux is plotted against the wave number k , defined here as $1/\lambda$.



Stahler & Palla

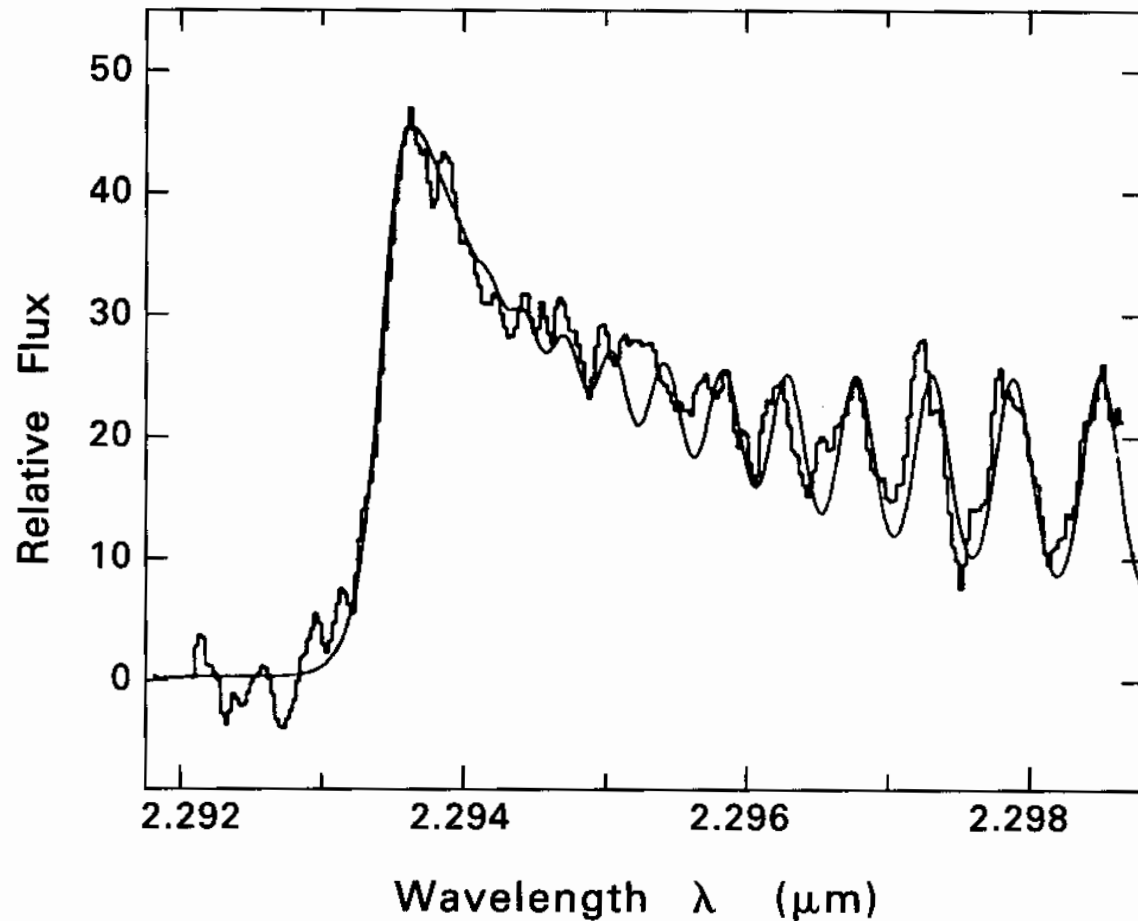
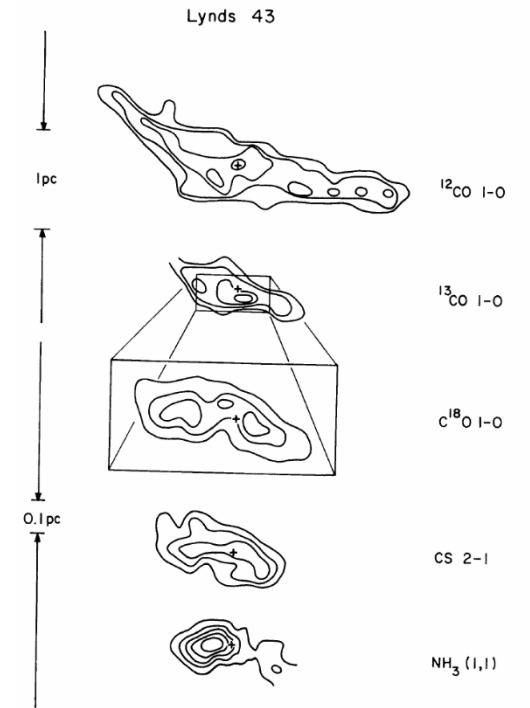


Figure 5.9 High-resolution near-infrared spectrum of the embedded stellar source SSV 13. The structure of the $v = 2 \rightarrow 0$ band head in $^{12}\text{C}^{16}\text{O}$ is evident. The smooth curve is from a theoretical model that employs an isothermal slab at 3500 K. Note that the spectrum here represents only a portion of the R -branch.

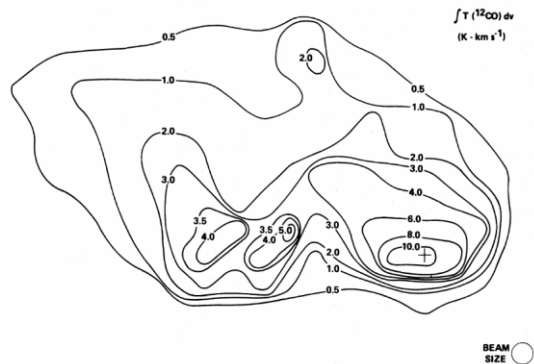
Each species has a different set of excitation conditions (density, temperature; cf. Boltzmann equation)

➔ Different molecules/isotopes serve as tracers of these conditions, e.g., C18O traces denser parts of a cloud than 12CO does; NH3 maps the dense cores where protostars are located.

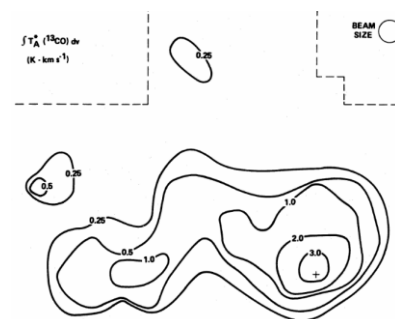


Myers et al. 1991

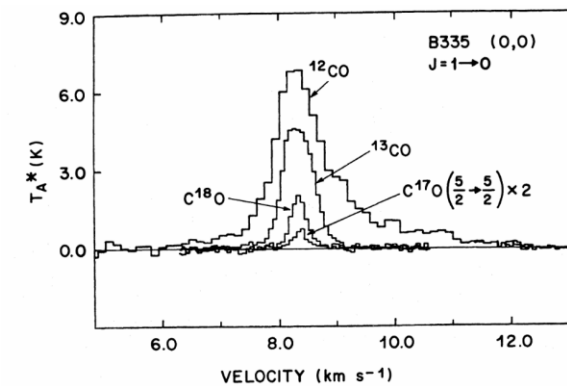
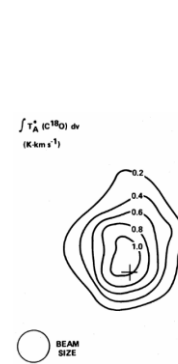
^{12}CO



^{13}CO



C^{18}O



Frerking et al. (1987)

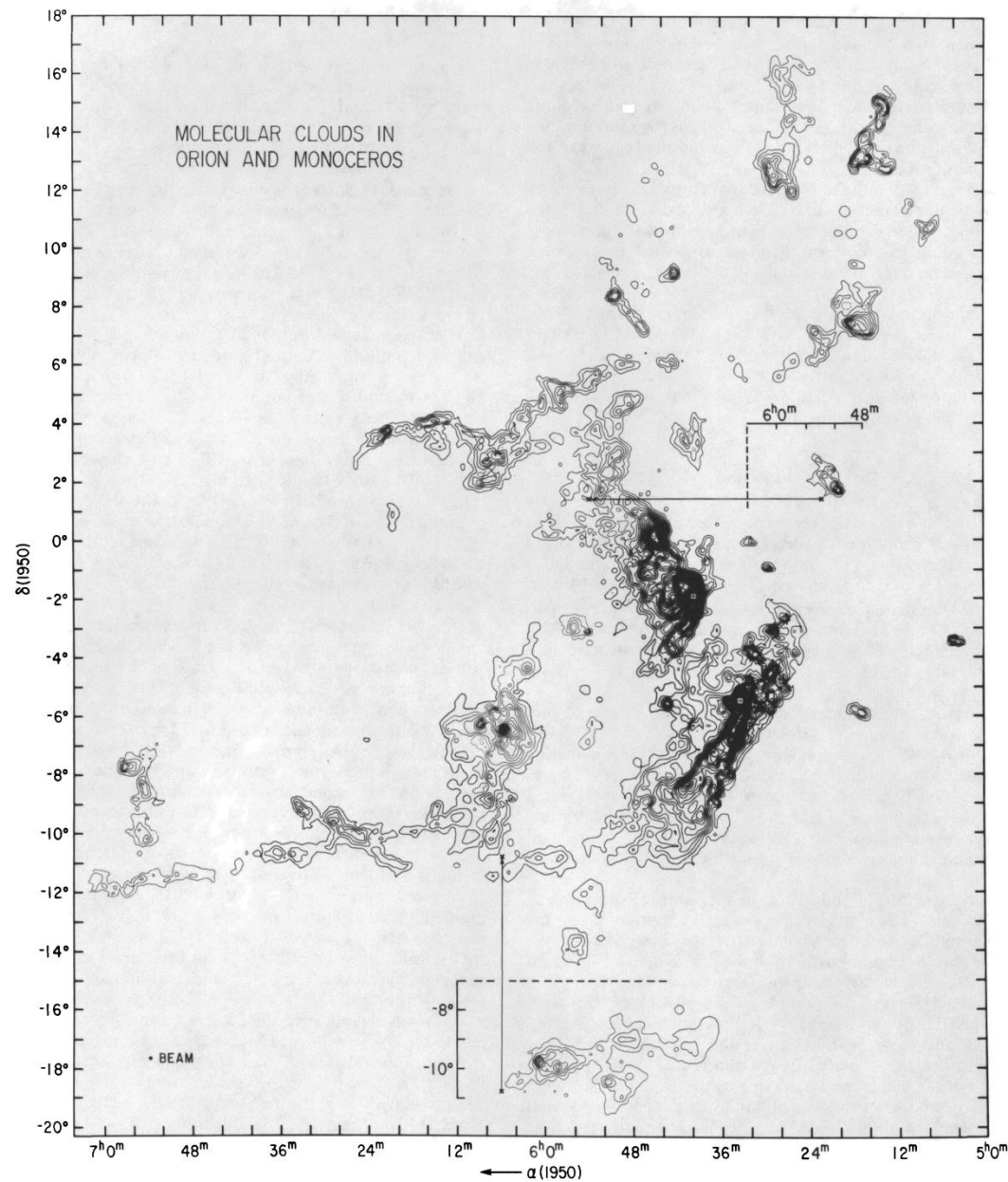
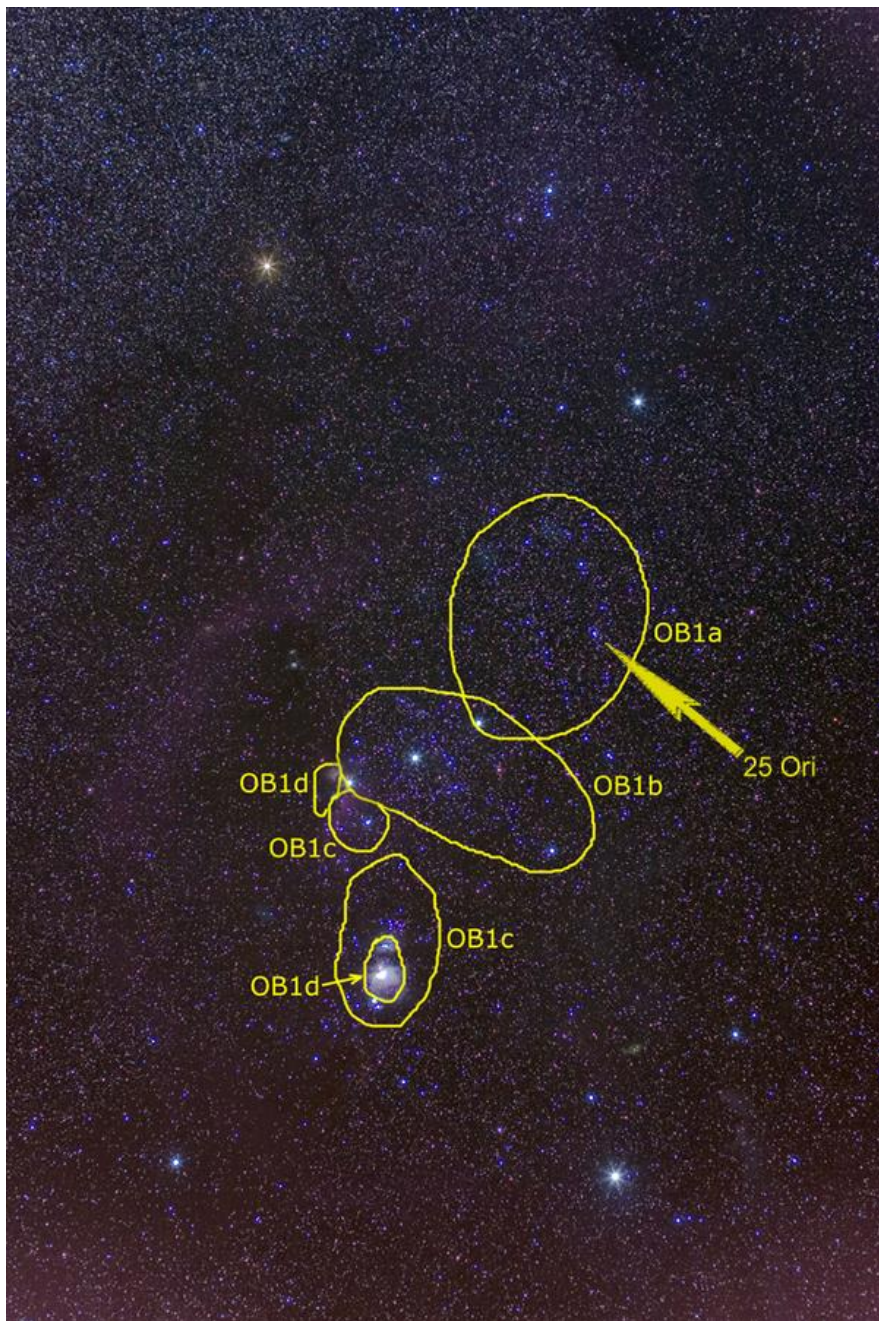
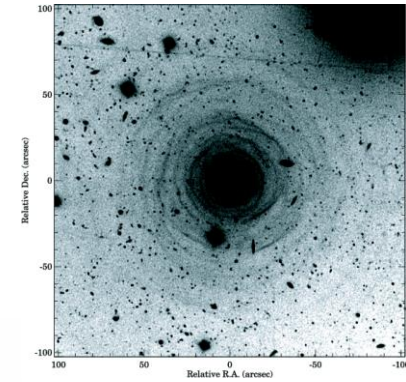


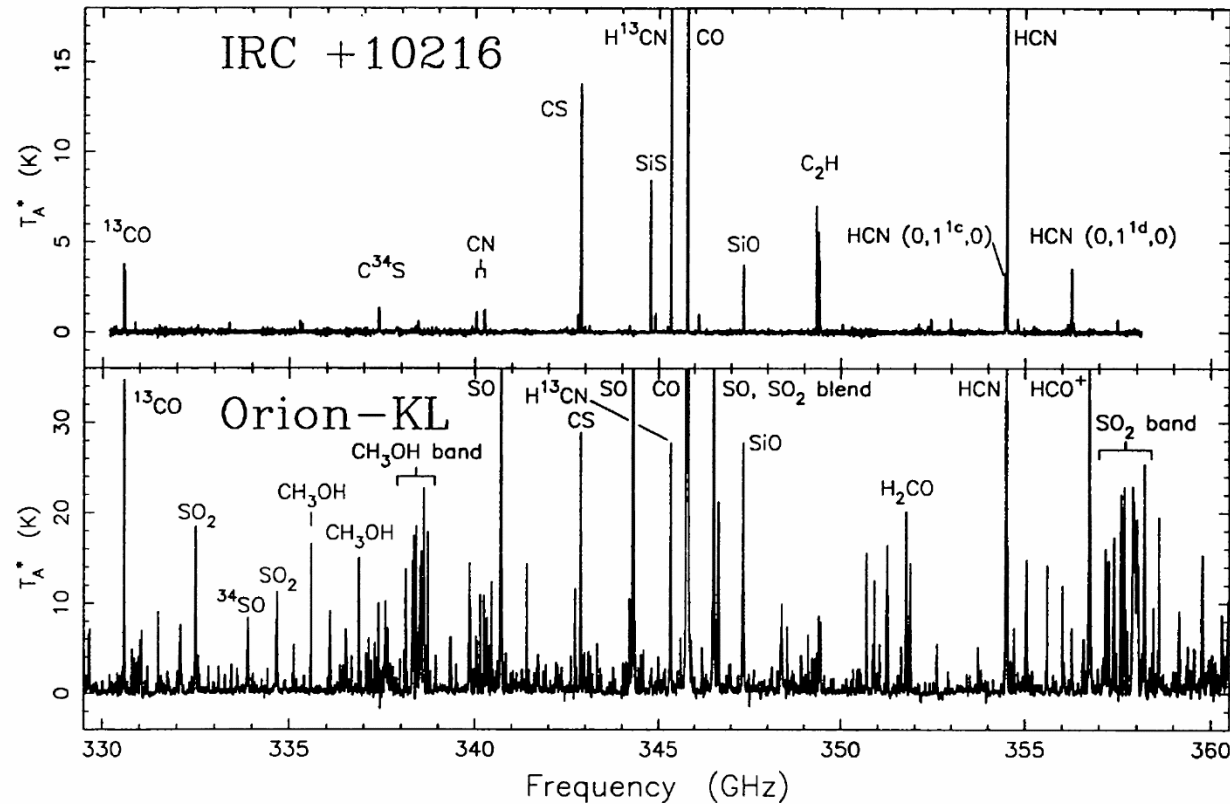
FIG. 2.—Contour map of integrated intensity of CO emission (W_{CO}) in the velocity range of -10 to 20 km s^{-1} . (Along the Galactic plane, CO emission was found at higher velocities, presumably from unrelated clouds more distant than the Orion clouds. These clouds are discussed elsewhere.) The lowest contour level is at 1.28 K km s^{-1} with subsequent levels at 3, 5, 7, ... times this value. The peaks of emission from the Orion Nebula and from NGC 2023 and 2024 (see Fig. 3) are designated by crosses. Two clouds, shown here in insets (see § III and also Figs. 3–5), that overlap other clouds in the survey lie at the positions indicated by arrows.

HCN (hydrogen cyanide) the poisonous gas? HCO^+ ?
 What is going on?

Layers of circumstellar envelope of IRC+10216 (Leão+06)



Kleinmann-Low (KL) object



= CW Leo, a carbon (i.e., evolved) star, puffing off its dusty atmosphere

A protostar in Orion

FIG. 4.—Comparison of the CSO spectral line surveys of IRC +10216 and Orion-KL. The data have been corrected by the main beam (0.6) and extended efficiencies (0.76) for IRC +10216 and Orion-KL, respectively. Note the difference in vertical scale between the two panels.

Star formation is not an isolated event.
Massive stars in particular may
trigger the birth of next-generation
stars → triggered star formation

... also possible by stellar jets, Galactic
density waves, cloud-cloud
collisions ...

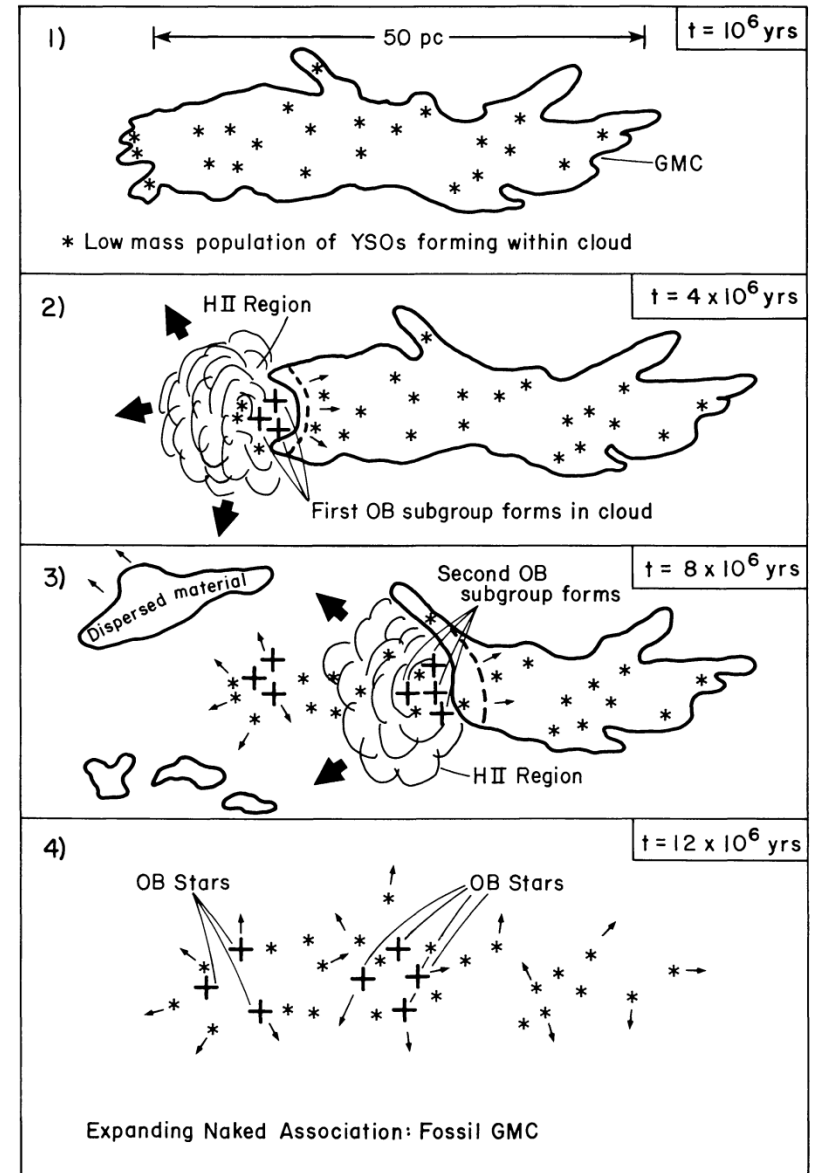


Figure 1. Probable stages in the formation of an expanding OB association from a giant molecular cloud. Low star formation efficiency in conjunction with efficient dispersal of residual, unprocessed molecular gas by OB stars result in a stellar system with positive total energy.

Luminous stars → photoionization of a nearby cloud
→ Radiative driven implosion

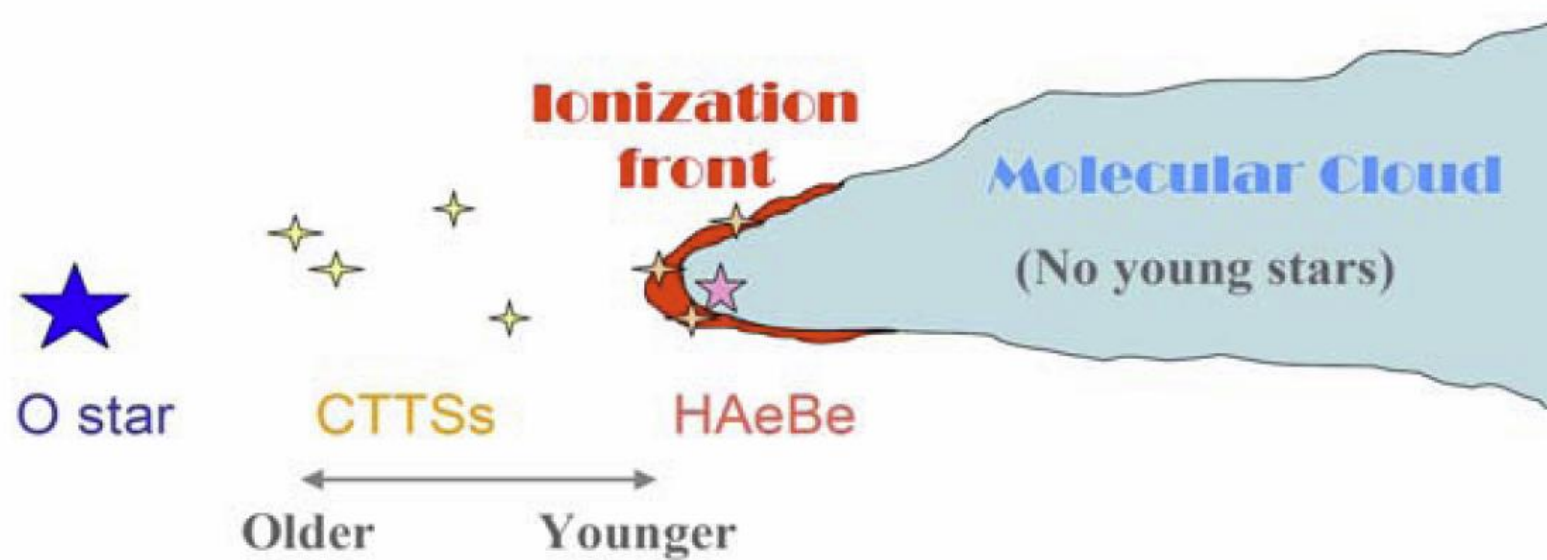
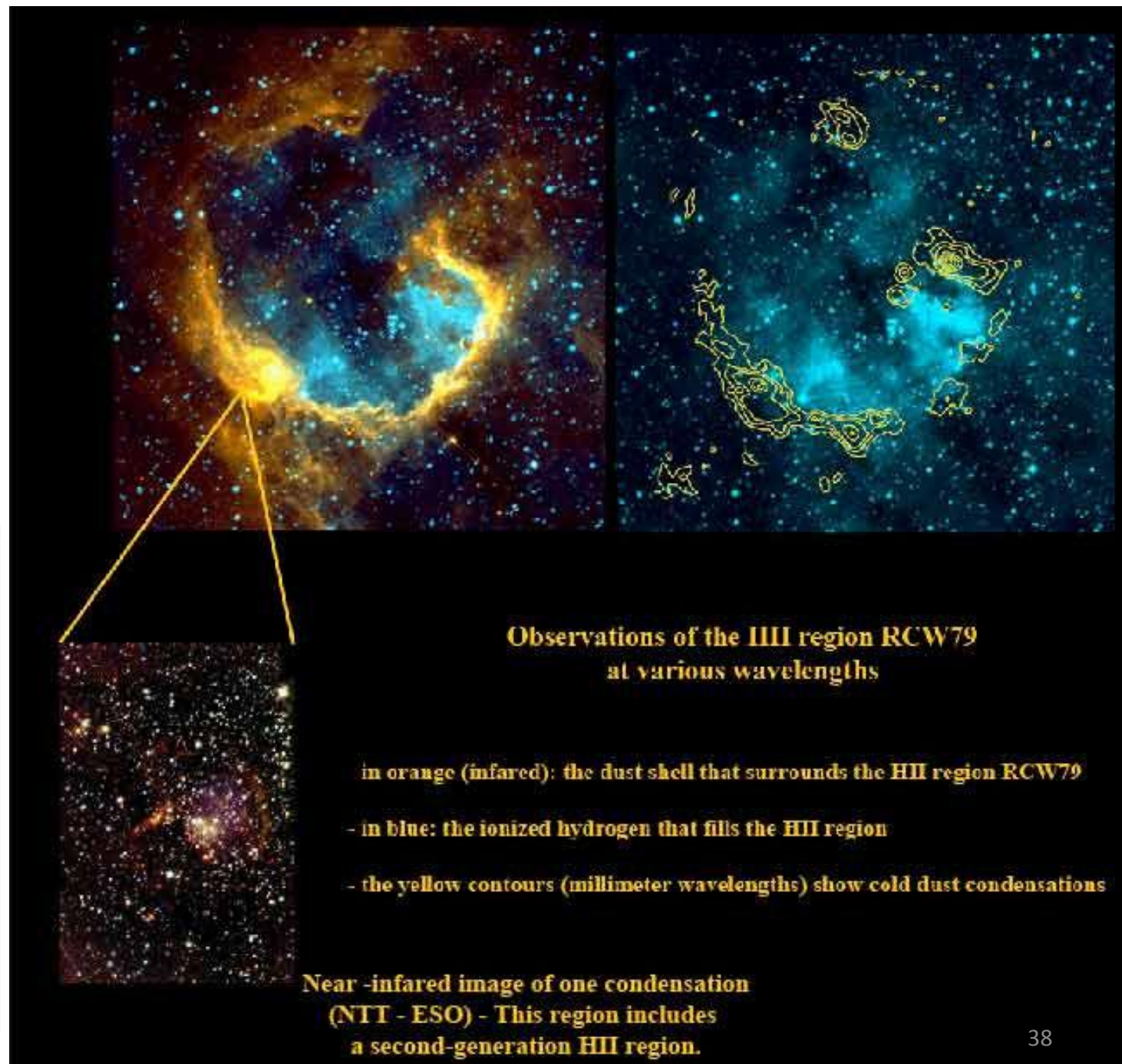
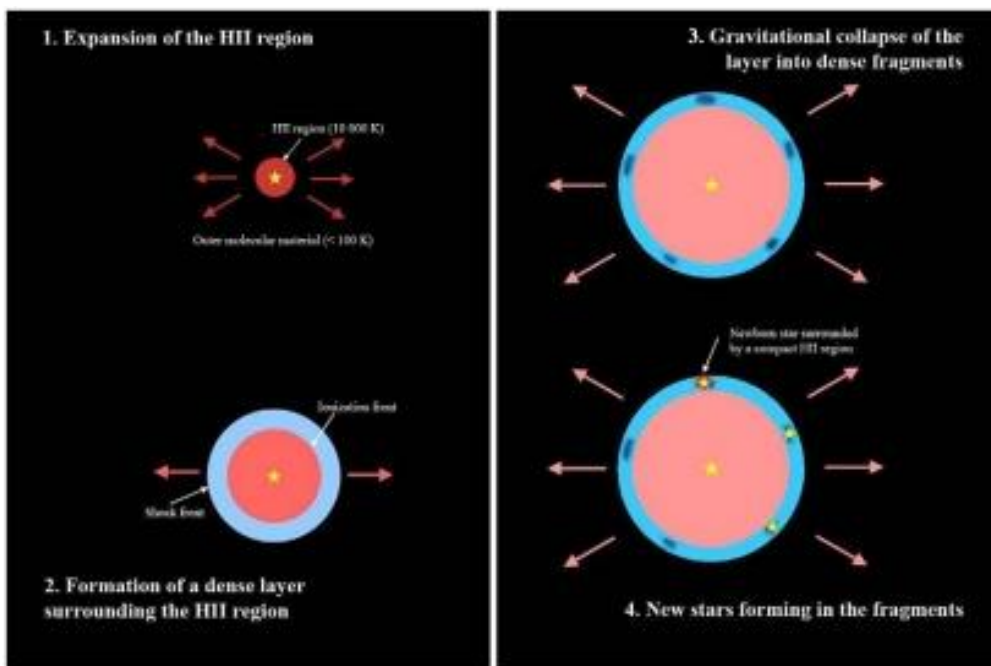


Figure 2. An illustration of a massive star to trigger star formation in a nearby molecular cloud.

Luminous stars →
 photoionization/winds
 on a surrounding cloud
 → Collect and collapse



Size Scales for Star Formation.

Object	log size scale [cm]
Galactic spiral arm	22
Giant molecular cloud	20
Molecular dense core	17
Protostellar accretion disk	15
Protostar	11

Mass Inventory in a Star-Forming Galaxy

Component	log M [M_{\odot}]
Molecular clouds	9
H ₂	9
He	8
CO	7
Young stars	5

Myers in You & Yuan (1995), p. 47

Properties of Giant Molecular Clouds

Diameter [pc]	Mass [M_{\odot}]	Density [cm^{-3}]	T [K]	Velocity Width [km/s]
20-100	$10^5 - 10^6$	10-300	10-30	5-15

Exercise

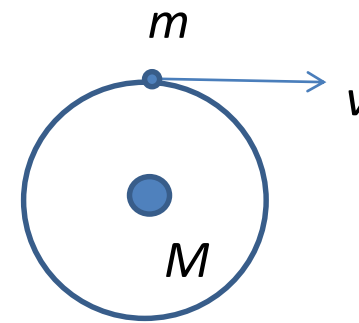
1. What is the BN object (why is it called an “object”)? What is its brightness, distance, luminosity, and mass (how are these known)?
2. Answer the same for the KL object. What is the relation between the two?
3. There is a class of objects called the “Herbig-Haro objects”. What are they?
4. “Quasi-Stellar Objects (QSOs)

Cloud Stability --- The Virial Theorem

Moment of Inertia $I = \int r^2 dm = \sum_i m_i r_i^2$

$$\begin{aligned} \frac{d^2 I}{dt^2} &= \frac{d^2}{dt^2} (mr^2) \dots (\text{if } \dot{m} = 0) \dots \\ &= 2m \frac{d}{dt} (r\dot{r}) = 2m(\dot{r}^2 + r\ddot{r}) \end{aligned}$$

$$\frac{1}{2} \frac{d^2 I}{dt^2} = 2E_K + E_P$$



$$\frac{GmM}{r^2} = m \frac{v^2}{r}$$

To be stable, LHS = 0

$$2E_K + E_P = 0$$

$$2 \left(\frac{1}{2} \right) m v^2 = GM/r$$

Virial Mass

MASS, LUMINOSITY, AND LINE WIDTH RELATIONS OF GALACTIC MOLECULAR CLOUDS

P. M. SOLOMON, A. R. RIVOLO, J. BARRETT, AND A. YAHIL

Astronomy Program, State University of New York–Stony Brook

Received 1986 October 2; accepted 1987 February 2

THE ASTROPHYSICAL JOURNAL, 319:730–741, 1987 August 15

ABSTRACT

We present measurements of the velocity line width, size, virial mass, and CO luminosity for 273 molecular clouds in the Galactic disk between longitudes of 8° and 90° . These are obtained from three-dimensional data in the Massachusetts–Stony Brook CO Galactic Plane Survey. From an analysis of these measurements we show that the molecular clouds are in or near virial equilibrium and are not confined by pressure equilibrium with a warm or hot phase of interstellar matter. The velocity line width is shown to be proportional to the 0.5 power of the size, $\sigma_v \propto S^{0.5}$. Combined with virial equilibrium, this shows that the clouds are characterized by a constant mean surface density of $170 M_\odot \text{ pc}^{-2}$ and have a mass $M \propto \sigma_v^4$. A tight relationship, over four orders of magnitude, is found between the cloud dynamical mass, as measured by the virial theorem, and the CO luminosity $M \propto (L_{\text{CO}})^{0.81}$. This relationship establishes a calibration for measuring the total molecular cloud mass from CO luminosity for individual clouds and for the Galactic disk. The cloud CO luminosity is $L_{\text{CO}} \propto \sigma_v^5$, which is the molecular cloud analog of the Tully-Fisher or Faber-Jackson law for galaxies.

The mass-luminosity law is accounted for by a cloud model consisting of a large number of optically thick clumps in virial equilibrium, each with a thermal internal velocity dispersion, but with the clouds effectively optically thin at a fixed velocity along the line of sight. The typical clump mass is of order a stellar mass and approximately equal to the Jeans mass at the clump density and thermal velocity dispersion.

TABLE 1
GALACTIC FIRST QUADRANT MOLECULAR CLOUD CATALOG



(1)	(2)	(3)	(4)	(5)	(6)	(7)	(8)	(9)	(10)	(11)	(12)	(13)	(14)	(15)
No.	$T_{\text{min}}-I$	ℓ_p	b_p	v_p	T_p	R	D	z	σ_ℓ	σ_b	σ_v	$L_{\text{CO}}/10^4$	$M_{\text{VT}}/10^4$	Flag
	(K)	(Deg.)	(Deg.)	(km·s ⁻¹)	(K)	(kpc)	(kpc)	(pc)	(Deg.)	(Deg.)	(km·s ⁻¹)	(K·km·s ⁻¹ ·pc ²)	(M _⊙)	
1	4-3	8.00	-0.50	128.	5.7	1.4	10.1	-89.	0.06	0.07	4.4	7.27	44.4	T
2	5-3	8.20	0.20	20.	10.2	6.2	15.9	56.	0.17	0.21	4.1	140.2	176.3	F,V
3	4-4	8.30	0.00	3.	5.7	4.0	6.2	0.	0.40	0.11	3.8	22.6	65.4	X
4	4-5	8.30	-0.10	48.	8.2	3.6	13.2	-23.	0.05	0.05	2.2	5.02	11.1	F,U
5	5-6	8.40	-0.30	37.	17.0	4.4	5.7	-30.	0.32	0.15	3.9	23.3	66.5	N,H

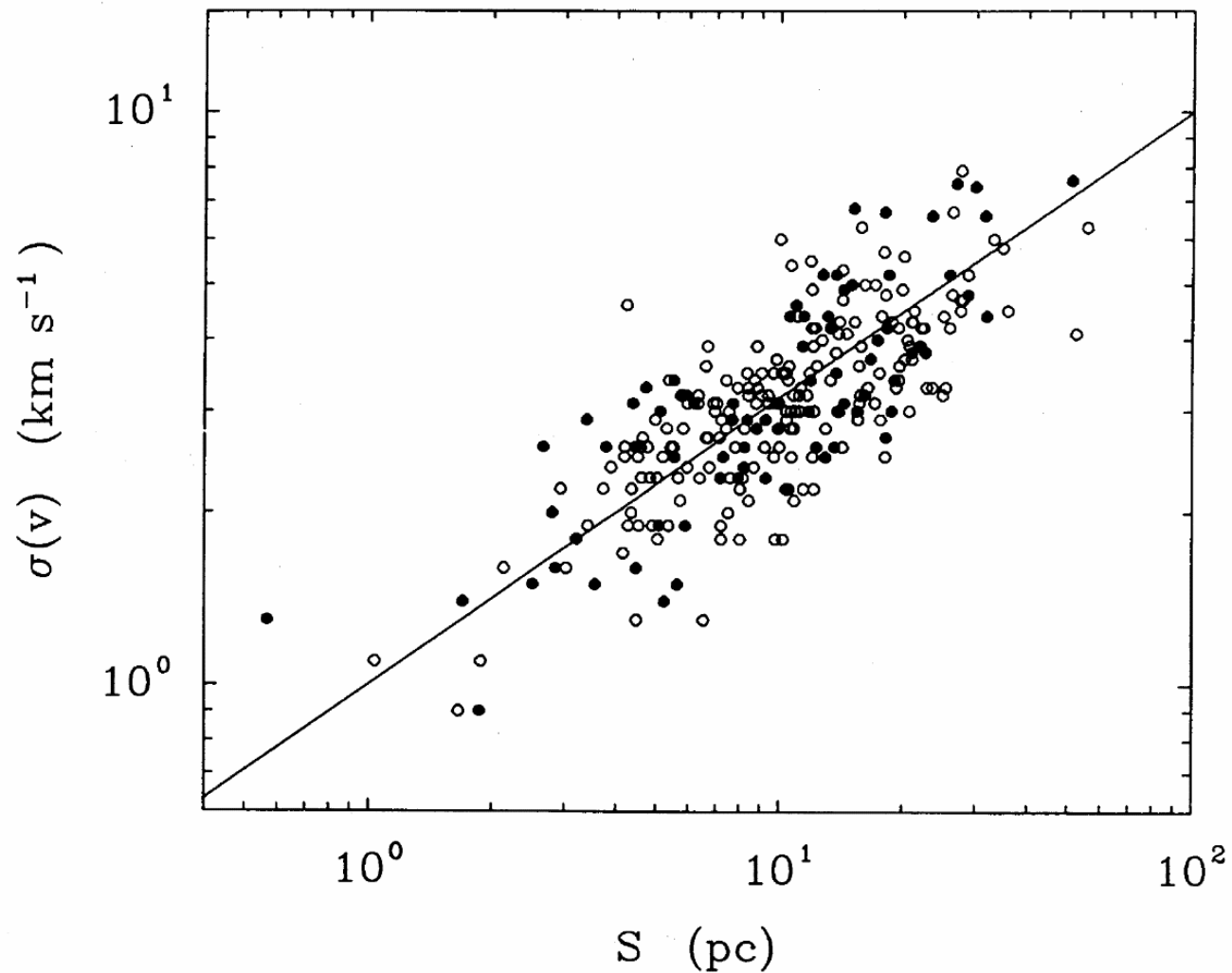


FIG. 1.—Molecular cloud velocity dispersion $\sigma(v)$ as a function of size S (defined in text) for 273 clouds in the Galaxy. The solid circles are calibrator clouds with known distances and the open circles are for clouds with the near-far distance ambiguity resolved by the method discussed in the text. The fitted line is $\sigma(v) = S^{0.5} \text{ km s}^{-1}$. For virial equilibrium the 0.5 power law requires clouds of constant average surface density.

LHS = 0 \rightarrow stable

LHS < 0 \rightarrow collapsing

LHS > 0 \rightarrow expanding

E_K

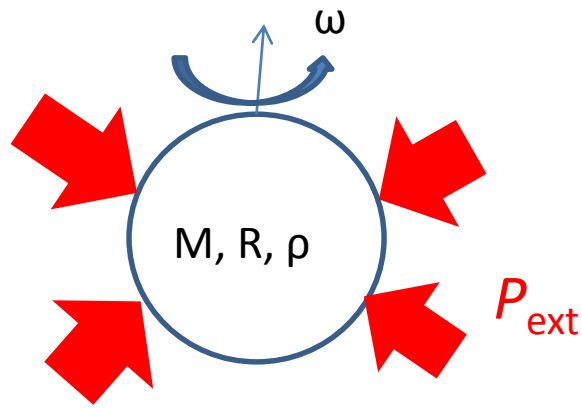
- Kinetic energy of molecules
- Bulk motion of clouds
- Rotation
- ...

E_P

- Gravitation
- Magnetic field
- Electrical field
- ...

$$E_{\text{total}} = E_K + E_P$$

$$E_{\text{total}} = E_K + \Omega \text{ (mostly)}$$



Cloud of mass M , radius R , rotating at ω

$$E_{rot} = \frac{1}{2} I \omega^2$$

$$I = \frac{2}{5} M R^2$$

$$\Omega = -\frac{3}{5} \frac{GM^2}{R}$$

Generalized virial theorem

$$\frac{1}{2} \frac{d^2 I}{dt^2} = 2 \langle E_K \rangle + \int \vec{r} \cdot \vec{F} dm + 3 \int P dV - \oint P \vec{r} \cdot d\vec{s}$$

If $\omega = 0$, and $P_{ext} = 0$

$$2 \cdot \frac{3}{2} \frac{M}{\mu m_H} kT - \frac{3}{5} \frac{GM^2}{R} = 0$$

$$R_J = \frac{1}{5} \frac{GM \mu m_H}{kT}$$

This is the **Jeans length**.

$\mu \approx 2.37$ for solar abundance with H_2

Jeans length = critical spatial wavelength

If perturbation length scale is longer

→ Medium is decoupled from self-gravity → stable

$$M_J = \frac{4}{3}\pi R_J^3 \rho$$

$$R_J = \left(\frac{15}{4\pi} \frac{kT}{\mu m_H G \rho}\right)^{1/2} \sim \sqrt{\frac{T}{\rho}}$$

$$M_J = \left(\frac{\pi kT}{4\mu m_H G}\right)^{3/2} \sqrt{\frac{1}{\rho}} \sim \frac{T^{3/2}}{\rho^{1/2}}$$

This is the **Jeans mass** ... the **critical** mass for onset of gravitational collapse

If cloud mass $M > M_{\text{Jeans}}$ → cloud collapse

Note the above does not consider external pressure, or other internal supporting mechanisms.

A non-magnetic, isothermal cloud in equilibrium with external pressure
→ a **Bonnor-Ebert sphere** (Bonnor 1956, Ebert 1955)

$$2E_K + E_P - 3P_{\text{ext}}V = 0$$

The potential term can include, other than the gravitational force, also rotation, magnetic field, etc.

At first, the cloud is optically **thin**.

Contraction → density ↑ → collisions more frequent
→ molecules excited and radiated → radiation escapes
→ cooling → less resistance to the contraction
→ collapse (free fall)

$$R_J \approx c_s \tau_{\text{ff}} = [\text{isothermal sound speed}] * [\text{free fall time}]$$

A spherical symmetric gas cloud with temperature T and external pressure P

For one particle, $F_i = m_i \ddot{r}_i \leftarrow \frac{\partial}{\partial r}$

$$\begin{aligned} m_i r_i \cdot \ddot{r}_i &= m_i \frac{d}{dt} (\dot{r}_i \cdot r_i) - m_i \dot{r}_i \cdot \dot{r}_i \\ &= \frac{1}{2} m_i \frac{d^2}{dt^2} (r_i^2) - m \dot{r}_i^2 \end{aligned}$$

Summing over all particles

$$\frac{1}{2} \frac{d^2}{dt^2} \left[\sum_i m_i r_i^2 \right] - 2 \sum_i \frac{1}{2} m_i \dot{r}_i^2 = \sum_i r_i F_i$$

Moment of inertial

Kinetic energy

To maintain $2E_K + E_P = 0$, the total energy $E_t = E_K + E_P$ must change.
The gravitational energy

$$\Omega \sim -\frac{GM^2}{r} \rightarrow d\Omega \sim \frac{dr}{r^2}$$

For contraction, $dr < 0$, so $d\Omega < 0 \rightarrow$ Then $dE_t = dE_K + d\Omega = \frac{1}{2} \Omega = L \Delta t$

This means to maintain quasistatic contraction, **half** of the gravitation energy from the contraction is radiated away.

Eventually the cloud becomes dense enough (i.e., optically **thick**) and contraction leads to temperature increase.

The cloud's temperature increases while energy is taken away
 \rightarrow negative heat capacity

- H I clouds

$$R_J \approx 25 \text{ pc}; M_J \approx 120 M_\odot > M_{\text{obs}}$$

So H I clouds are not collapsing.

- Dark molecular clouds

$$M_{\text{obs}} \approx 100\text{-}1000 M_\odot > M_J \approx 10 M_\odot$$

So H₂ clouds should be collapsing. But observations show that most are not.

→ There is additional support other than the thermal pressure, e.g., rotation, magnetic field, turbulence, etc.

Roughly, the requirement for a cloud to be gravitational stable is

$$|E_{\text{grav}}| > E_{\text{th}} + E_{\text{rot}} + E_{\text{turb}} + E_{\text{mag}} + \dots$$

For a spherical cloud, $E_{\text{grav}} = -C_{\text{grav}} GM^2/R$, where C_{grav} is a constant depending on the mass distribution ($=3/5$ for uniform density).

The thermal energy, $E_{\text{th}} = \frac{3}{2} \frac{m}{\mu m_H} k_B T$, where μ is the mean molecular weight of the gas in atomic mass units.

The rotational energy $E_{\text{rot}} = C_{\text{rot}} M R^2 \omega^2$, where C_{rot} depends on the mass distribution and is $1/5$ for uniform density; ω is the (assumed) uniform angular velocity.

The turbulent kinetic energy $E_{\text{turb}} = \frac{1}{2} M \sigma^2$, where σ is the mean turbulent velocity.

The magnetic energy $E_{\text{mag}} = \frac{1}{8} \int B^2 dV \approx \frac{1}{6} B^2 R^3$, where B is the uniform magnetic field.

For **rotational support** to be important,

$$\frac{3}{5} \frac{GM}{R} = \frac{1}{2} I \omega^2 = \frac{1}{2} \left(\frac{2}{5} MR^2 \right) \left(\frac{v_{\text{crit}}}{R} \right)^2 = \frac{1}{5} M v_{\text{crit}}^2$$

So $v_{\text{crit}} = (3GM/R)^{1/2}$, where v_{crit} is the critical rotation velocity at the equator.

$$\text{Numerically, } v_{\text{crit}} = 0.11 \left[\frac{M}{M_{\odot}} \frac{\text{pc}}{R} \right]^{1/2} \text{ [km/s]}$$

$$\text{For HI clouds, } v_{\text{crit}} = 0.11 \left[\frac{50}{2.5} \right]^{1/2} \approx 0.5 \text{ [km/s]}$$

Typically, $\omega \approx 10^{-16} \text{ s}^{-1}$, so $v \approx 0.01$ to 0.1 [km/s]

→ Clouds are generally **not** rotationally supported.

Measuring the ISM Magnetic Fields

Method	Medium	Info
Polarization of starlight	Dust	B_{\perp}
Zeeman effect	Neutral hydrogen; a few mol. lines	B_{\parallel}
Synchrotron radiation	Relativistic electrons	B_{\perp}
Faraday rotation	Thermal electrons	B_{\parallel}

The Zeeman effect is the only technique for **direct** measurements of magnetic field strengths.

Polarization of Starlight

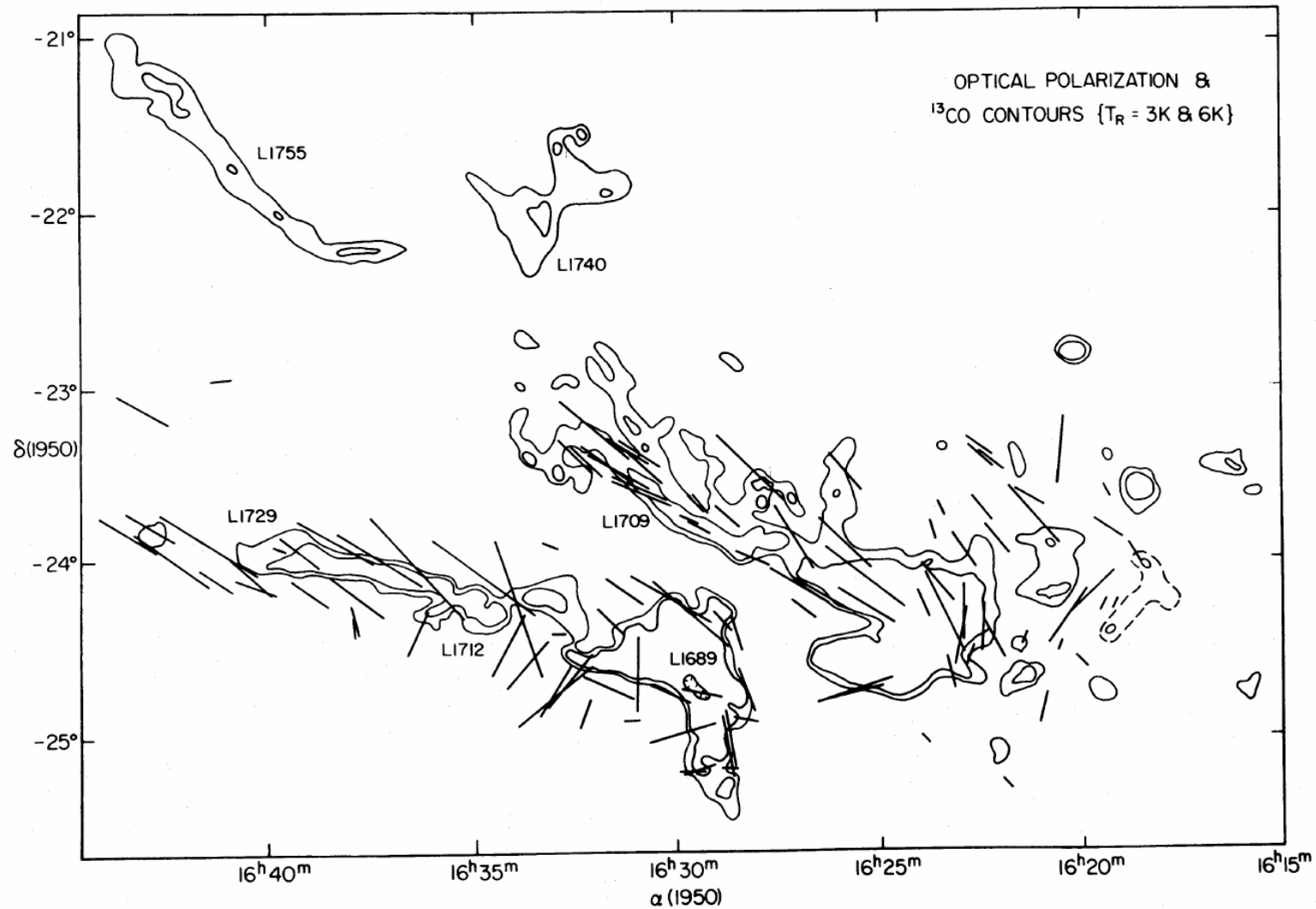
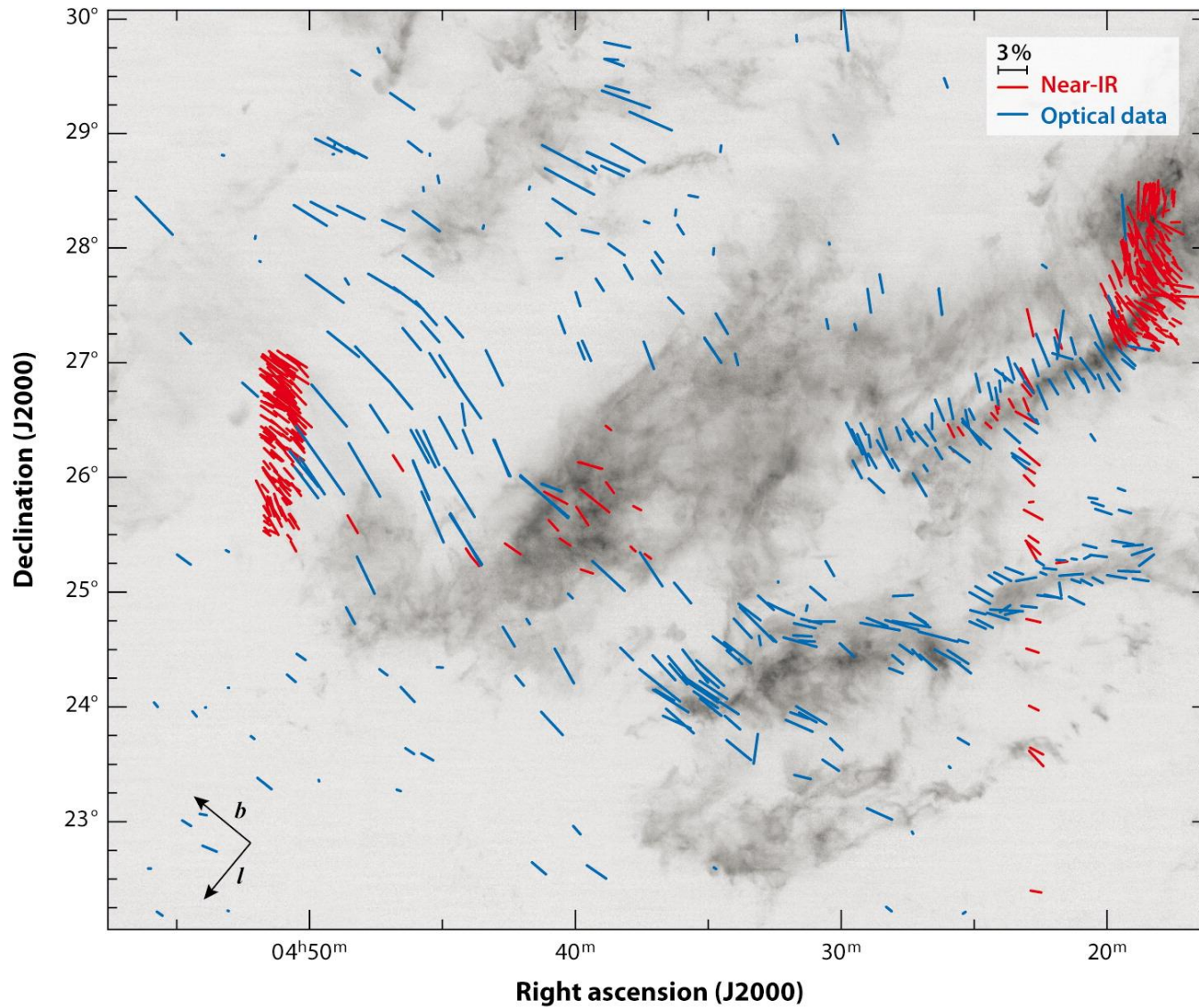


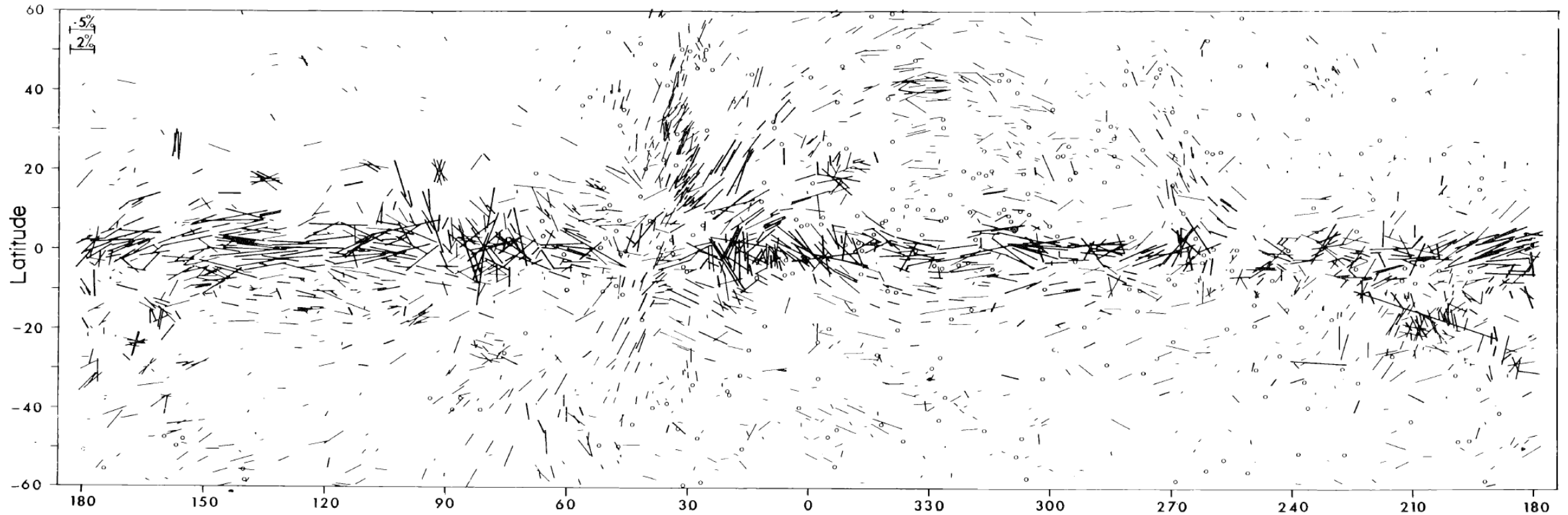
FIG. 7.—Orientation and relative magnitude of optical polarization vectors toward field stars at the cloud edges (Vrba, Strom, and Strom 1976). Solid contours of $T_R(^{13}\text{CO})$ are at 3 and 6 K, with a dotted 1 K contour added around R5–R6 and R8–R9.



Organized magnetic field morphology in the Taurus dark-cloud complex superposed on a ^{13}CO map (Chapman et al. 2011). **Blue** lines show polarization measured at optical wavelengths and **red** lines show near-IR (H-band and I-band) polarization.

Dichroic extinction by dust (optical and near-IR) $\vec{P} \parallel \vec{B}$

Interstellar Polarization



Mathewson & Ford (1970)

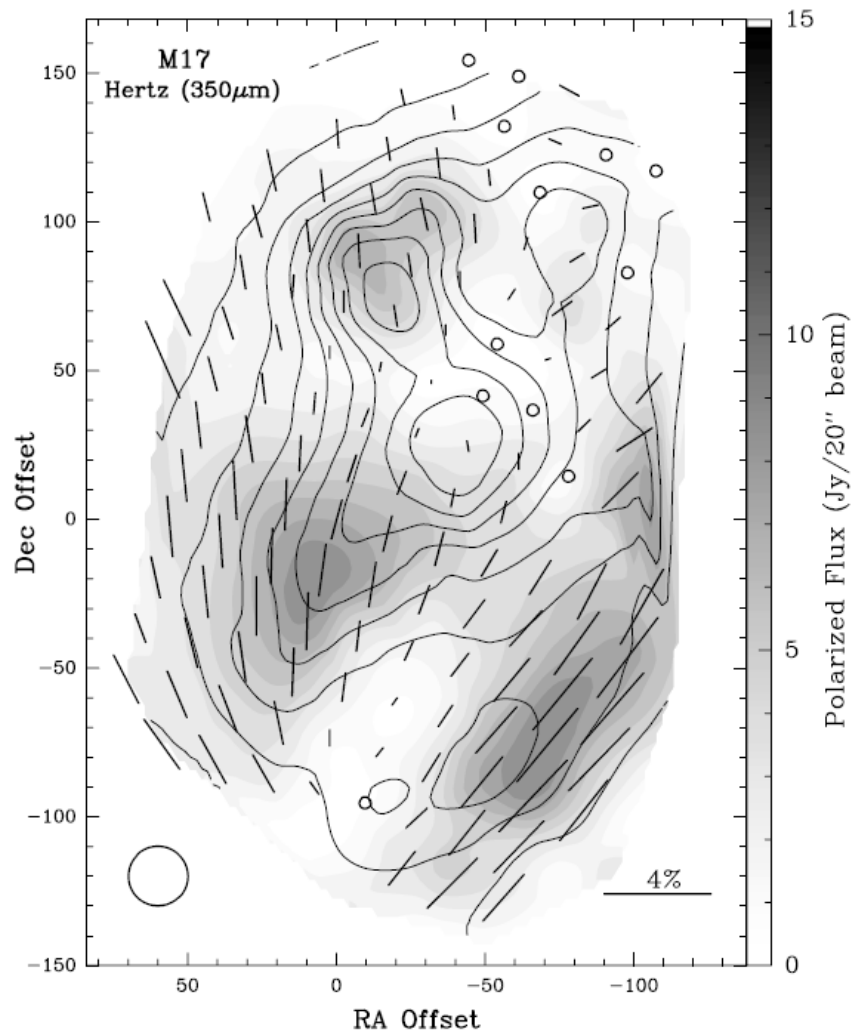


FIG. 6.—HERTZ polarization map of M17 at $350\ \mu\text{m}$. All of the polarization vectors shown have a polarization level and error such that $P > 3\sigma_P$. Circles indicate cases where $P + 2\sigma_P < 1\%$. The contours delineate the total continuum flux (from 10% to 90% with a maximum flux of ≈ 700 Jy), whereas the underlying gray scale gives the polarized flux according to the scale on the right. The beam width ($\approx 20''$) is shown in the lower left corner and the origin of the map is at R.A. = $18^{\text{h}}17^{\text{m}}31^{\text{s}}.4$, decl. = $-16^{\circ}14'25''.0$ (B1950.0).

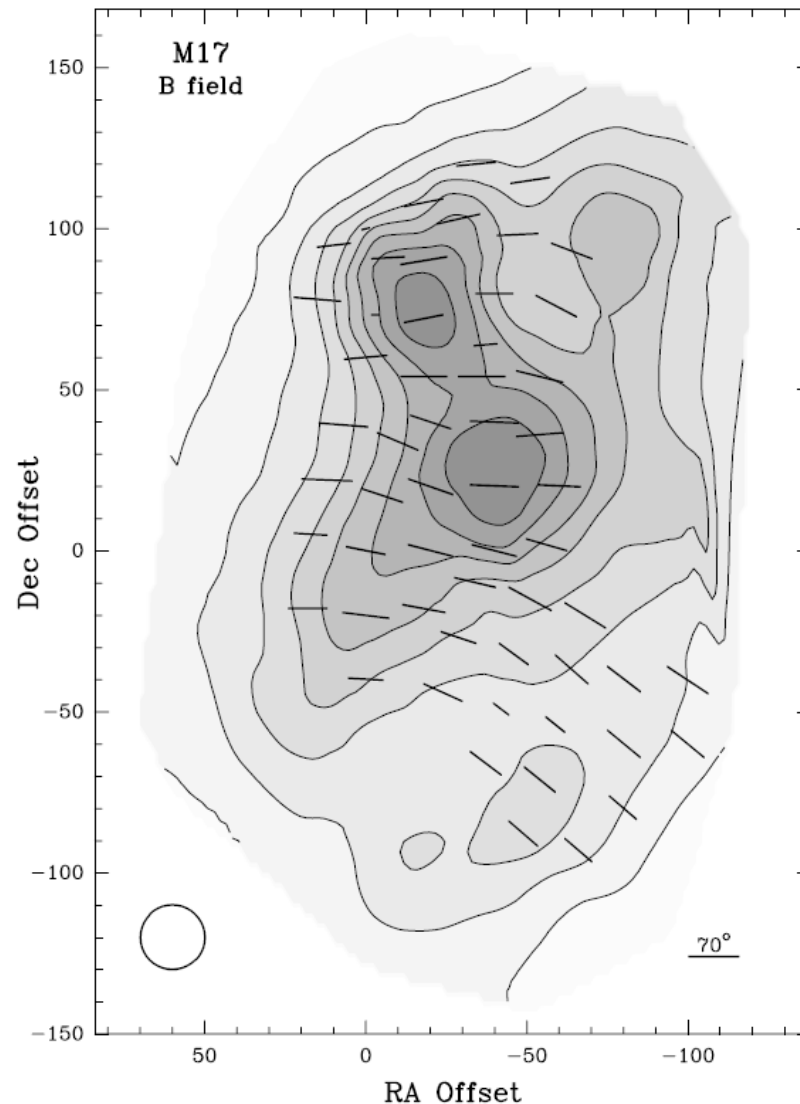
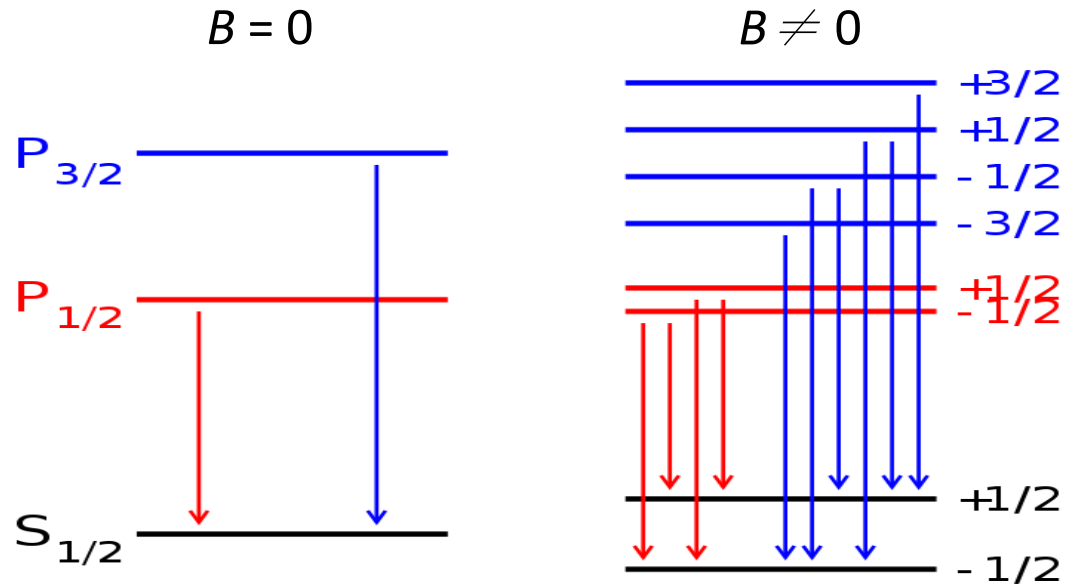


FIG. 11.—Orientation of the magnetic field in M17. The orientation of the projection of the magnetic field in the plane of the sky is shown by the vectors and the viewing angle is given by the length of the vectors (using the scale shown in the bottom right corner). The contours and the gray scale delineate the total continuum flux. The beam width ($\approx 20''$) is shown in the lower left corner, and the origin of the map is at R.A. = $18^{\text{h}}17^{\text{m}}31^{\text{s}}.4$, decl. = $-16^{\circ}14'25''.0$ (B1950.0).

Thermal emission
by dust (far-IR, and
smm) $\vec{P} \perp \vec{B}$

Houde et al. (2002)

Zeeman effect



$$\Delta \nu_B \text{ [Hz]} = 1.40 \times 10^{10} g B[\text{T}]$$

$$\Delta \lambda_B \text{ [nm]} = 4.67 \times 10^{-8} g (\lambda_0 \text{ [nm]})^2 B[\text{T}]$$

g : Landé or g factor (L, S, J) ~ 1

Ex: $B = 0.1 \text{ T}$ (1 kG) for a typical sunspot, at 500 nm, $g = 1$

→ wavelength shift 0.001 nm \approx natural line width

→ difficult to measure

Letter to the Editor

The magnetic field of the NGC 2024 molecular cloud: detection of OH line Zeeman splitting

Richard M. Crutcher^{1,2} and Ilya Kazès¹

¹ Department de Radioastronomie, Observatoire de Paris-Meudon, F-92195 Meudon, France

² Department of Astronomy, University of Illinois, Urbana, IL 61801, USA

Summary

Zeeman splitting of the main lines of OH in absorption has been detected for the first time. The derived magnetic field for a clump in the NGC 2024 molecular cloud is -38 ± 1 microgauss.

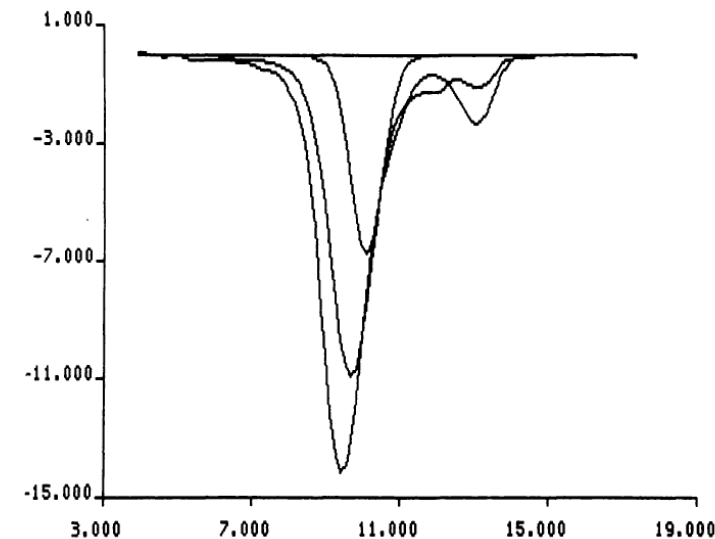


Fig. 1. Spectra of the 1667 (strongest) and 1665 lines observed for $13^{\text{h}} 18^{\text{m}}$ toward NGC 2024 (RA/DEC [1950.0] $05^{\text{h}} 39^{\text{m}} 14^{\text{s}}.3 / -01^{\circ} 55' 57''$). The weakest line is the assumed gaussian component used for Zeeman analysis.

The abscissa scale in all figures is the same and is given in km s^{-1} relative to the LSR. The ordinate scale in $^{\circ}\text{K}$ antenna temperature is correct except that displacements of zero have been made in most figures.

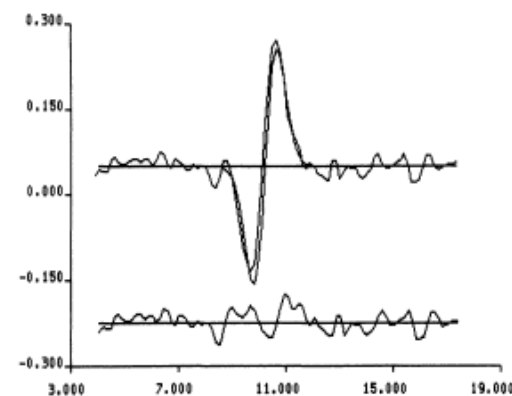


Fig. 4. Stokes V spectrum of the 1667 line together with a fit derived from the gaussian of figure 1. At the bottom the fitted minus the observed residuals are shown.

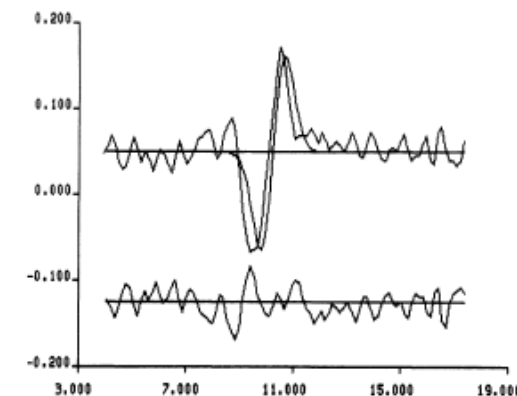
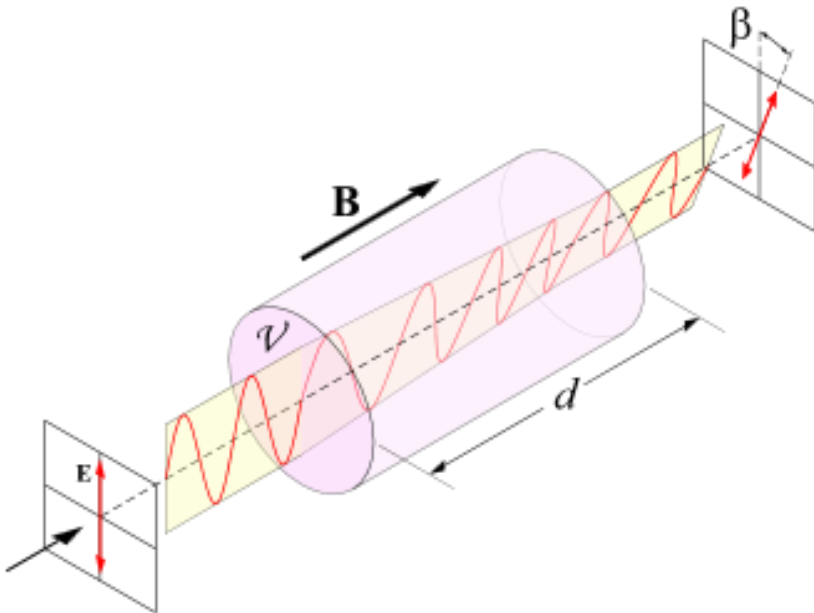


Fig. 5. Stokes V spectrum of the 1665 line together with a fit derived from the gaussian of figure 1. At the bottom the observed minus the fitted residuals are shown.

Faraday Rotation --- rotation of the plane of polarization when light passes through a magnetic field

Circularly polarized light \rightarrow E field rotates \rightarrow force on the charged particles to make circular motion \rightarrow creating its own B field, either parallel or in opposite direction to the external field \rightarrow phase difference \rightarrow Change of position angle of the linear polarization



Faraday rotation angle $\beta = RM \lambda^2$
where the rotation measure (RM) is

$$RM = \frac{e^3}{2\pi m^2 c^4} \int_0^d n_e(s) B_{\parallel}(s) ds$$

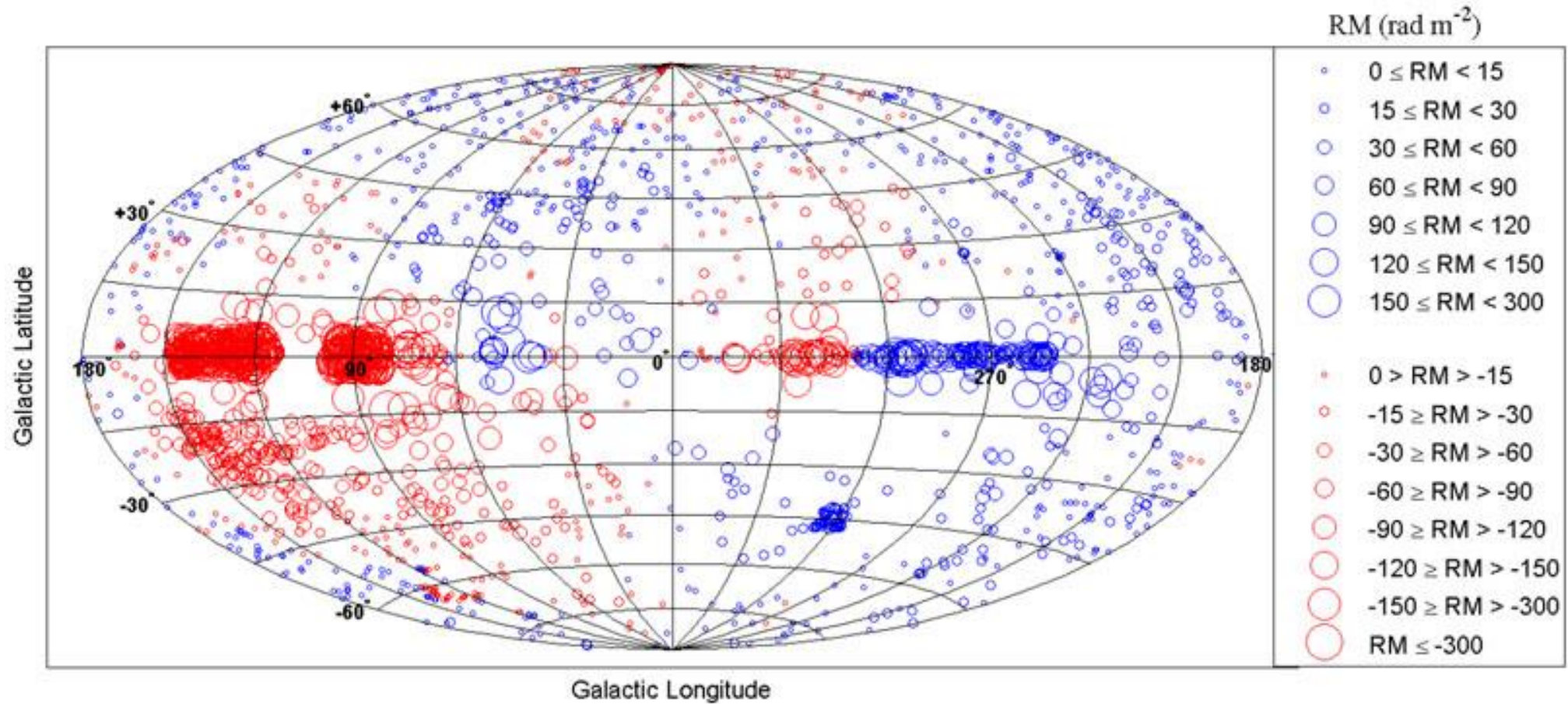


Figure 3. A smoothed representation of 2257 **Faraday rotation** measures in Galactic coordinates with the Galactic center at (0,0). (Kronberg & Newton-McGee, [3]). Blue and red circles represent positive and negative RM's respectively, and the circle size is proportional to RM strength.

<http://ned.ipac.caltech.edu/level5/Sept10/Kronberg/Figures/figure3.jpg>

For **magnetic support** to be important,

$$\frac{3}{5} \frac{GM^2}{R} = \frac{B^2}{8\pi} \left(\frac{4}{3} \pi R^3 \right) = \frac{1}{6} B^2 R^3$$

So, $M \propto BR^2$, and since $M \propto \rho R^3$, we get $R \propto \frac{B}{\rho}$

The magnetic Jeans mass becomes

$$M_{\text{Jeans}}^B \propto BR^2 \propto B^3 / \rho^2$$

Numerically, $M_{\text{Jeans}}^B \approx 2.4 \times 10^4 B_{\mu\text{G}}^3 n_H^{-2} [M_{\odot}]$

and $B_{\text{crit}} = 0.1 \frac{M}{M_{\odot}} \left(\frac{\text{pc}}{R} \right)^2 [\mu\text{G}]$

If the magnetic flux is conserved, $\mathbf{B} \propto \frac{1}{R^2}$

Because $M \propto R^3 \rho = \text{constant}$, the **frozen-in** (i.e., flux conservation) condition would have led to $\mathbf{B} \propto R^{-2} \sim \rho^{2/3}$

If flux is conserved, \mathbf{B}_0 (ISM) $\sim 10^{-6}$ [G]

$$R_0 \approx 0.1 \text{ [pc]} \rightarrow R = R_{\odot} \rightarrow \mathbf{B} \approx 10^7 \text{ [G]}$$

But what has been actually observed is

$$\mathbf{B} \propto \rho^{1/3} \text{ to } \rho^{1/2},$$

Implying magnetic flux loss.

INTERSTELLAR MAGNETIC FIELD STRENGTHS AND GAS DENSITIES: OBSERVATIONAL AND THEORETICAL PERSPECTIVES

T. H. TROLAND

Physics and Astronomy Department, University of Kentucky

AND

CARL HEILES

Astronomy Department, University of California, Berkeley

Received 1985 January 31, accepted 1985 July 16

ABSTRACT

We present an updated compilation of observational data concerning the relationship between the interstellar magnetic field strength and the gas density. Pulsar and Zeeman-effect data provide the only reliable information about the (B, n) relationship, and they now span nearly six orders of magnitude in gas density. Field strengths show no evidence of increase over the density range $0.1\text{--}\sim 100\text{ cm}^{-3}$. At higher densities, a modest increase in field strength is observed in some regions, in line with theoretical expectations for self-gravitating clouds. In two regions of the interstellar medium, the magnetic field is unusually high; however, these are not locales where self-gravitation is important. Despite the consistency between observations and theory, questions still exist about how the magnetic field strength remains constant for densities up to $\sim 100\text{ cm}^{-3}$. Further Zeeman effect studies and a better theoretical understanding of the formation of interstellar clouds and complexes will be necessary to answer these questions.

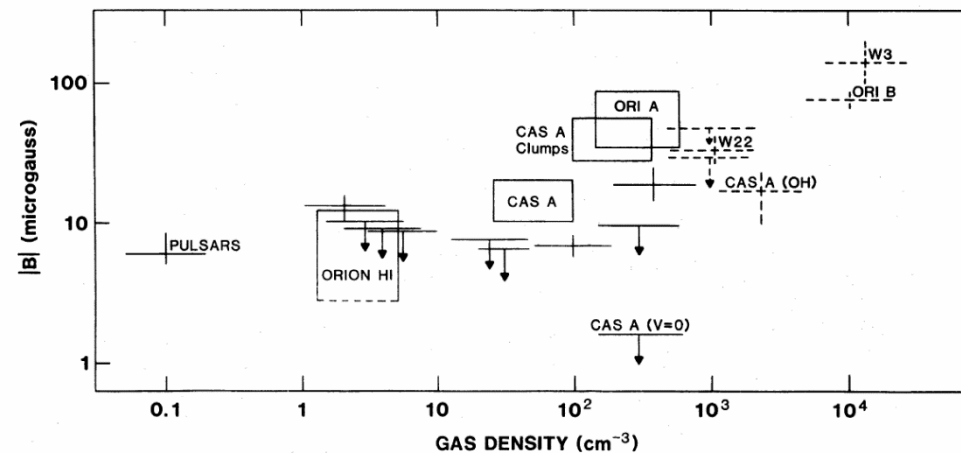


FIG. 1.—Observed magnetic field strengths as a function of estimated volume density. All results come from measurements of the H I (solid lines) and OH (dashed lines) Zeeman effect, except for the point labeled “pulsars.” This point is derived from pulsar rotation and dispersion measures. Rectangular boxes represent ranges of field strengths encountered in Zeeman effect maps made either with a single-dish or with aperture synthesis instruments. See § II for further details.

A new probe of magnetic fields during high-mass star formation

Zeeman splitting of 6.7 GHz methanol masers

W. H. T. Vlemmings

Argelander Institute for Astronomy, University of Bonn, Auf dem Hügel 71, 53121 Bonn, Germany

Received 24 January 2008 / Accepted 30 March 2008

Abstract

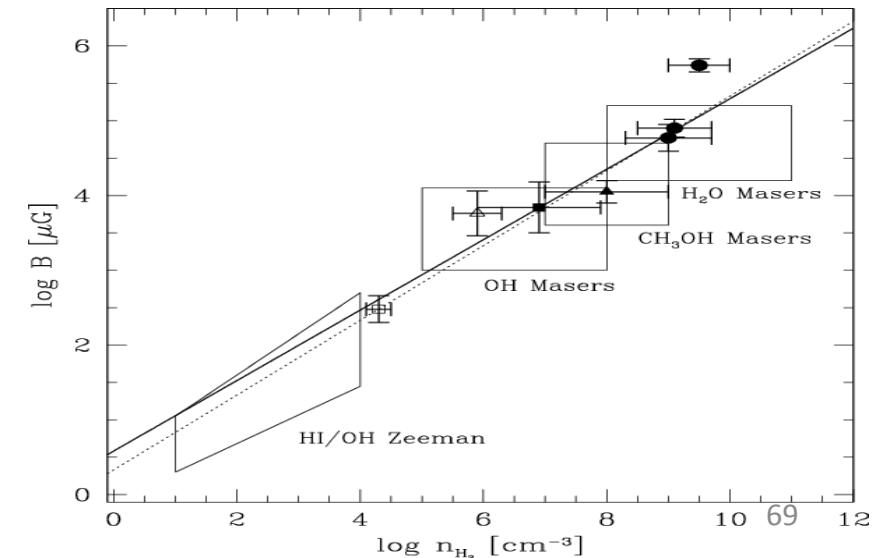
Context. The role of magnetic fields during high-mass star formation is a matter of fierce debate, yet only a few direct probes of magnetic field strengths are available.

Aims. The magnetic field is detected in a number of massive star-forming regions through polarization observations of 6.7 GHz methanol masers. Although these masers are the most abundant of the maser species occurring during high-mass star formation, most magnetic field measurements in the high-density gas currently come from OH and H₂O maser observations.

Methods. The 100-m Effelsberg telescope was used to measure the Zeeman splitting of 6.7 GHz methanol masers for the first time. The observations were performed on a sample of 24 bright northern maser sources.

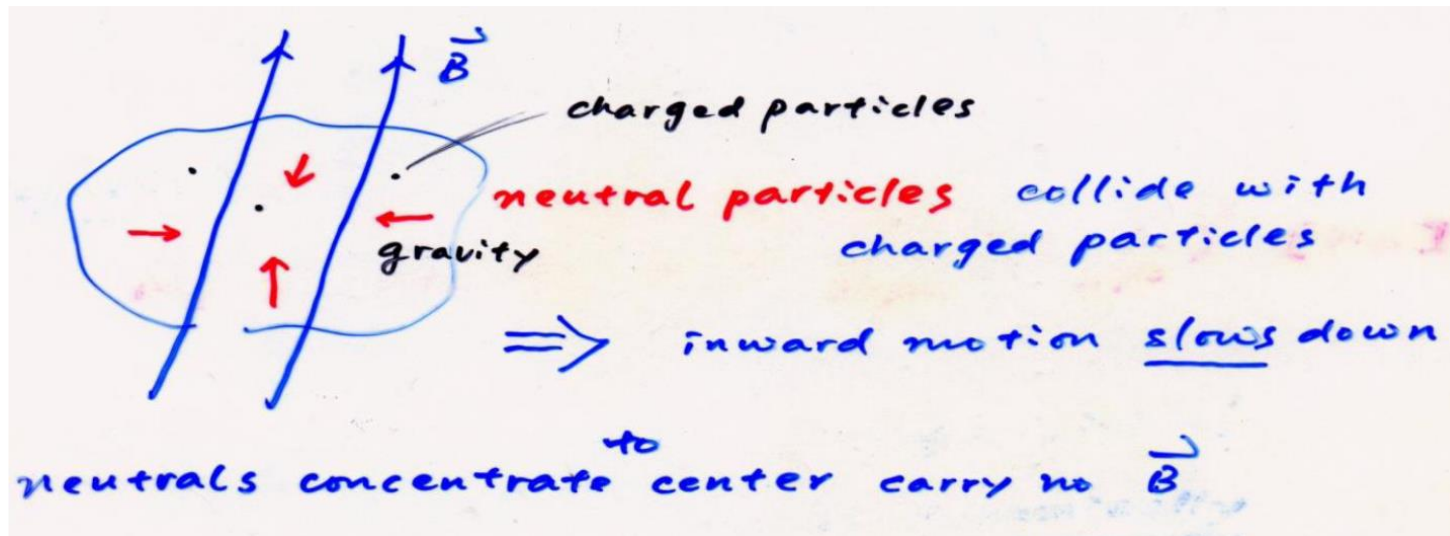
Results. Significant Zeeman splitting is detected in 17 of the sources with an average magnitude of 0.56 m s⁻¹. Using the current best estimate of the 6.7 GHz methanol maser Zeeman splitting coefficient and a geometrical correction, this corresponds to an absolute magnetic field strength of 23 mG in the methanol maser region.

Conclusions. The magnetic field is dynamically important in the dense maser regions. No clear relation is found with the available OH maser magnetic field measurements. The general sense of direction of the magnetic field is consistent with other Galactic magnetic field measurements, although a few of the masers display a change of direction between different maser features. Due to the abundance of methanol masers, measuring their Zeeman splitting provides the opportunity to construct a comprehensive sample of magnetic fields in high-mass star-forming regions.



\vec{B} confines motion of charged particles.

Molecular clouds \rightarrow most neutral with only a tiny fraction of particles;
ionized by cosmic rays or by natural radioactivity



= decoupling of neutral particles from plasma in the initial stage of star formation

- \rightarrow 1. leakage of \vec{B}
- 2. charged particles escaped from magnetic poles
(**ampipolar diffusion=plasma drift**)

If $\mathcal{M}_{\text{cloud}} > \mathcal{M}_{\text{crit}} \rightarrow$ supercritical \rightarrow Cloud will collapse dynamically
 \rightarrow Massive star formation

If $\mathcal{M}_{\text{cloud}} < \mathcal{M}_{\text{crit}} \rightarrow$ subcritical \rightarrow Cloud collapses, if ever, quasi-statically
 \rightarrow Low-mass star formation

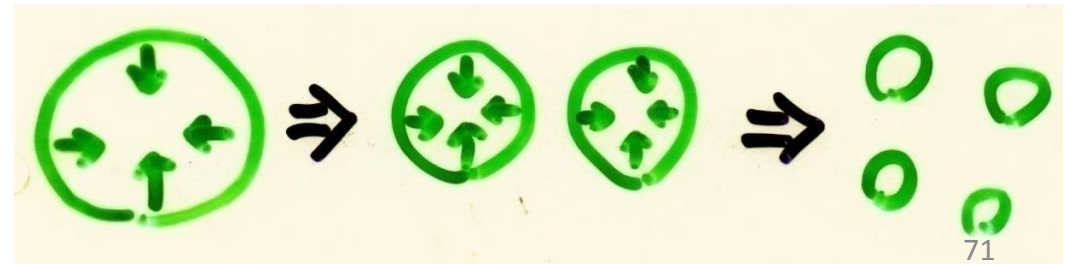
Clouds tend to condense with $\mathcal{M} \sim 10^4 M_{\odot}$, but observed stellar mass ranges $0.05 \leq \mathcal{M}/M_{\odot} \leq 100$

Why is there a lower mass limit and an upper mass limit for stars?

Cloud collapse \rightarrow (local) density increase \rightarrow (local) M_j decrease
 \rightarrow easier to satisfy $M > M_j$, i.e., cloud becomes more unstable

\rightarrow fragmentation

Formation of a cluster of stars $\sim\sim$



Recall Jeans mass $M_J \approx 1.2 \times 10^5 \left(\frac{T}{100 \text{ K}}\right)^{3/2} \left(\frac{\rho_0}{10^{-24} \text{ g cm}^{-3}}\right)^{-1/2} \frac{1}{\mu^{3/2}} [M_\odot]$

$$\propto T^{2/3} / \rho^{1/2}$$

If during collapse, $M_J \downarrow \rightarrow$ subregions become unstable and continue to collapse to smaller and smaller scales (**fragmentation**).

Since during collapse ρ always \uparrow , the behavior of M_J depends on T .

If gravitational energy is radiated away, i.e., $\tau_{\text{cooling}} \ll \tau_{\text{ff}}$ and collapse is **isothermal**, $T = \text{const}$, so $M_J \propto \rho^{-1/2} \rightarrow$ collapse continues

However, once the isothermal condition is no longer valid, e.g., when the cloud becomes optically thick, the collapse is **adiabatical**.

$$T \propto P^{2/5} \propto \rho^{2/3}$$

So $M_J \propto \frac{\rho}{\rho^{1/2}} = \rho^{1/2}$, i.e., grows with time (ever more difficult to overcome/collapse), so the collapse halts

For a monatomic idea gas, the adabatic index

$$\gamma \equiv c_p/c_v = \frac{f+2}{f} = \frac{5/2}{3/2} = 5/3$$

$$PV^\gamma = \text{const}; TV^{\gamma-1} = \text{const};$$

Equation of motion for a spherical surface at r is

$$\frac{d^2 r}{dt^2} = -\frac{Gm}{r^2}$$

with initial condition $r(0) = r_0$, $\frac{dr}{dt}(0) = 0$, $m = 4\pi r_0^3 \rho_0 / 3$.

Multiplying both sides by dr/dt , and since $\frac{d}{dt} \left(\frac{dr}{dt}\right)^2 = 2 \frac{dr}{dt} \frac{d^2 r}{dt^2}$,

$$\frac{d}{dt} \left(\frac{dr}{dt}\right)^2 = -\frac{2Gm}{r^2} \frac{dr}{dt}$$

Integrating both sides, we get

$$\left(\frac{dr}{dt}\right)^2 = 2Gm \left(\frac{1}{r} - \frac{1}{r_0}\right)$$

Substituting m , we get

$$\frac{dr}{dt} = - \left[\frac{8\pi G \rho_0 r_0^2}{3} \left(\frac{r_0}{r} - 1 \right) \right]^{\frac{1}{2}}$$

Define a new variable θ , so that $r(t) = r_0 \cos^2 \theta$, ($\theta = 0$ at $t = 0$) then

$$\frac{d\theta}{dt} \cos^2 \theta = \frac{1}{2} \left(\frac{8\pi G \rho_0}{3} \right)^{1/2}$$

Integrating this, we obtain $\theta + \frac{1}{2} \sin 2\theta = \left(\frac{8\pi G \rho_0}{3} \right)^{1/2} t$

The free-fall time is when $\theta = \pi/2$, $t_{\text{ff}} = \left(\frac{3\pi}{32 G \rho_0} \right)^{\frac{1}{2}} = \frac{3.4 \times 10^7}{\sqrt{n_0}} \text{ [yr]}$

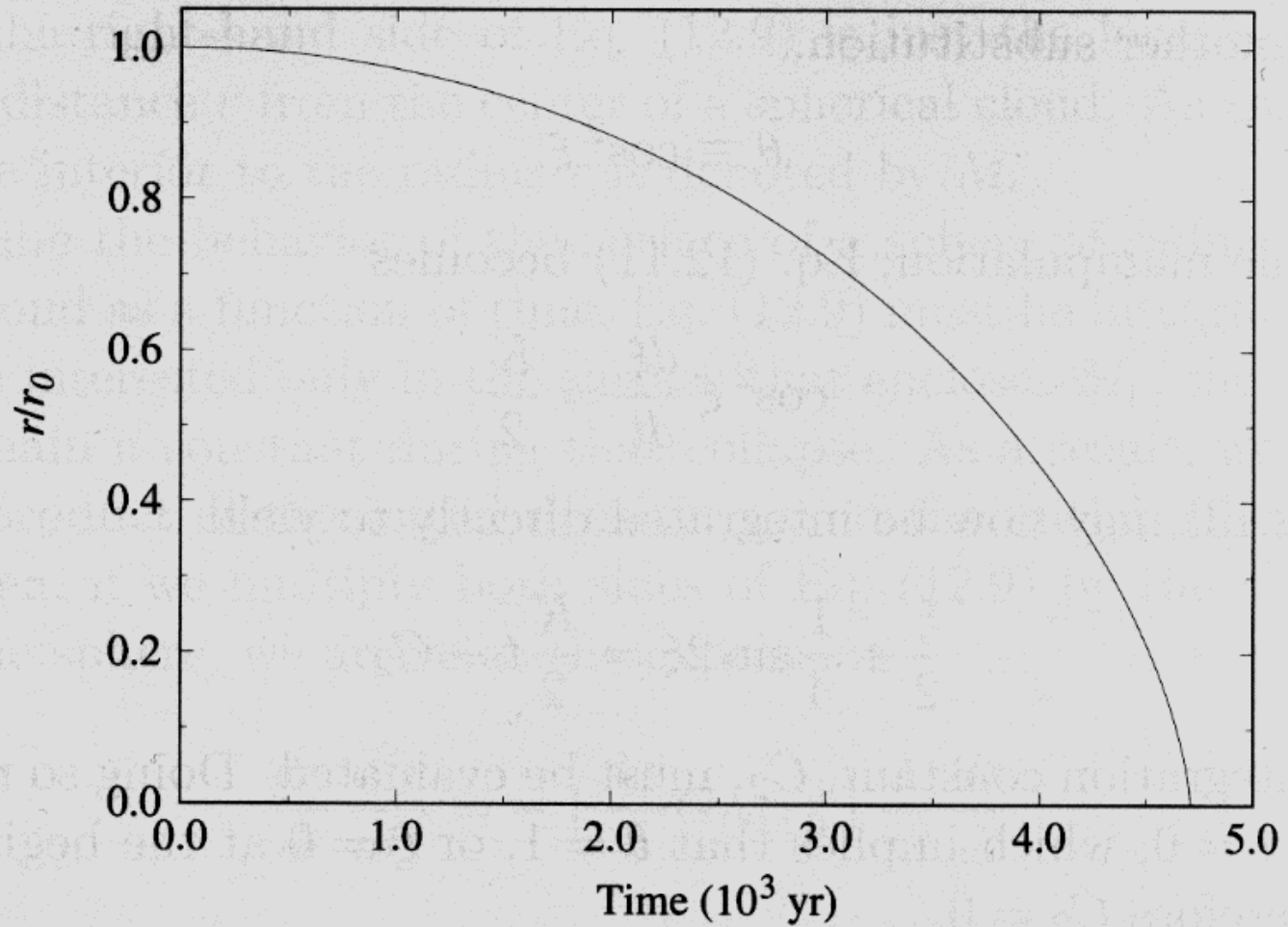


Figure 12.5 The ratio of the radius relative to its initial value as a function of time for the homologous collapse of a molecular cloud. The collapse is assumed to be isothermal, beginning with a density of $\rho_0 = 2 \times 10^{-16} \text{ g cm}^{-3}$.

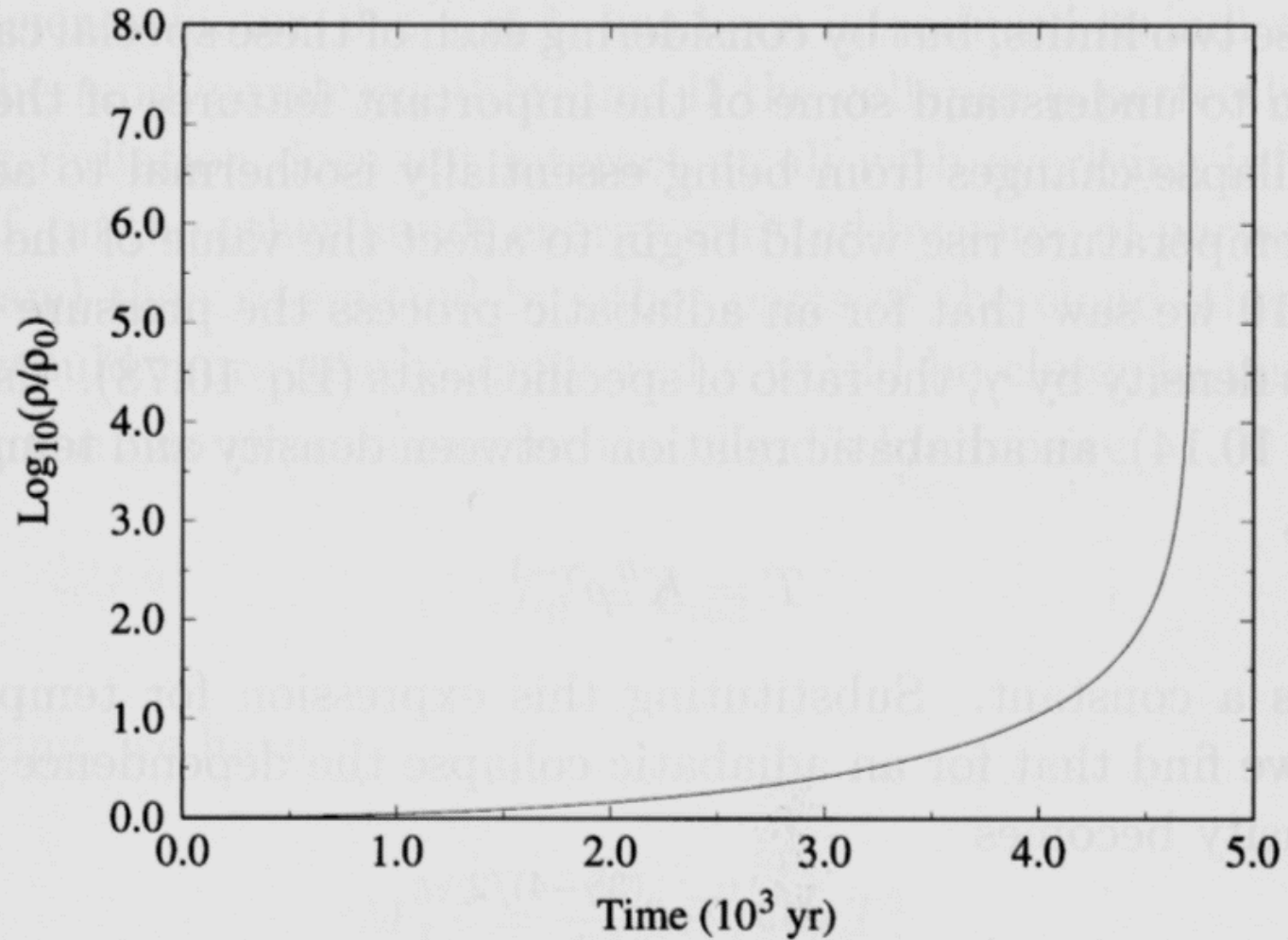


Figure 12.6 The ratio of the cloud's density relative to its initial value as a function of time for the isothermal, homologous collapse of a molecular cloud with an initial density of $\rho_0 = 2 \times 10^{-16} \text{ g cm}^{-3}$.

Note that $t_{\text{ff}} \propto \frac{1}{\sqrt{G\rho_0}}$ has no dependence on r_0 .

If ρ_0 is uniform, all m collapse to the center at the same time

→ **homologous collapse**

If ρ_0 is somewhat centrally condensed, as observed,

e.g., $\rho_0 \propto r^{-1}$ to r^{-2} , inner region (small r), $t_{\text{ff}} \downarrow\downarrow$

→ **inside-out collapse**

Gravitational energy available $E_G \sim \frac{GM^2}{R}$
 which is released during the contraction
 of mass M from ∞ to R

$$\tau_{KH} \sim \frac{GM^2}{R} / L \sim R^{-3} \quad (\because L \sim R^2 T^4)$$

const

$$\tau_{ff} \sim \frac{1}{\sqrt{G\rho}} \sim R^{3/2}$$

For an object already on the main sequence

$$\tau_{ff} \ll \tau_{KH}$$

Ex. For $1 M_{\odot}$, $1 L_{\odot}$ $\tau_{ff} \sim 10^4 \text{ yr}$
 $\tau_{KH} \sim 2 \times 10^7 \text{ yr}$

$$\tau_{ff} \ll \tau_{KH}$$

\therefore When $R \gtrsim 300 R_{\odot}$ $\tau_{ff} \gtrsim \tau_{KH}$

\Rightarrow protostellar collapse is a dynamical process.

$$\tau_{ff} \sim 66120 / \sqrt{\rho}_{\text{MKS}} \sim 35 / \sqrt{\rho}_{\text{cgs}} [\text{min}]$$

Free-Fall Collapse



$$m \frac{d^2 r}{dt^2} = \frac{GMm}{r^2}$$

Dimension analysis

$$\frac{R}{t^2} \sim \frac{GM}{R^2} \Rightarrow \boxed{t_{ff} \sim \frac{1}{\sqrt{G\rho}}} \approx \frac{4.3 \times 10^7 \text{ [yrs]}}{\sqrt{n_{H_0}}}$$

or

$$2 E_K + E_p = \dots < 0$$

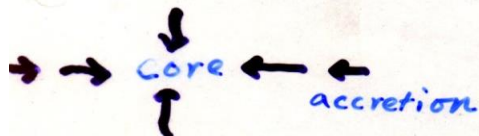
$$t_s = \frac{R}{v_{\text{sound}}} \sim \frac{1}{\sqrt{G\rho}}, \quad v_s \sim \sqrt{\frac{RT}{\mu}}$$

e.g. $\rho \sim 10^3 \times 1.6 \times 10^{-24}$, $t_{ff} \sim \frac{1}{\sqrt{6.6 \times 10^{-8} \times 10^{-21}}} \sim 10^{14} \text{ s}$
 $\sim 3 \times 10^6 \text{ yr}$

In reality, $\rho \uparrow$ as $r \downarrow$ (i.e., density concentration
e.g. $\rho \sim r^{-1.5}$)

$\therefore t_{ff}$ shorter for smaller r

\Rightarrow Collapse proceeds in an inside-out fashion.



$$\boxed{L_{\text{acc}} \sim GM_* \dot{M}_{\text{acc}} / R_*}$$

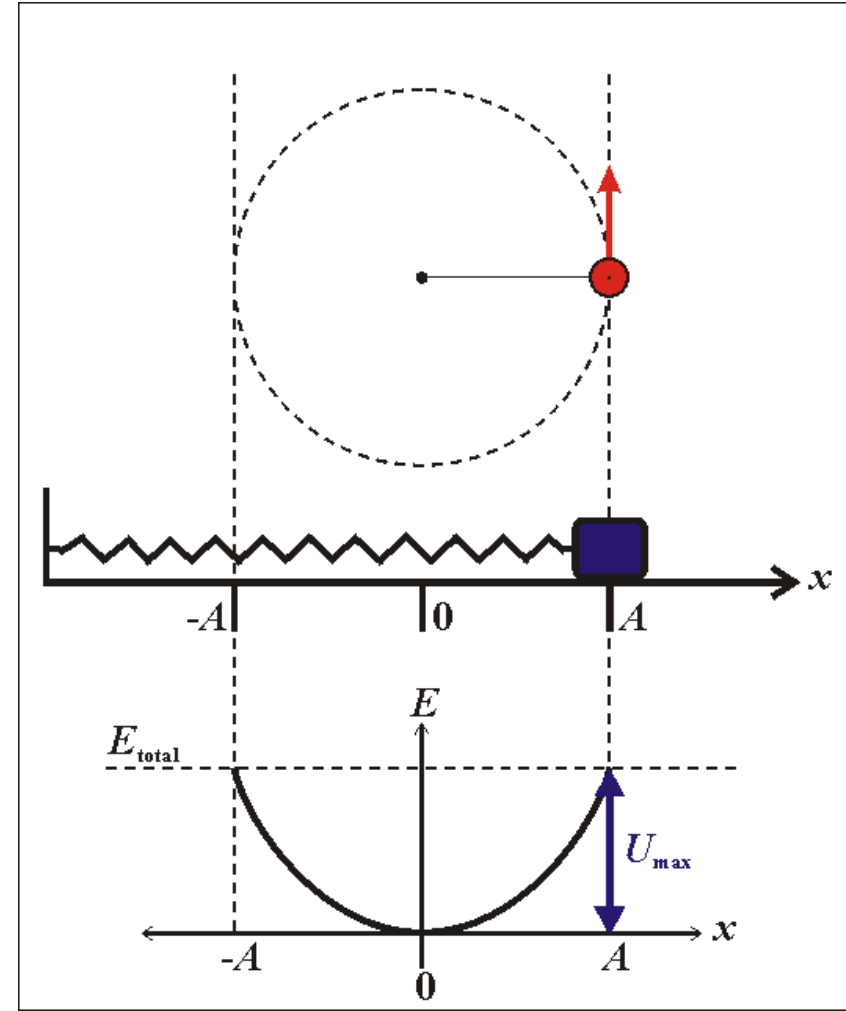
Recall the relation between **a circular motion** and **a simple harmonic motion**.

Acceleration to the center

Time scale = $\frac{1}{4}$ period

Applications:

- Gas in a collapsing cloud
- Stars in a globular cluster
- Galaxies in a galaxy cluster



Exercise

1. For a the sun, i.e., a mass $\mathcal{M} = 1 \mathcal{M}_{\odot}$, a luminosity $\mathcal{L} = 1 \mathcal{L}_{\odot}$, and a radius $\mathcal{R} = 1 \mathcal{R}_{\odot}$, compute the free-fall time scale τ_{ff} and the Kelvin-Helmholtz time scale $\tau_{\text{KH}} \approx G\mathcal{M}^2 / RL$. Which time scale is longer?
2. Note that both time scales have different dependence on the size scale. At what size, do the two time scales equal?

STAR FORMATION IN MOLECULAR CLOUDS: OBSERVATION AND THEORY

Frank H. Shu, Fred C. Adams, and Susana Lizano

Astronomy Department, University of California, Berkeley,
California 94720

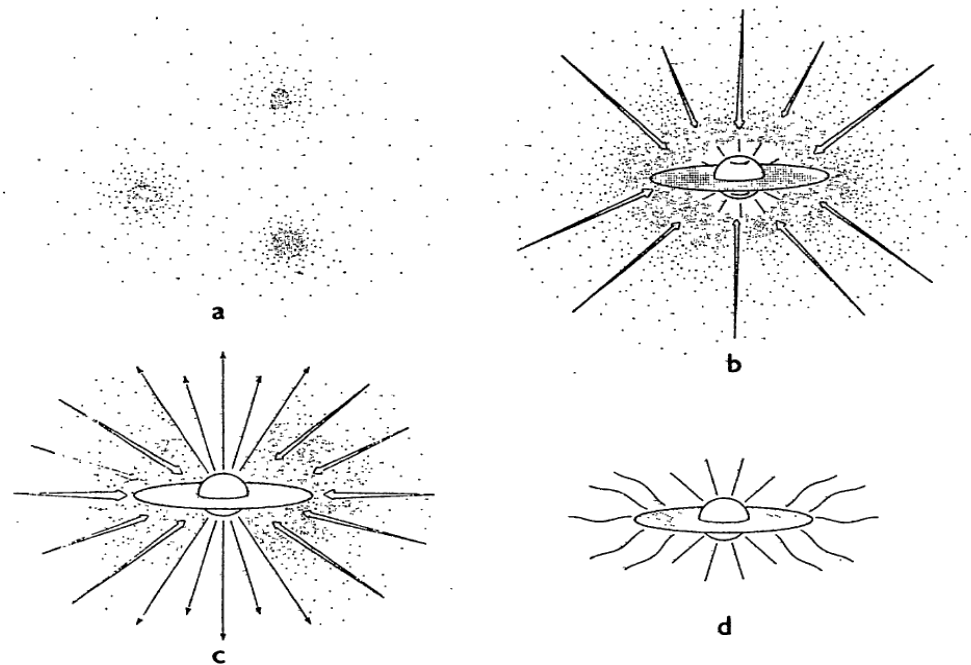


Figure 7 The four stages of star formation. (a) Cores form within molecular clouds as magnetic and turbulent support is lost through ambipolar diffusion. (b) A protostar with a surrounding nebular disk forms at the center of a cloud core collapsing from inside-out. (c) A stellar wind breaks out along the rotational axis of the system, creating a bipolar flow. (d) The infall terminates, revealing a newly formed star with a circumstellar disk.

A TWO MICRON POLARIZATION SURVEY OF T TAURI STARS

MOTOHIDE TAMURA^{a)}

Department of Physics, Kyoto University, Sakyo-ku, Kyoto 606, Japan

and

Department of Astronomy, University of Massachusetts, Amherst, Massachusetts 01003

SHUJI SATO

National Astronomical Observatory, Mitaka, Tokyo 181, Japan

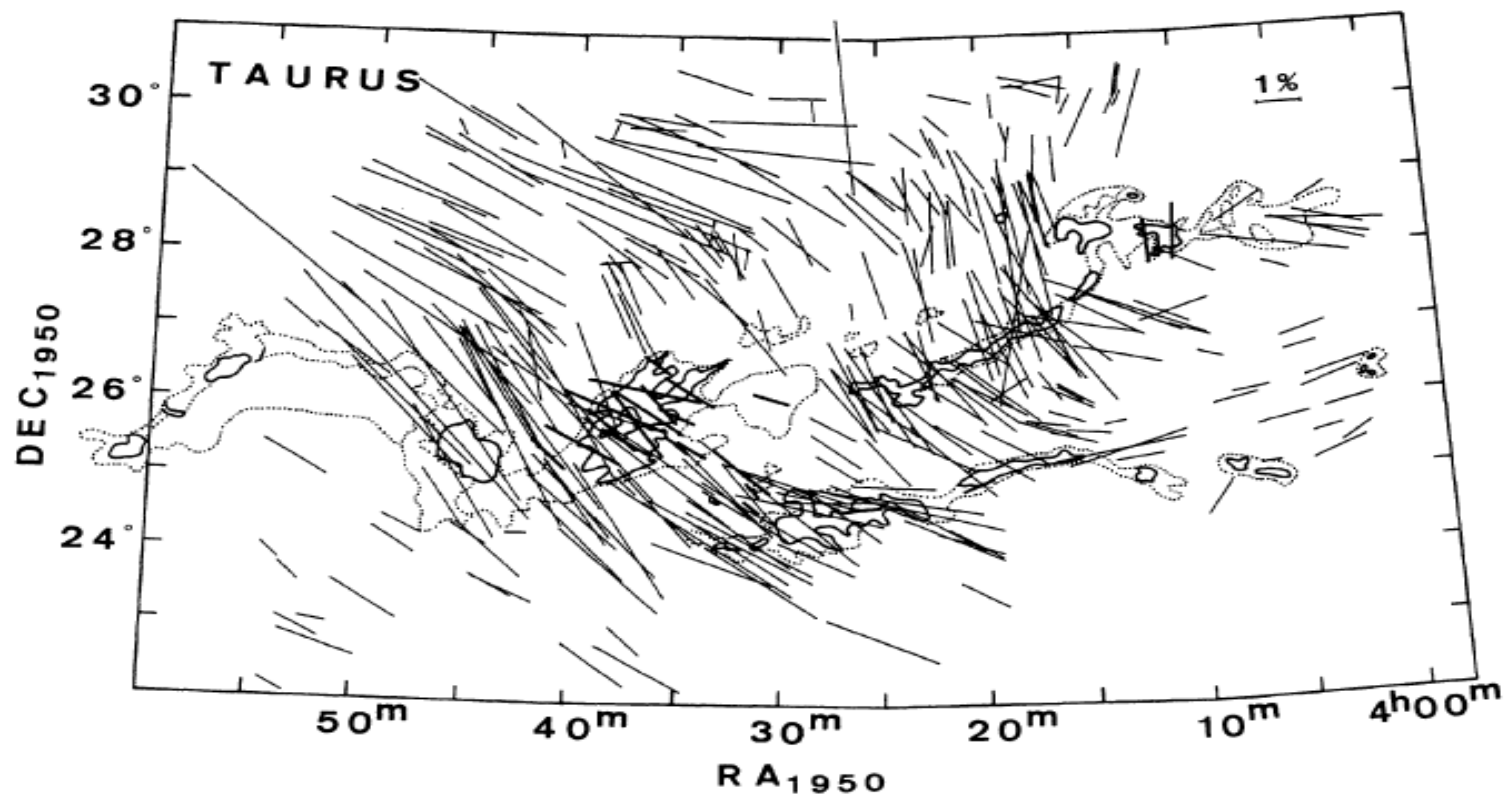
Received 30 September 1988; revised 23 May 1989

FIG. 2. Polarization map at optical (thin vectors) and at infrared (thick vectors) towards background stars in the Taurus dark cloud complex, compiled from the data in the literature (Moneti *et al.* 1984; Hsu 1984; Heyer *et al.* 1987; Tamura *et al.* 1987).

Evolution from a circumstellar toroid (geometrically thick) to a disk; opening angle of the outflow widened

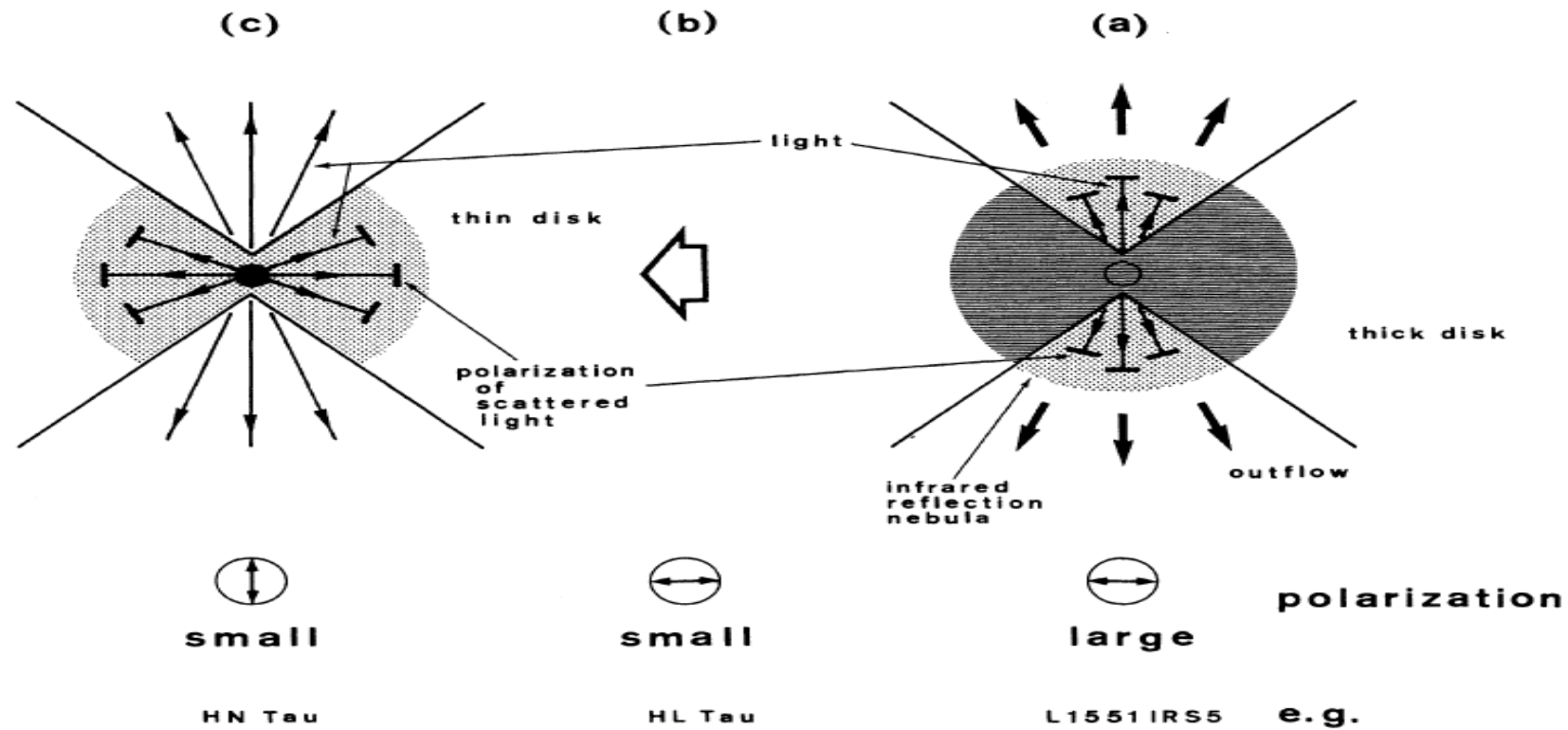


FIG. 10. Model of infrared polarization of (a) young stellar objects with mass outflows, (b) T Tauri stars with extreme mass-outflow phenomena, and (c) T Tauri stars without extreme mass outflow.

OBSERVATIONS OF CO IN L1551: EVIDENCE FOR STELLAR WIND DRIVEN SHOCKS

RONALD L. SNELL

Astronomy Department and Electrical Engineering Research Laboratory, University of Texas at Austin; and
Five College Radio Astronomy Observatory, University of Massachusetts at Amherst

ROBERT B. LOREN

Electrical Engineering Research Laboratory and McDonald Observatory, University of Texas at Austin

RICHARD L. PLAMBECK

Radio Astronomy Laboratory, University of California at Berkeley

ABSTRACT

CO observations reveal the presence of a remarkable, double-lobed structure in the molecular cloud L1551. The two lobes extend for ~ 0.5 pc in opposite directions from an infrared source buried within the cloud; one lobe is associated with the Herbig-Haro objects HH28, HH29, and HH102. We suggest that the CO emission in the double-lobed structure arises from a dense shell of material which has been swept up by a strong stellar wind from the infrared source. This wind has a velocity of ~ 200 km s $^{-1}$, and evidently is channeled into two oppositely directed streams. The CO observations indicate that the shell has a velocity of ~ 15 km s $^{-1}$, a mass of $0.3 M_{\odot}$, and a kinetic temperature of 8–35 K. Its age is roughly 3×10^4 years. A stellar mass-loss rate of $\sim 8 \times 10^{-7} M_{\odot} \text{ yr}^{-1}$ would be sufficient to create such a shell.

Data cube (sky position and frequency)

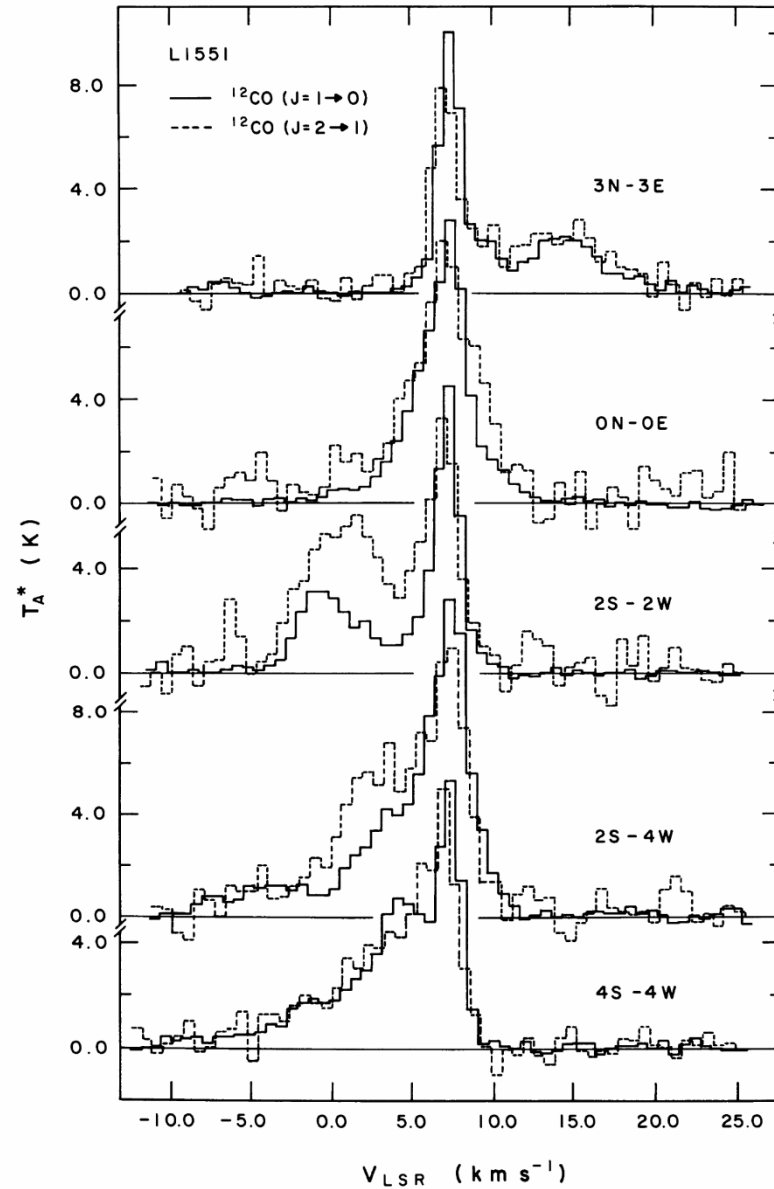
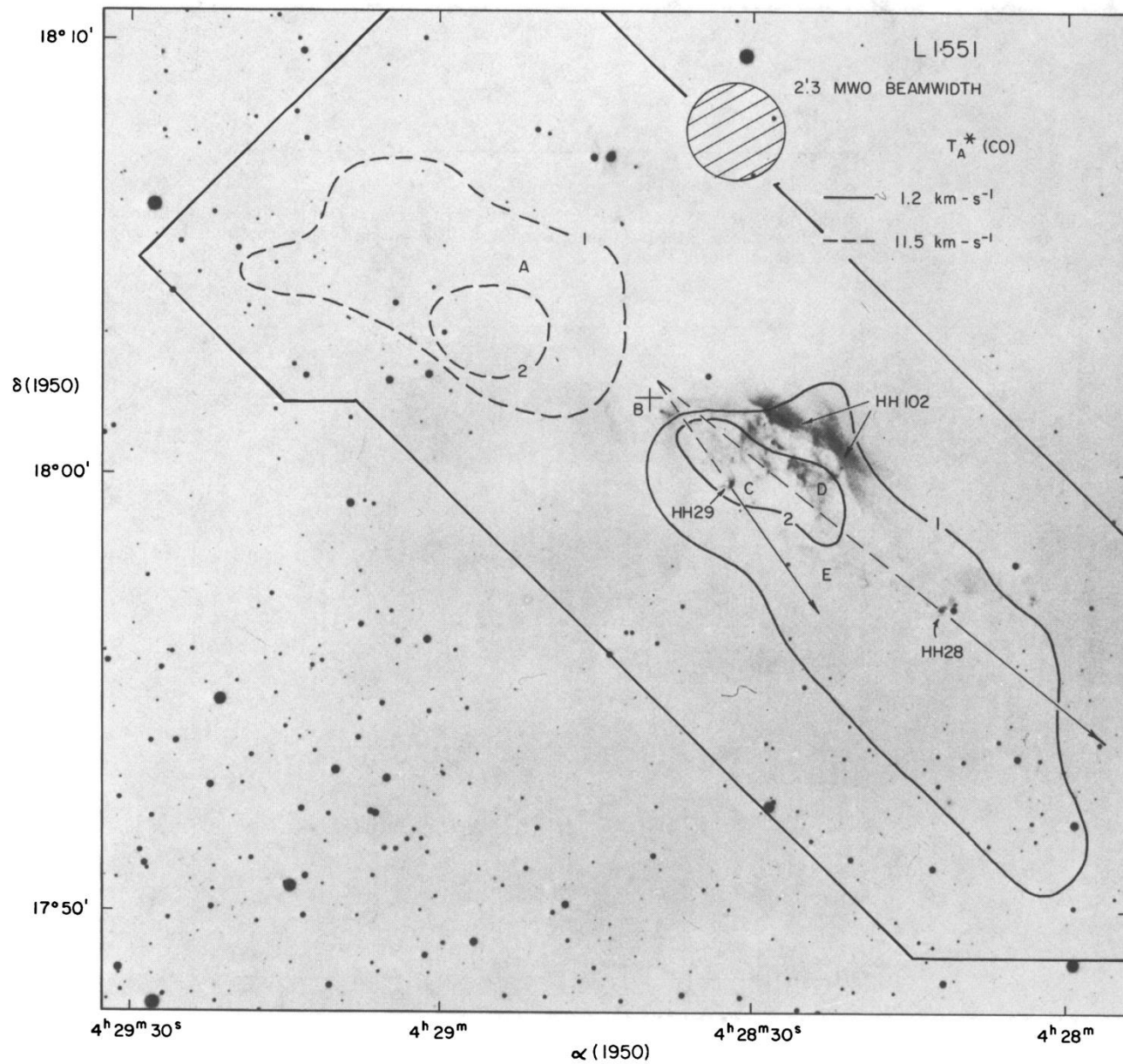


FIG. 1.—Spectra of the $J = 1-0$ (solid) and $J = 2-1$ (dashed) lines of ^{12}CO taken toward five selected positions in L1551. Offsets are measured in arcmin relative to the position of IRS-5 at $\alpha(1950) = 04^{\text{h}}28^{\text{m}}40^{\text{s}}$, $\delta(1950) = 18^{\circ}01'52''$. The $J = 1-0$ spectra were taken at NRAO with a $1'.1$ beam; the $J = 2-1$ spectra were taken at the MWO with a $1'.2$ beam. The ratio of the 2-1 and 1-0 antenna temperatures in the broad velocity features can be used to infer the kinetic temperature of the gas responsible for these features.



Snell et al. (1980)

FIG. 2.—Contour map of the $J = 1-0$ ^{12}CO antenna temperatures in the broad velocity components, superposed on an optical photo of the region taken by Strom with the 4 m telescope at KPNO. The map is based on CO spectra taken at 115 positions within the enclosed border with $1''-2''$ spacings. A cross indicates the position of IRS-5; letters A-E indicate the positions of the five spectra in Fig. 1 from top to bottom. Also shown are the directions of the proper motions of the two compact Herbig-Haro objects, HH 28 and HH 29; tracing their motion backward suggests a common origin at the infrared source.

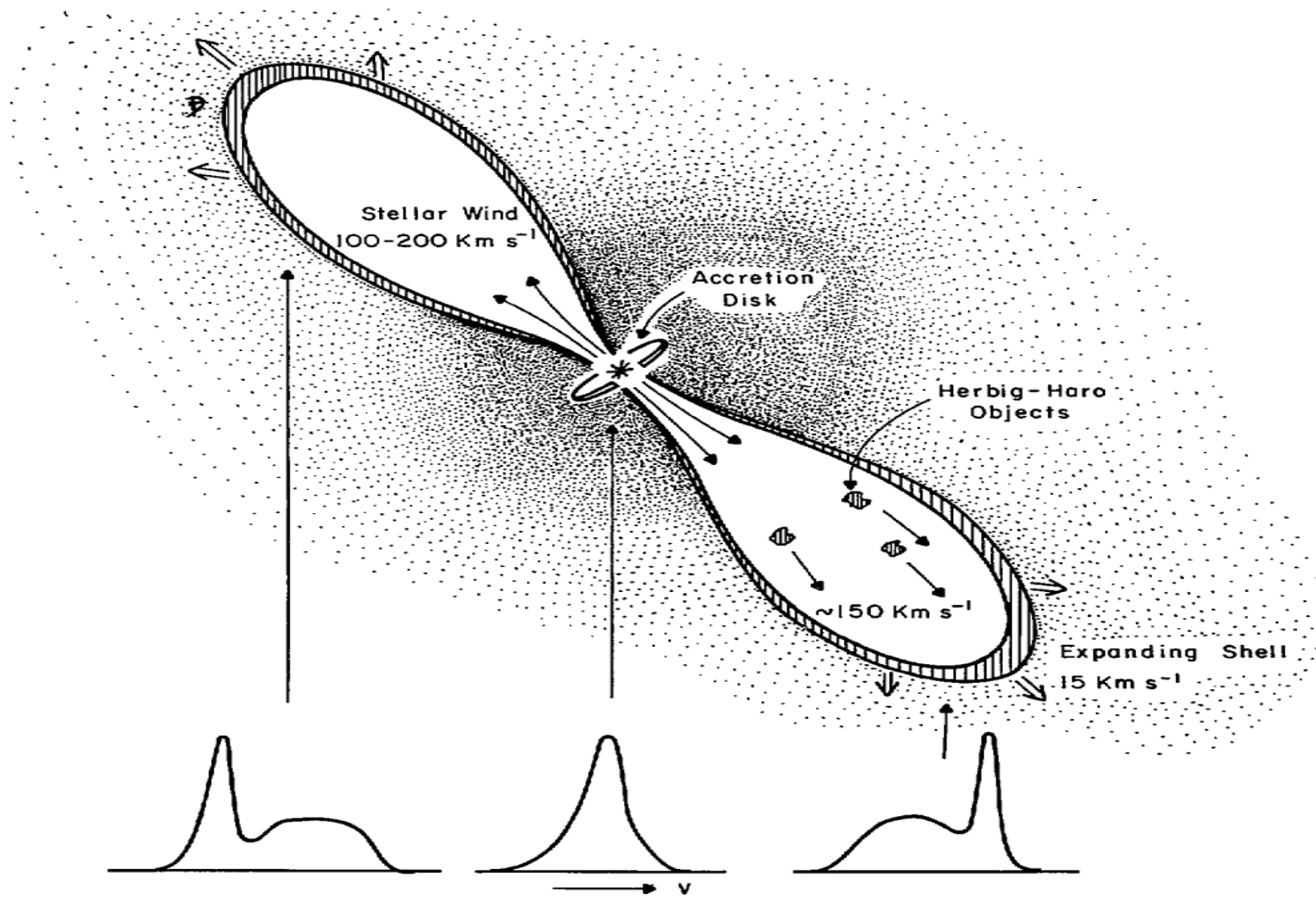


FIG. 5.—A schematic picture of the stellar wind driven shock model for L1551, indicating the CO line profiles which would be expected at different positions across the source. The Herbig-Haro objects are not necessarily located inside the shell; because of their high velocities, they may have been ejected through the shell and into the surrounding medium.

Snell et al. (1980)

BIPOLAR MOLECULAR OUTFLOWS FROM YOUNG STARS AND PROTOSTARS

Rafael Bachiller

Observatorio Astronómico Nacional (IGN), Campus Universitario, Apartado 1143, E-28800 Alcalá de Henares (Madrid), Spain

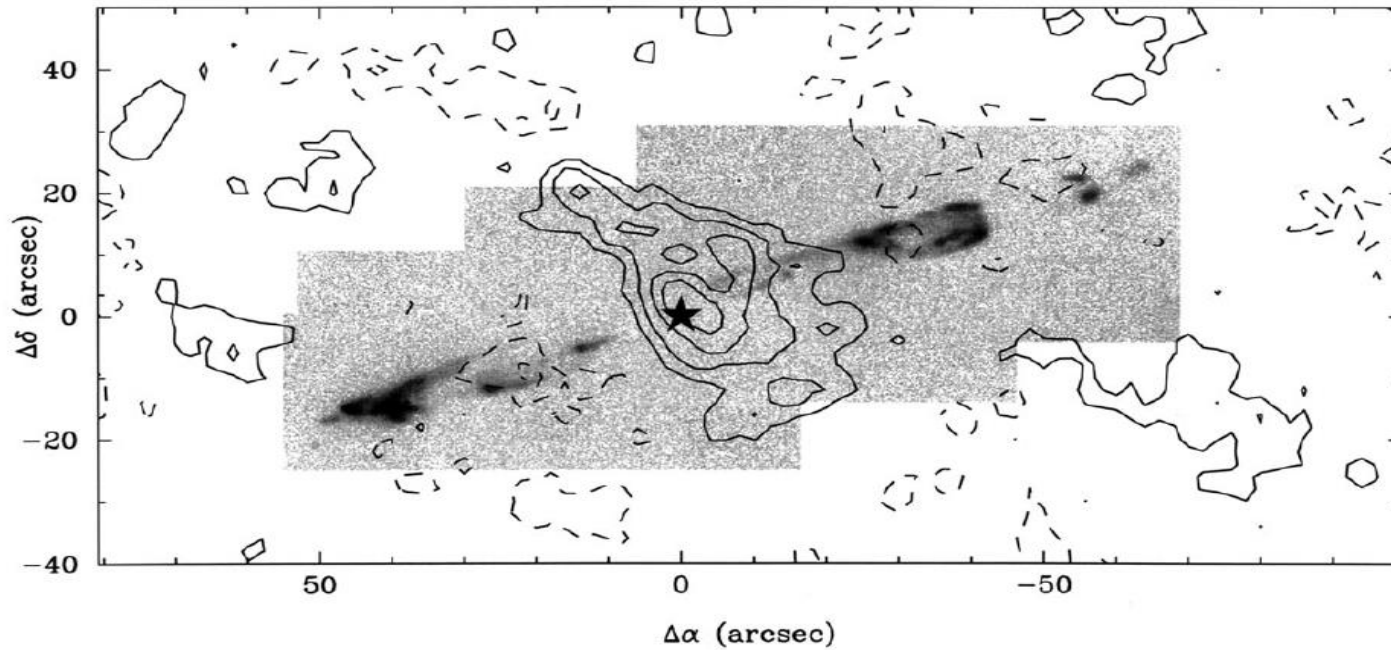
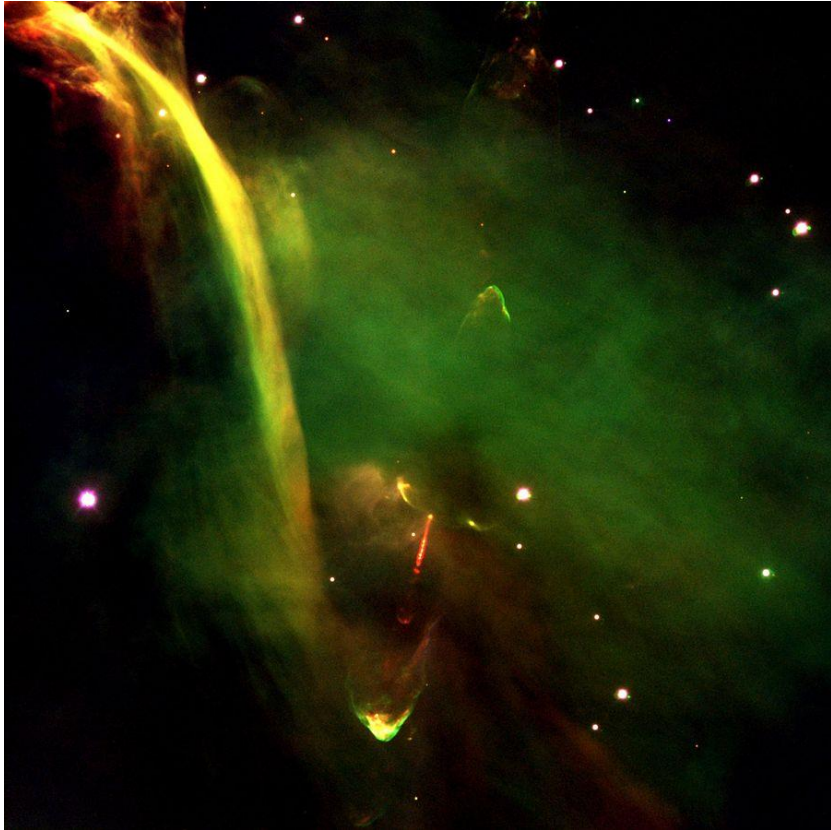


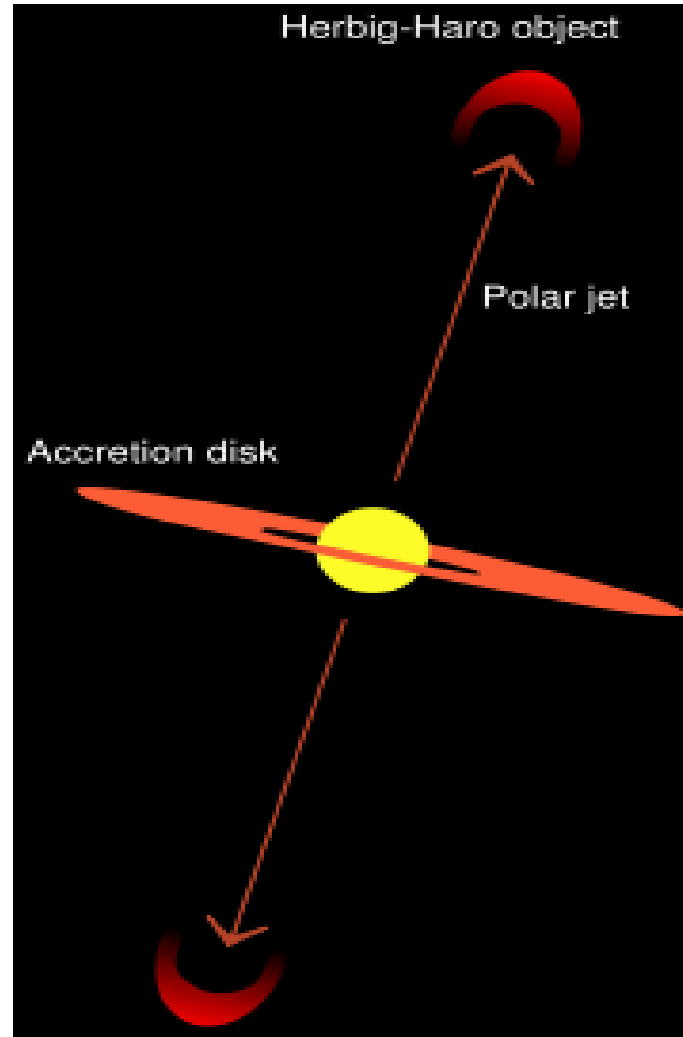
Figure 4 Superposition of a gray-scaled image of the HH 211 jet taken in the H₂ $v = 1-0$ S(1) line at 2.122 μm (from McCaughrean et al 1994) with a NH₃ (1,1) image obtained with the VLA at its D configuration (6'' angular resolution) (R Bachiller & M Tafalla 1995, unpublished data). The star marks the position of the jet source HH 211-mm (see also Table 1).

Herbig-Haro (HH) Objects

-- (shock) *excited nebulosity*



HH 34



HH 47 91

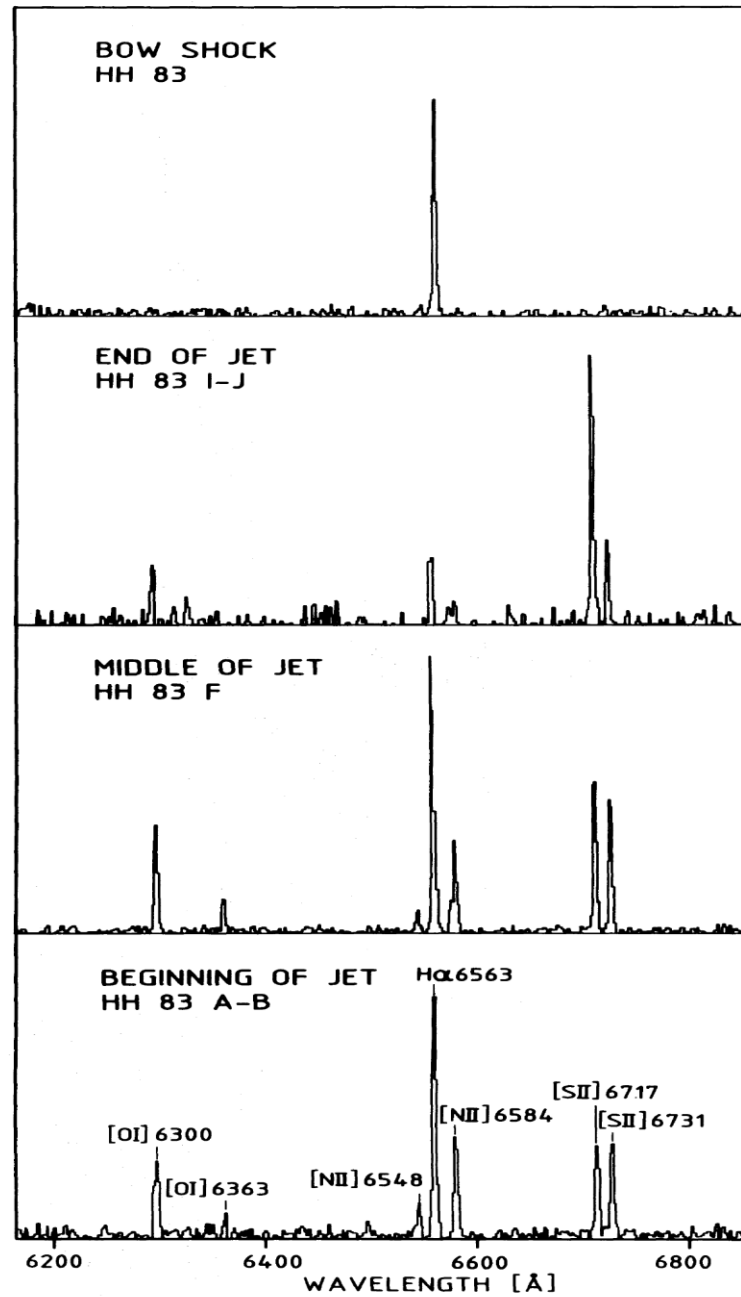


Fig. 5. Spectra of knots A-B, F, I-J in the HH 83 jet and of the bow shock in the wavelength range approx. 6200 Å to 6800 Å. Note the increasing [S II] 6717/H α ratio as one moves out along the jet, as well as the changing sulphur line ratio, indicating decreasing electron density. The bow shock is pure H α emission

Reipurth (1989)

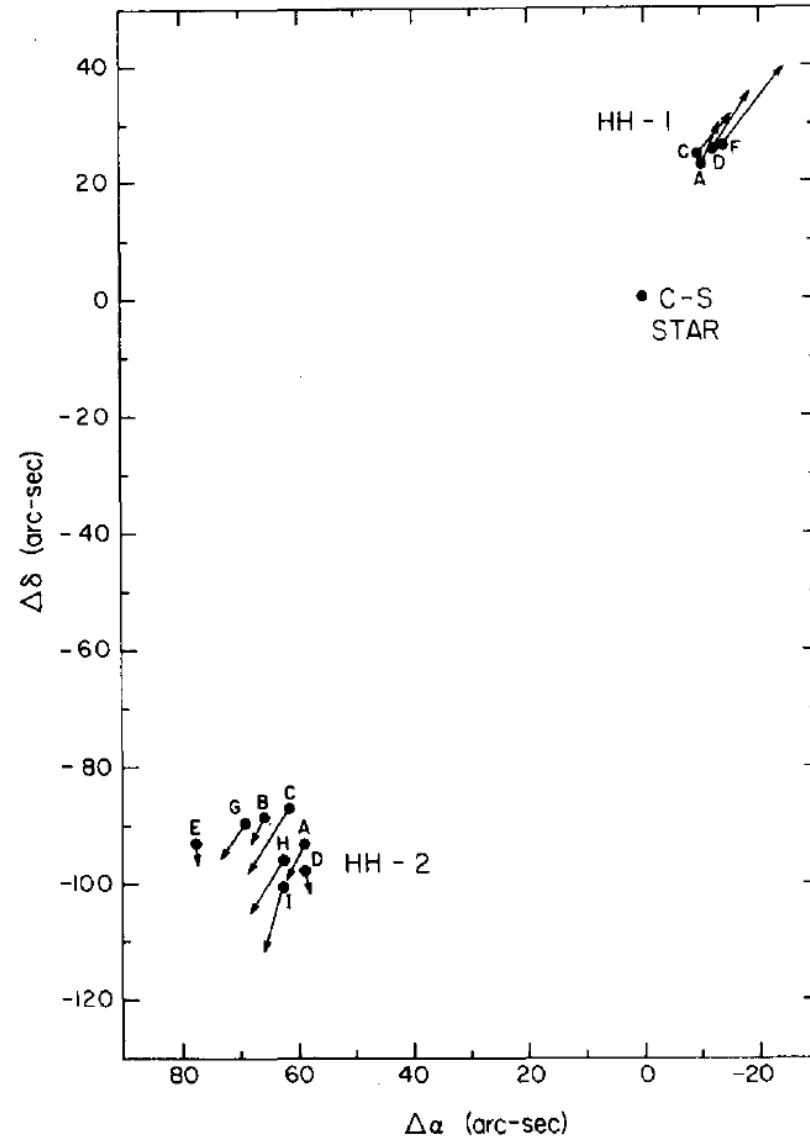


Fig. 39. Proper motions for individual knots of HH1, 2 and the Cohen-Schwartz star [161].

Molecular Hydrogen Objects (MHOs) 1000+ now known



Infrared image of molecular bow shocks (MHO 27) associated with bipolar outflows in Orion. Credit: UKIRT/Joint Astronomy Centre

Spectral Energy Distribution

Optical depth

$\tau \sim 1$ at $100 \mu\text{m}$

~ 0.01 at 1 mm

$\tau > 100$ at $1 \mu\text{m}$

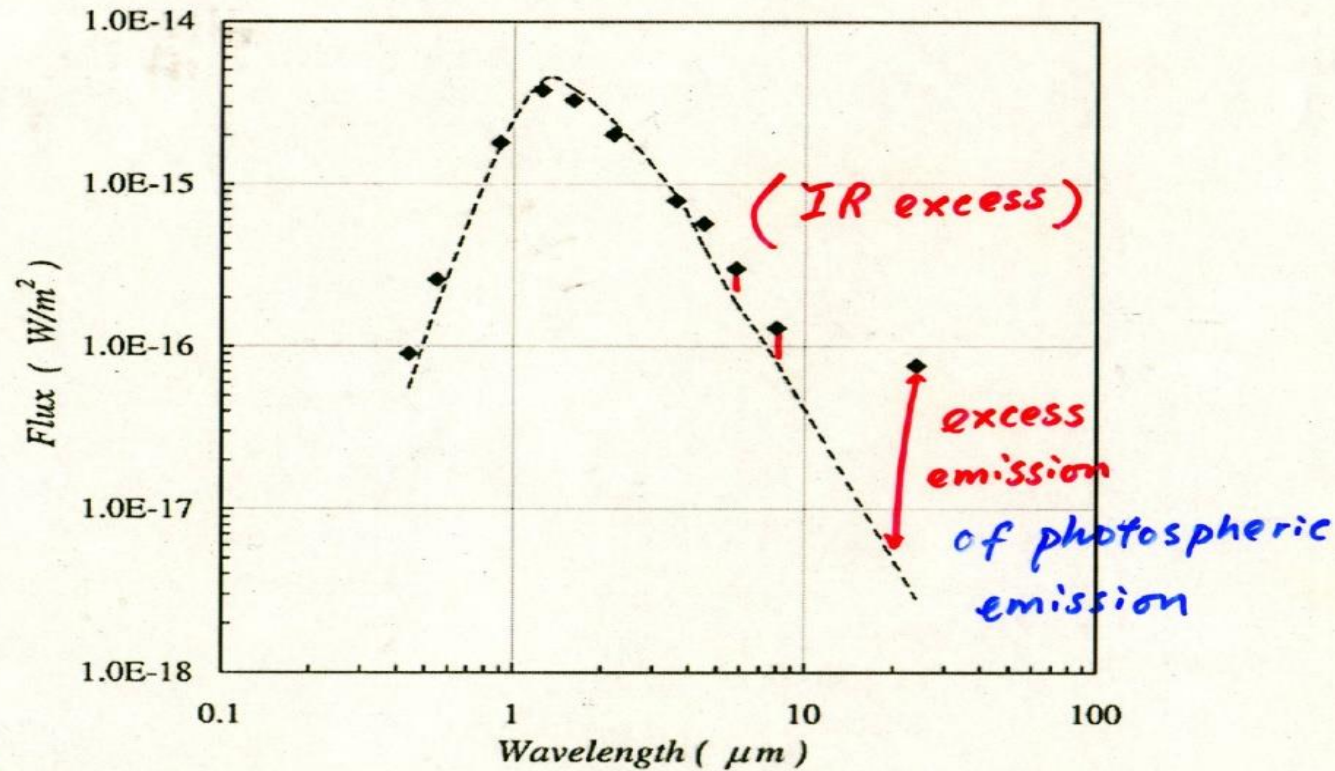
Obs. at mm

→ total dust mass

⇒ $A_V \gtrsim 300$!

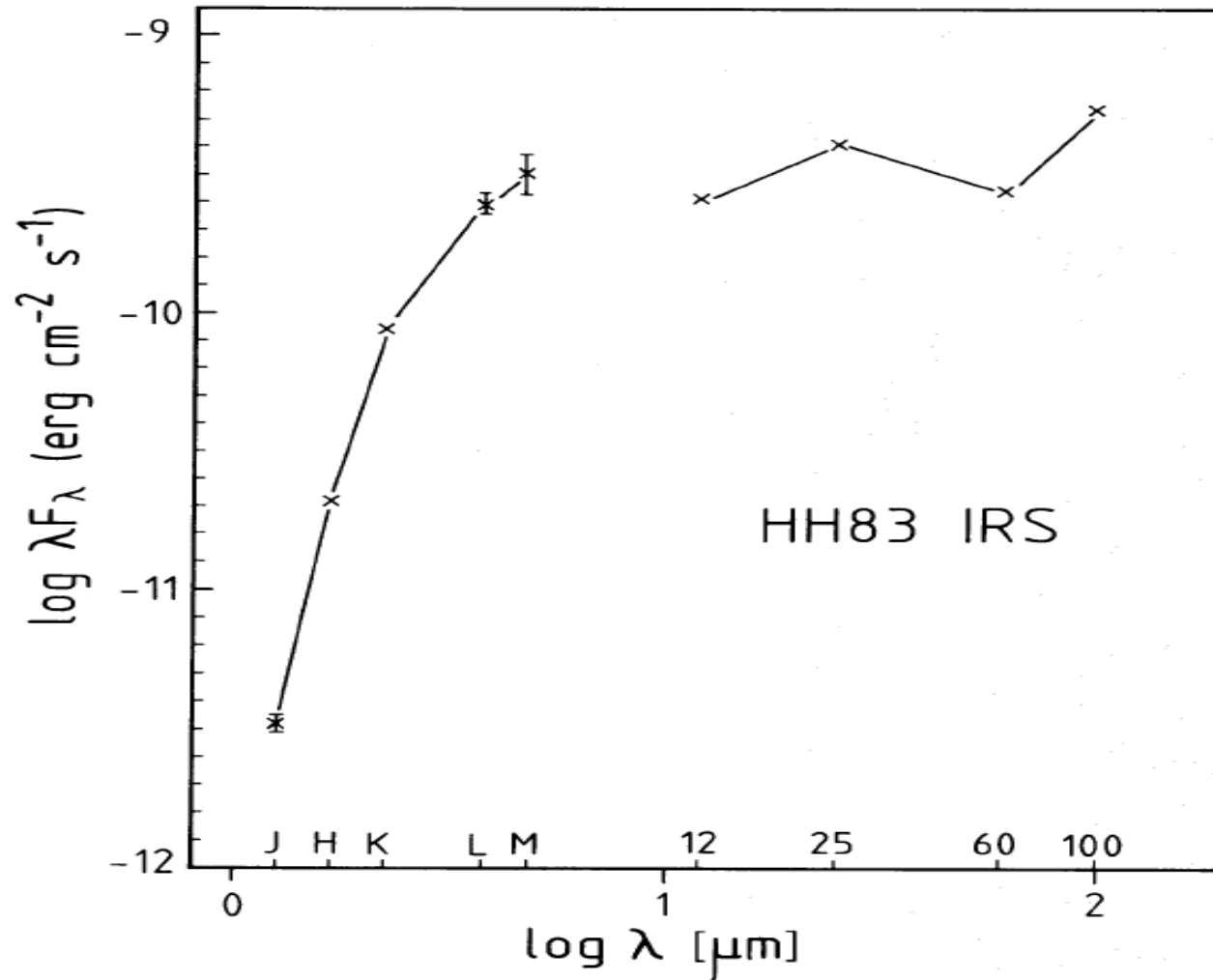
i.e. Star should be invisible

But obs'd $A_V \sim 3$



SED for 2MASS 08093547-4913033, with that of an M5 star (Young et al. 2004, ApJS, 154, 428)

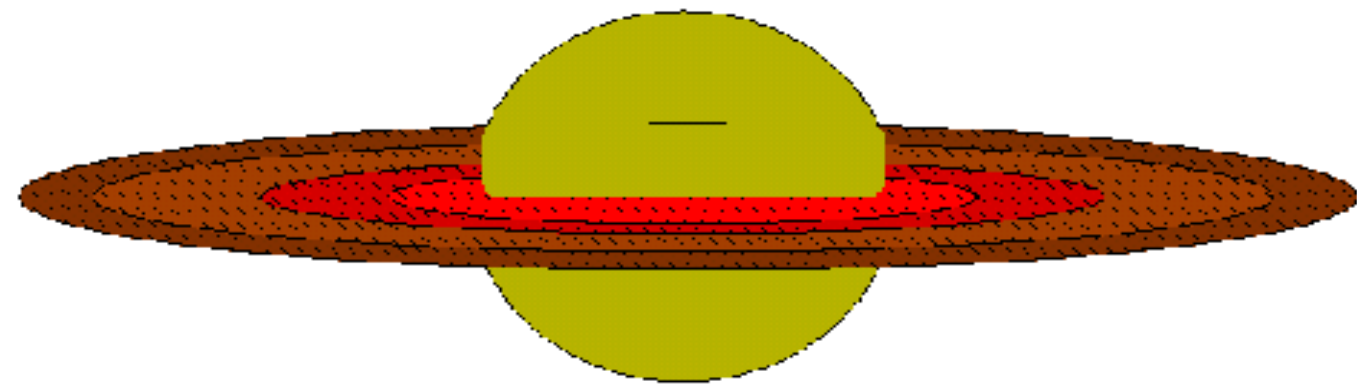
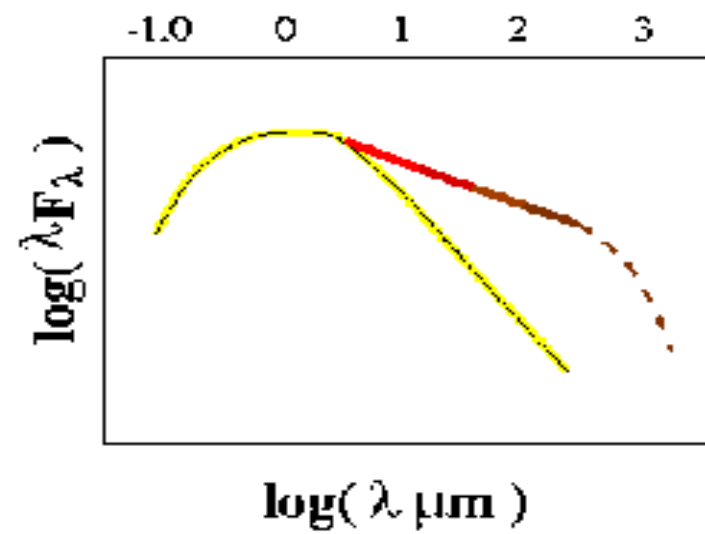
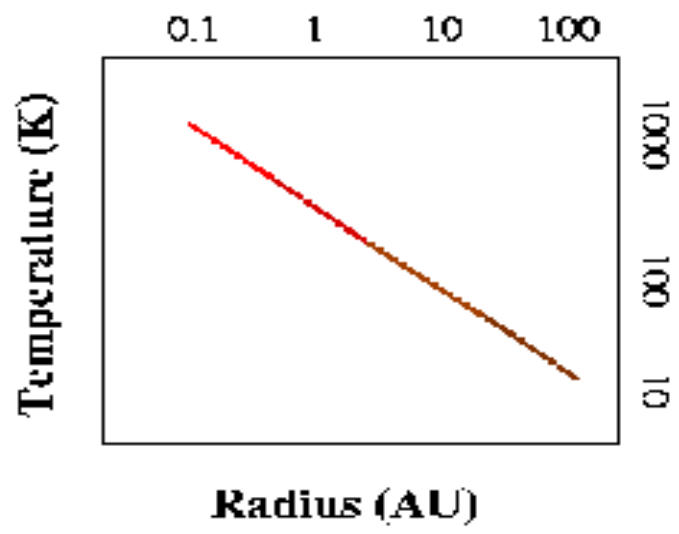
⇒ clear line-of-sight ⇒ disk or thin shell



Exciting source of an
HH object = protostar

Fig. 6. The energy distribution of the infrared source of HH 83 based on near- and far-infrared photometry. Error bars are shown for the near-infrared data points where the errors are larger than the extent of the crosses. No error bars are given for the far-infrared IRAS data

very prominent IR excess; lots of dust; a very young age



Accretion Disks

- Found in YSOs, supermassive BHs in AGB, binaries, Saturnian rings
- Turbulent viscosity important
 - generating heat
 - transporting angular momentum outwards
 - transporting matter inwards

Fact: The Sun has $> 99\%$ of the total mass in the solar system, but accounts for $\sim 3\%$ of the total angular momentum (rotation), whereas Jupiter's orbital angular moment accounts for 60% .

Fact: Outer planets rotate fast (thus are flattened.)

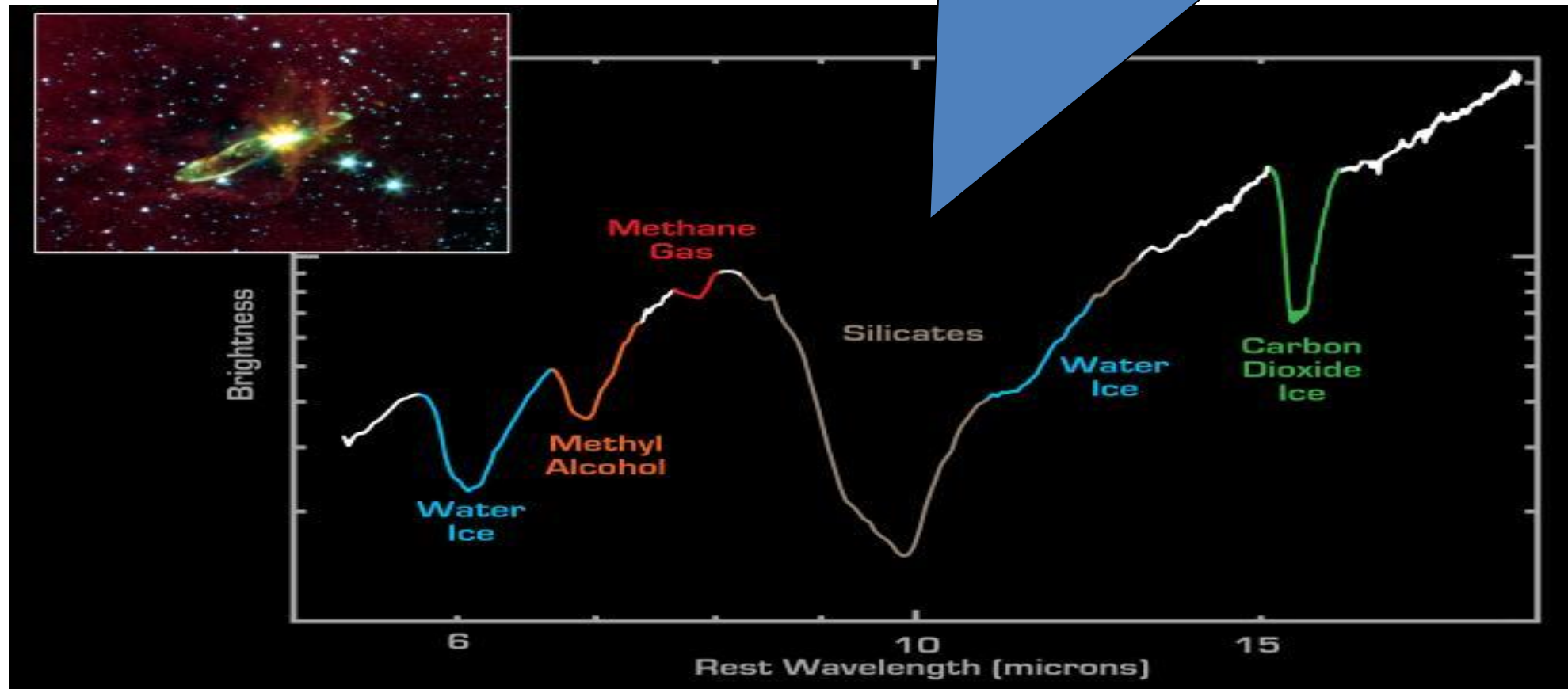
Exercise

1. Compare the angular momenta of the Sun, Jupiter, and Earth.
2. What is the specific angular momentum of the Earth versus Jupiter?
3. How round (or flat) is the shape of the Earth, of Jupiter, and of the Sun?

http://www.zipcon.net/~swhite/docs/astronomy/Angular_Momentum.html

Water and carbon dioxide in solid form
→ cold materials near the protostar

Silicate feature → thick dusty cocoon



Spitzer IRS

T Tauri stars (= PMS sun-like stars) are seen against dark nebosity and characterized by emission-line spectra.

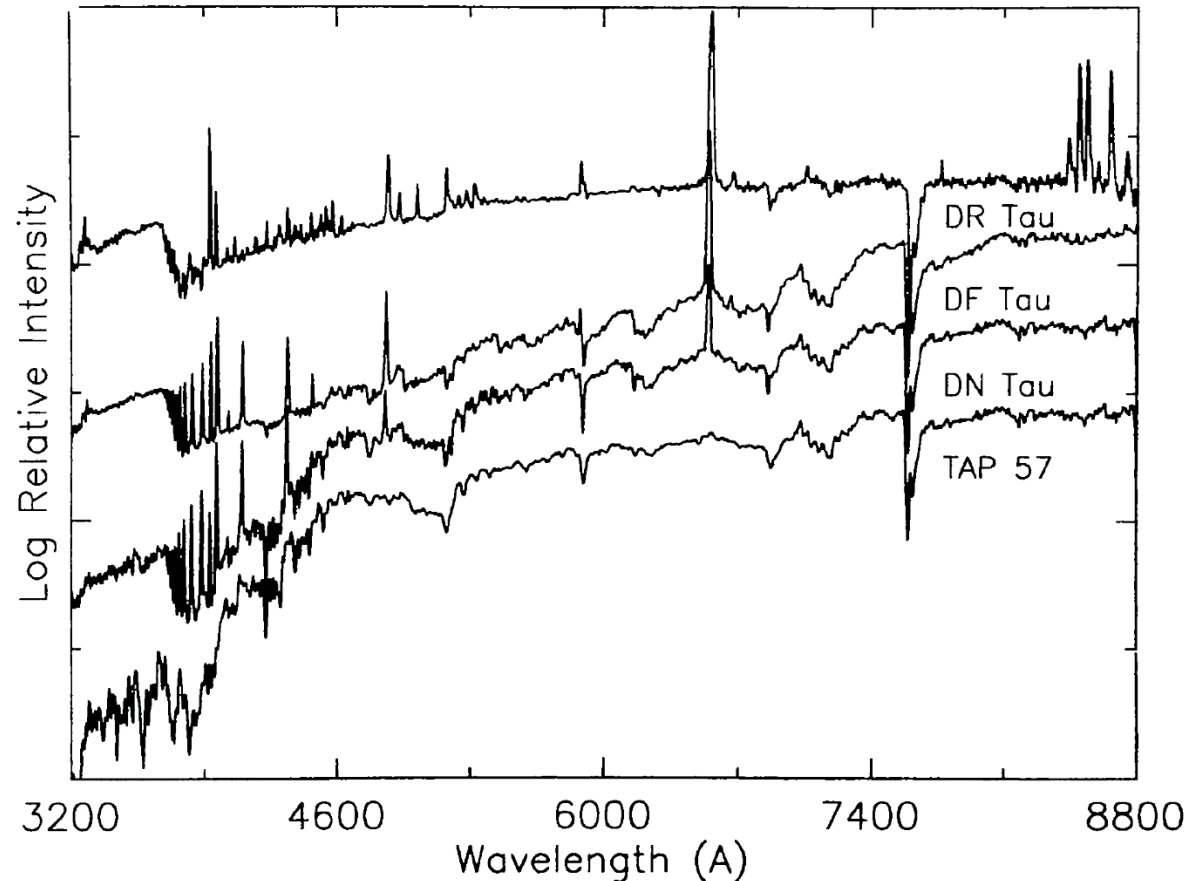


Figure 2 Medium-resolution spectrograms covering the spectral range 3200–8800 Å of four late-K or early-M T Tauri stars, shown in order of increasing emission levels. The relative intensity is displayed in wavelength units.

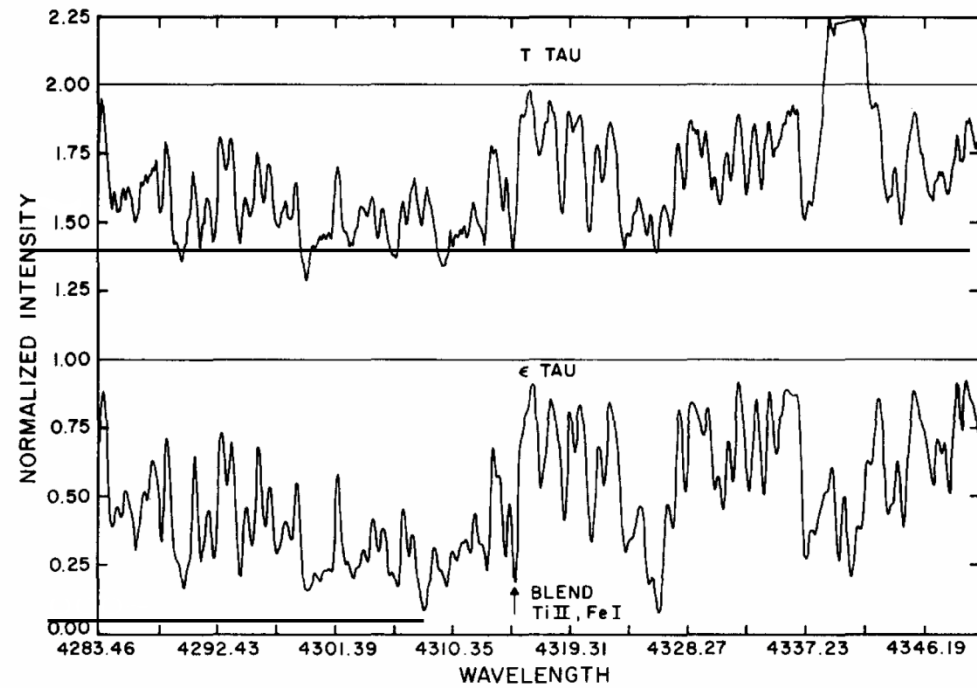


Fig. 3a. Spectrum of T Tau and of ϵ Tau, a standard star of the same temperature.

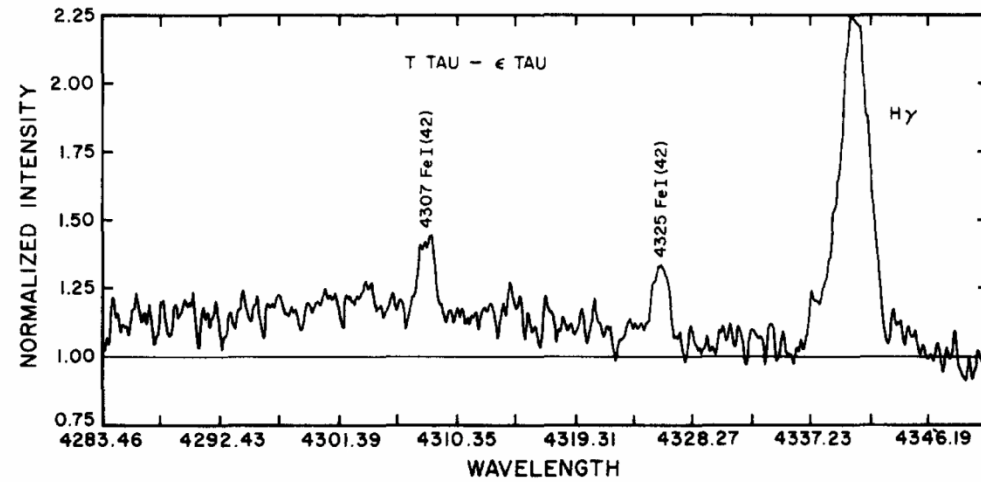
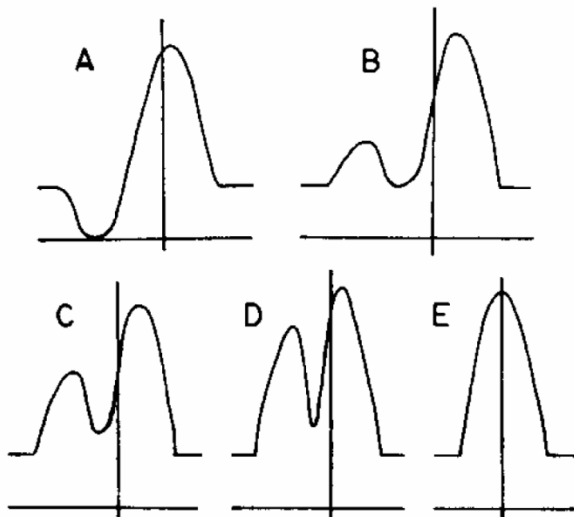
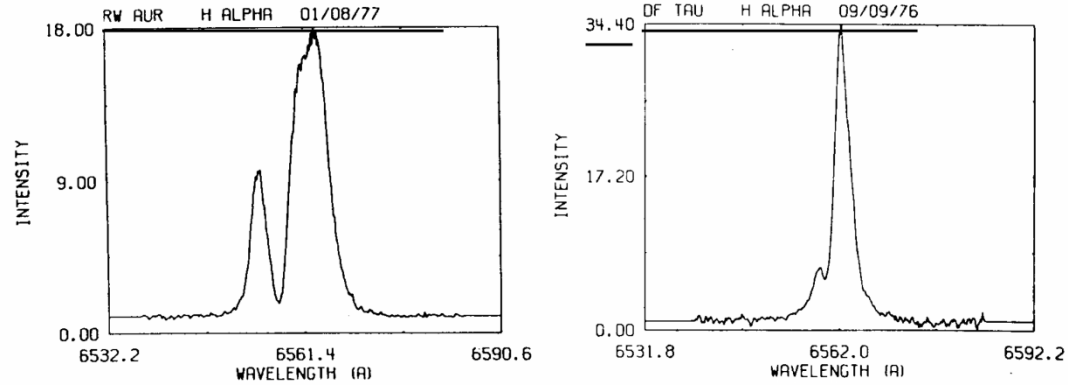
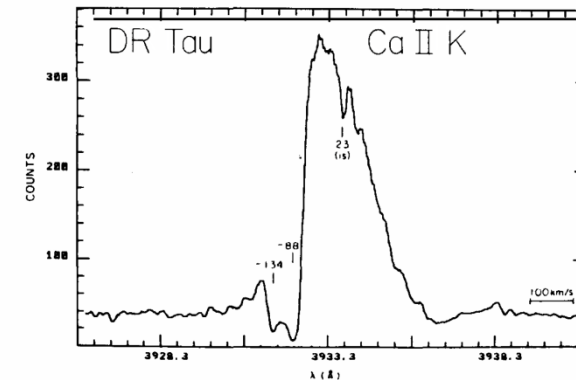
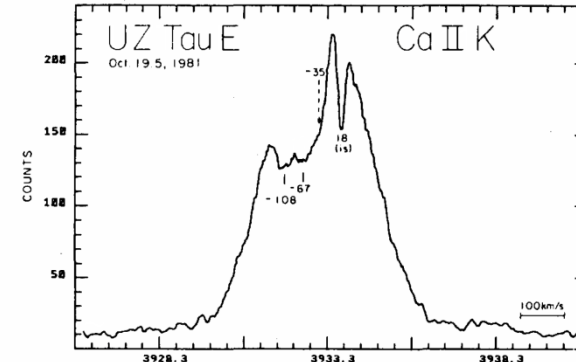
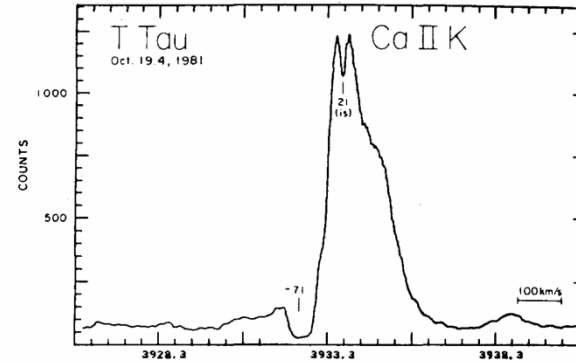


Fig. 3b. The result of subtracting the optical spectrum of a standard stellar spectrum from that of a T Tau star, suitably normalised, having the same photospheric temperature. Note the set of discrete emission lines in the T Tau spectrum. (From [17].)

P Cygni profile → A spectral profile showing an expanding envelope



Stellar velocity



T Tauri stars also show infrared excess in the SEDs.

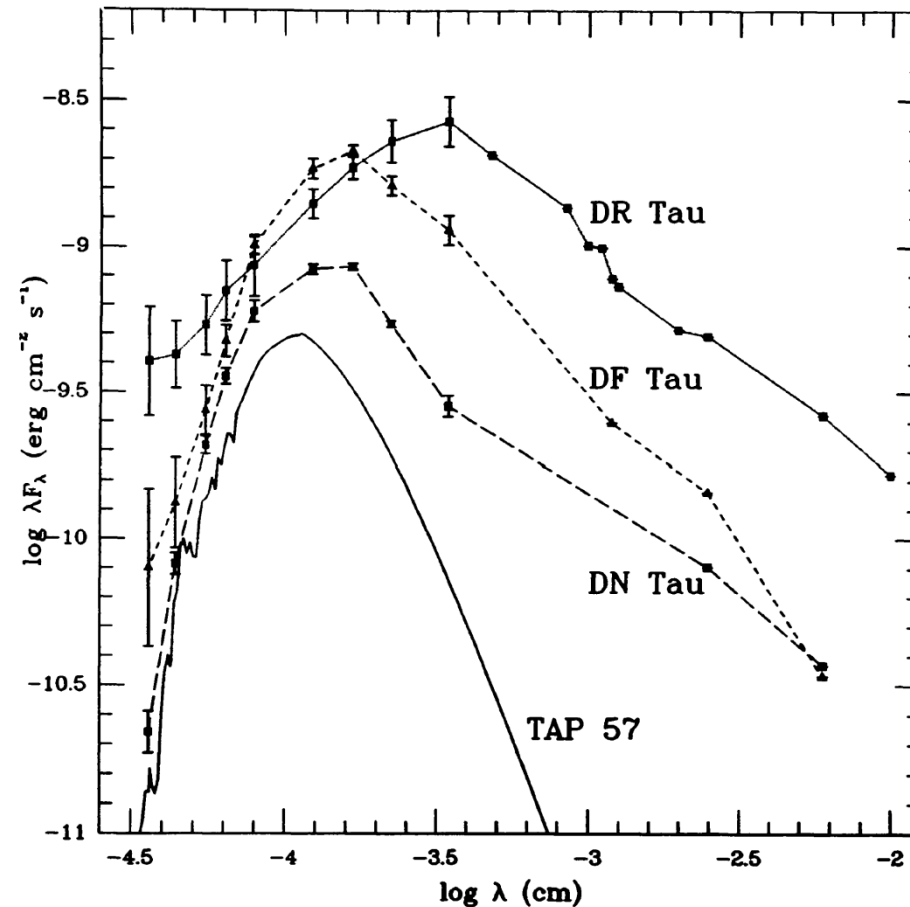


Figure 3 Observed spectral energy distributions from 3600 Å to 100 μm of the stars whose spectra are shown in Figure 2. The energy distribution of the K7V WTTS TAP 57, shown as a solid line, has been displaced downward by 0.3 dex. The filled symbols are simultaneous (for DN Tau and DF Tau) or averaged (for DR Tau) photometric data (cf. Bertout et al. 1988) supplemented by *IRAS* data (Rucinski 1985). When available, observed variability is indicated by error bars. When compared with WTTSs such as TAP 57, CTTSs display prominent ultraviolet and infrared excesses. Excess continuum flux and optical emission-line activity are often correlated.

... and also UV excess
→ spectral “veiling”

INTERPRETATION OF T TAURI STARS

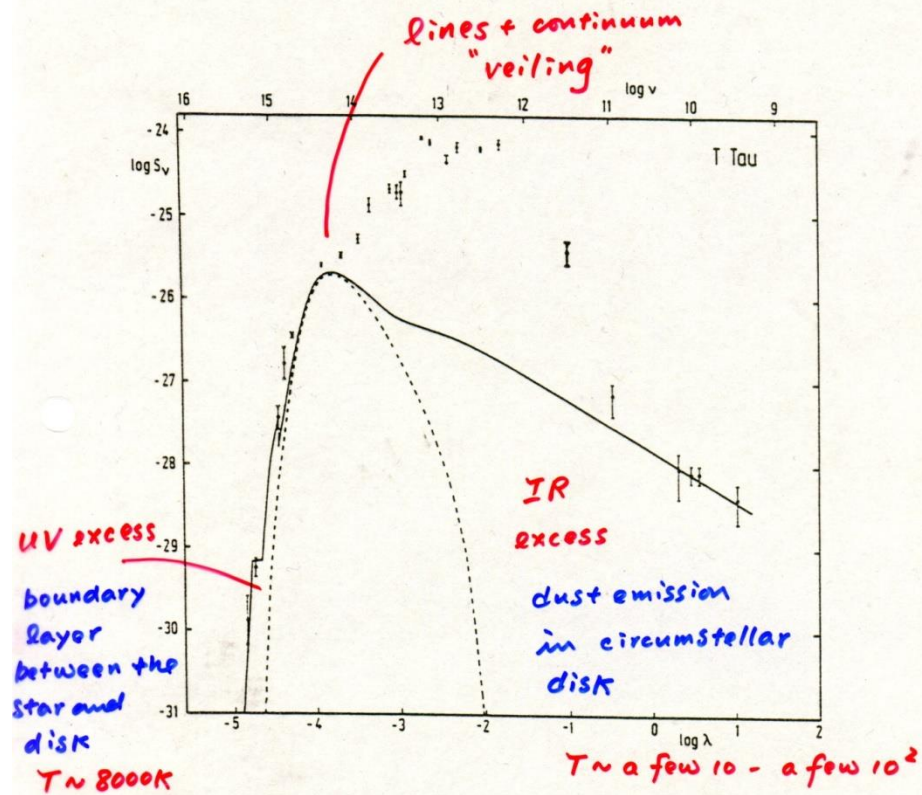


Figure 3: Continuum energy distribution of the star T Tau (according to Bertout 1980). The $\lambda = 1$ mm point is a new measurement by Chini et al. (1983). The units of S_ν are $\text{Wm}^{-2}\text{Hz}^{-1}$, λ is given in cm, ν in Hz. The broken line indicates the contribution of the star's photosphere, the solid line the combined contribution of the photosphere and the ionized part of the circumstellar gaseous envelope. The remaining IR excess is attributed to dust emission.

Appenzeller (1983) RMAA

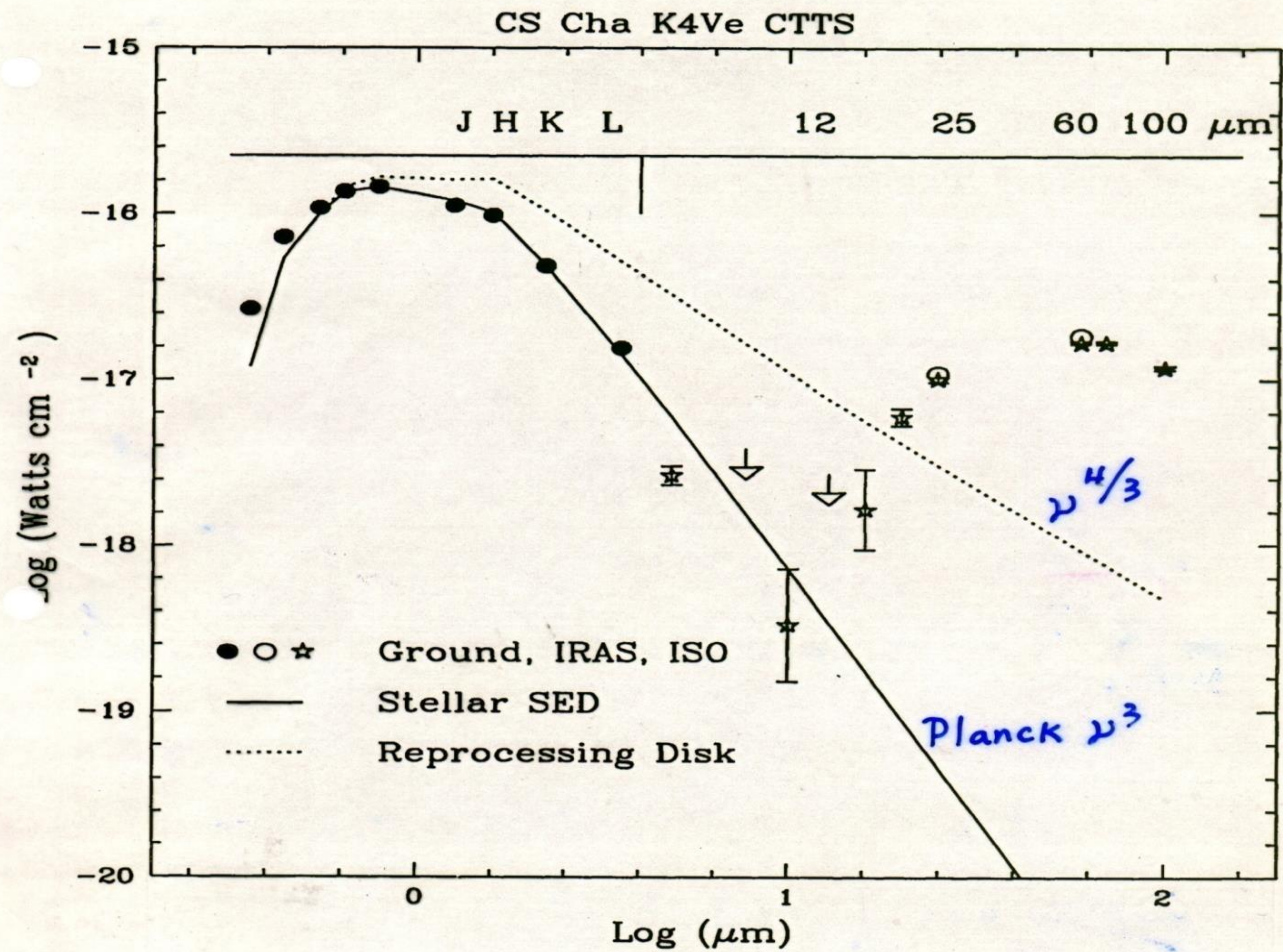


Figure 2. CS Cha SED. The ISO measurements are shown by stars. The two arrows denote upper limits from ISO observations. Filled circles are ground-based photometry. Open circles are IRAS measurements at 60 and 100 μm . The solid curve shows the SED of the stellar photosphere; the dotted curve the model prediction for a standard reprocessing disk seen face-on.

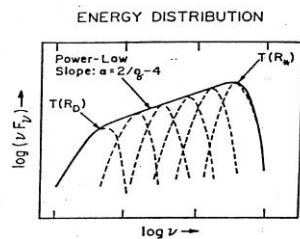
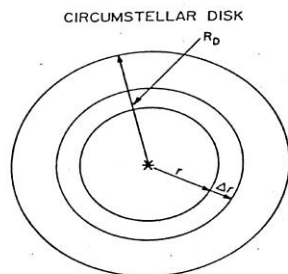
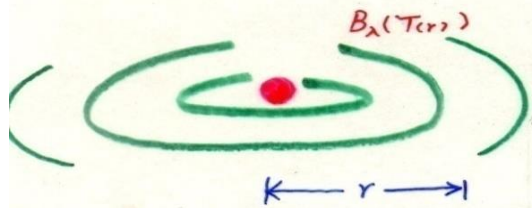


圖 8 理論模型環星盤輻射之能譜分佈示意圖，摘自 [Lada 1991]



Adams, Emerson, and Fuller (1990)

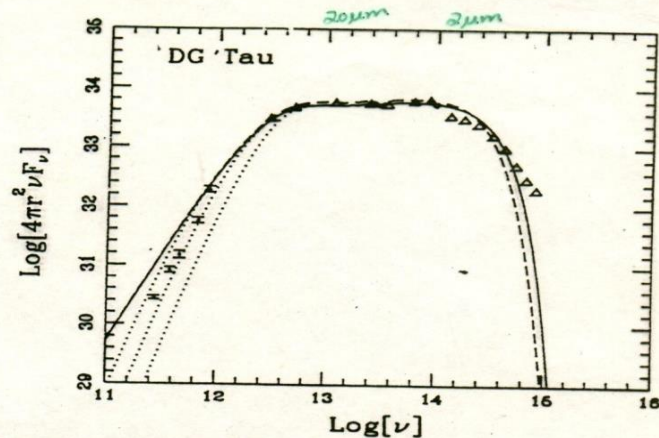


FIG. 2.—Spectral energy distribution of the infrared source DG Tauri (cgs units). Solid triangles are previously observed data points, solid triangles with error bars are the data points from this paper. Where no error bars are shown, they are smaller than the plotting symbols. Solid curve shows the theoretical spectrum in the optically thick ($M_D \rightarrow \infty$) limit for an assumed stellar photospheric temperature of 5495 K; the dashed curve assumes a cooler stellar surface temperature of 3500 K; dotted curves show spectra for finite disk masses of 0.01, 0.1, and 1.0 M_\odot .

$$\text{Assuming } T = T_0 \left(\frac{R_*}{r} \right)^p \propto r^{-p}$$

$$\text{Flux} = \sigma T^4 \propto r^{-4p}$$

$$\sum_{\text{annulus}} \text{Flux} = r^{-4p} \cdot r^2 = r^{2-4p}$$

\therefore Flat spectral energy distribution

$$\left(\text{i.e. } 2 F_\lambda \approx \text{const} \right) \implies T \propto r^{-1/2}$$

Spectral index useful to classify a young stellar object (YSO)

$$\alpha = \frac{d \log(\lambda F_\lambda)}{d \log(\lambda)}$$

Where λ =wavelength, between 2.2 and 20 μm ; F_λ =flux density

Class 0 sources --- undetectable at $\lambda < 20 \mu\text{m}$

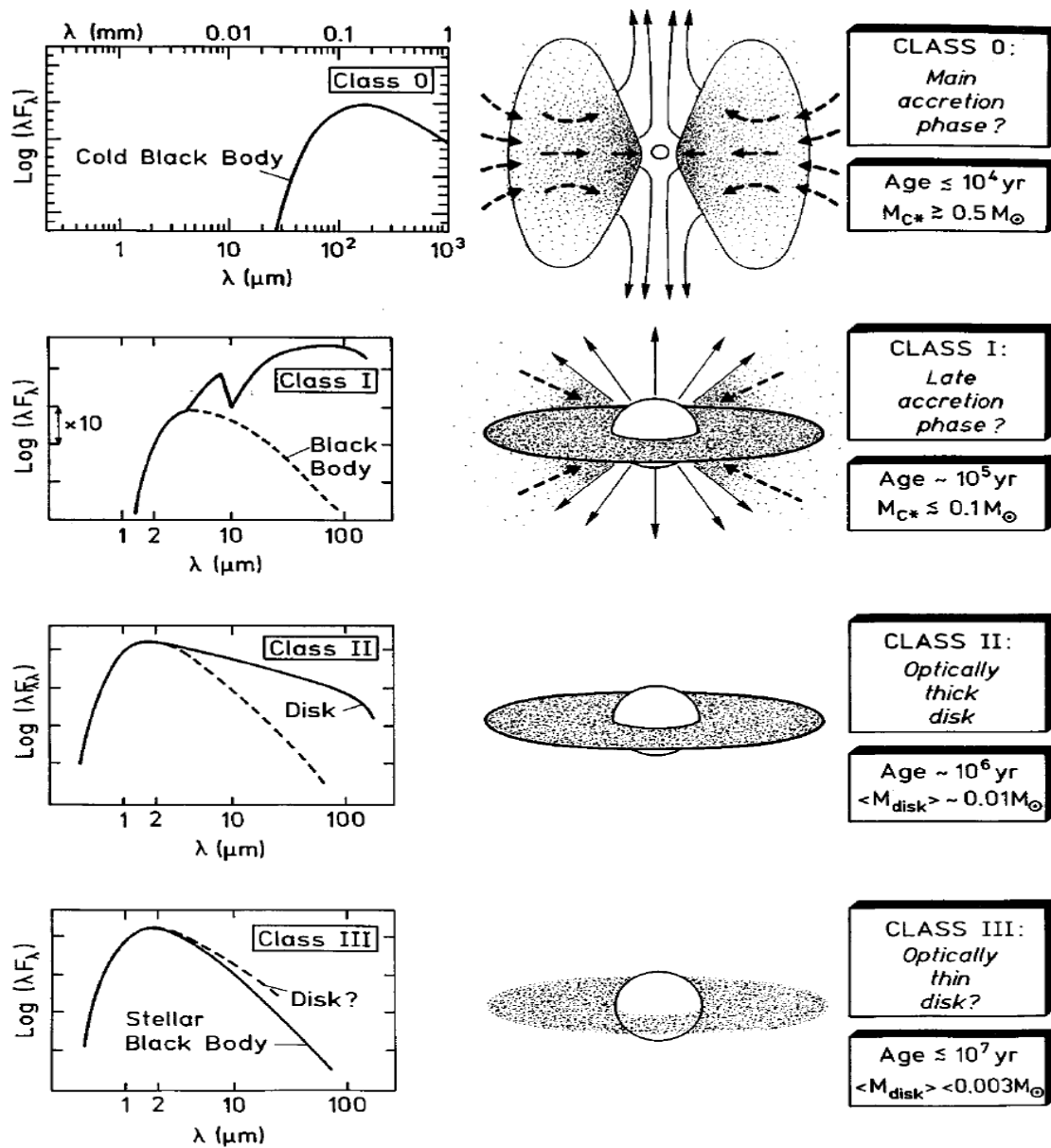
Class I sources --- $\alpha > 0.3$

Flat spectrum sources --- $0.3 > \alpha > -0.3$

Class II sources --- $0.3 > \alpha > -1.6$

Class III sources --- $\alpha < -1.6$

→ Evolutionary sequence in decreasing amounts of circumstellar material (disk clearing)



Submillimeter
cores

Protostars

Classical
T Tauri stars

Weak-lined
T Tauri stars

Figure 11 Evolutionary sequence of the spectral energy distributions for low-mass YSOs as proposed by André (1994). The four classes 0, I, II, and III correspond to successive stages of evolution.

T Tauri stars are PMS objects, contracting toward the **zero-age main sequence (ZAMS)**.

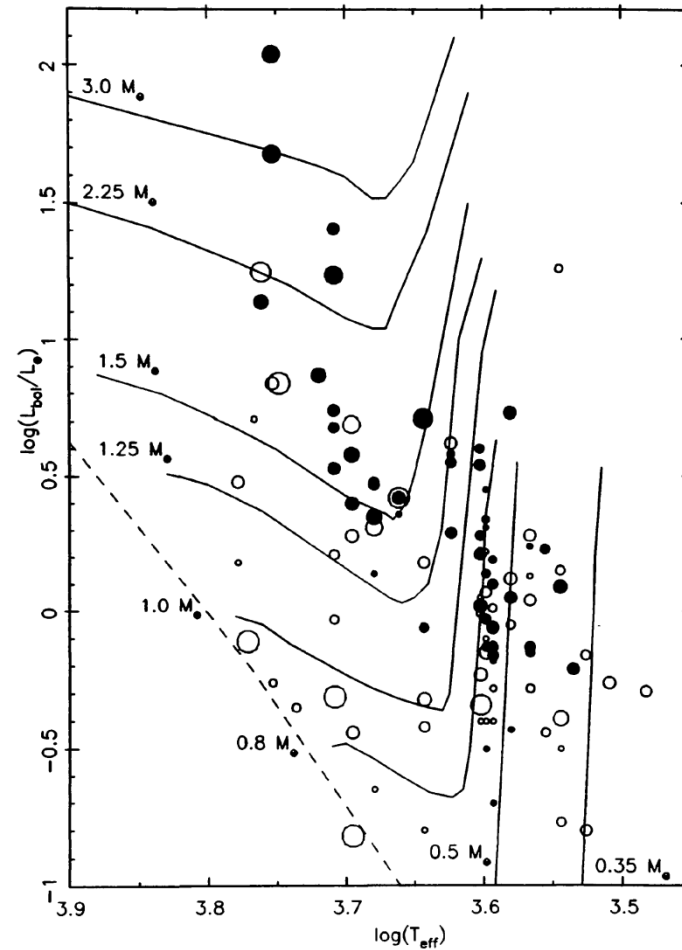


Figure 4 Position in the Hertzsprung-Russell diagram of all CTTSs and WTTSs with known $v \sin i$. WTTSs are represented by open circles, and CTTSs by dark circles. In both cases, the circle area is proportional to the stellar $v \sin i$. Approximate pre-main-sequence quasi-static evolutionary tracks for various masses are also plotted together with the zero-age main sequence (dashed line).

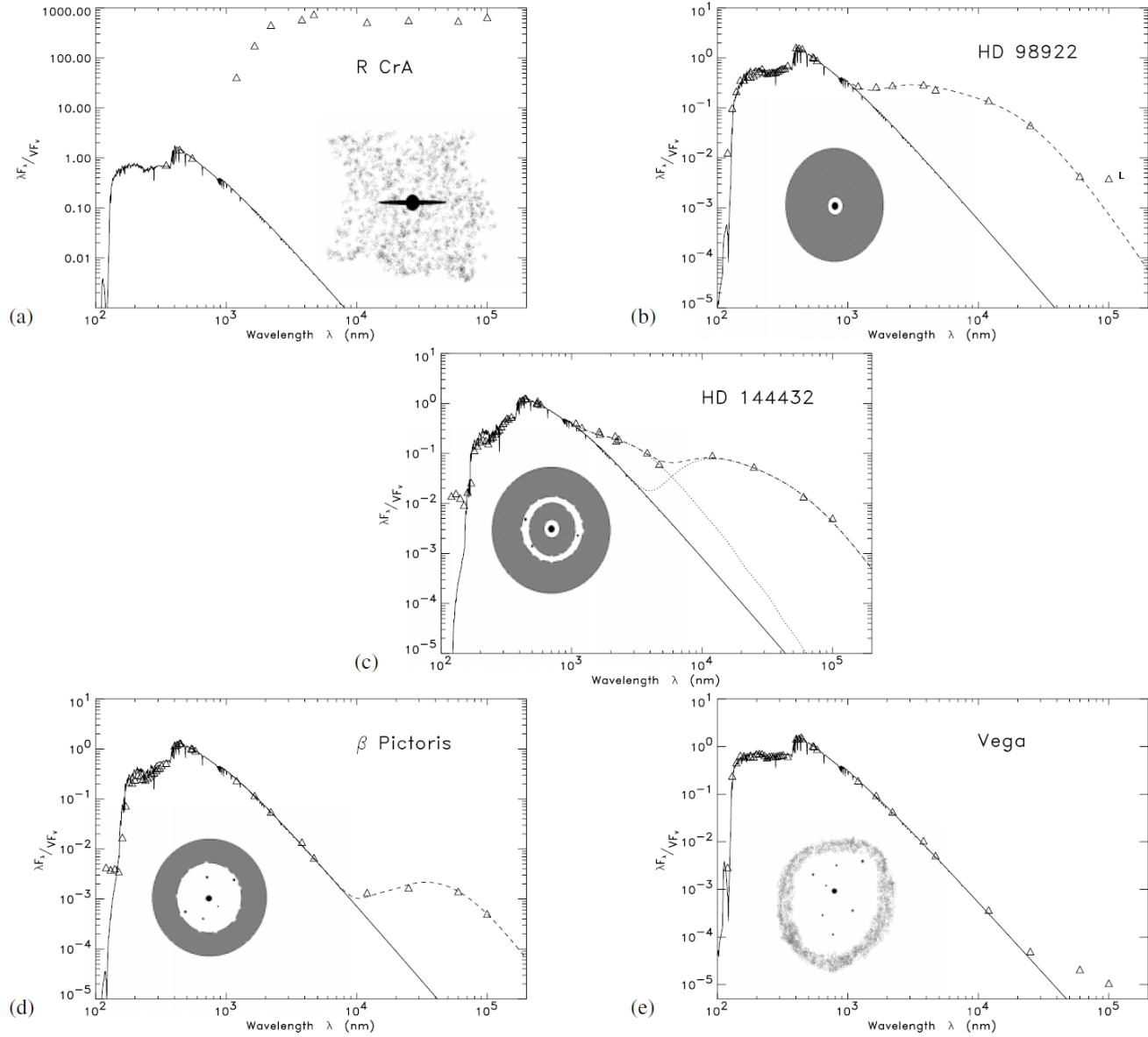
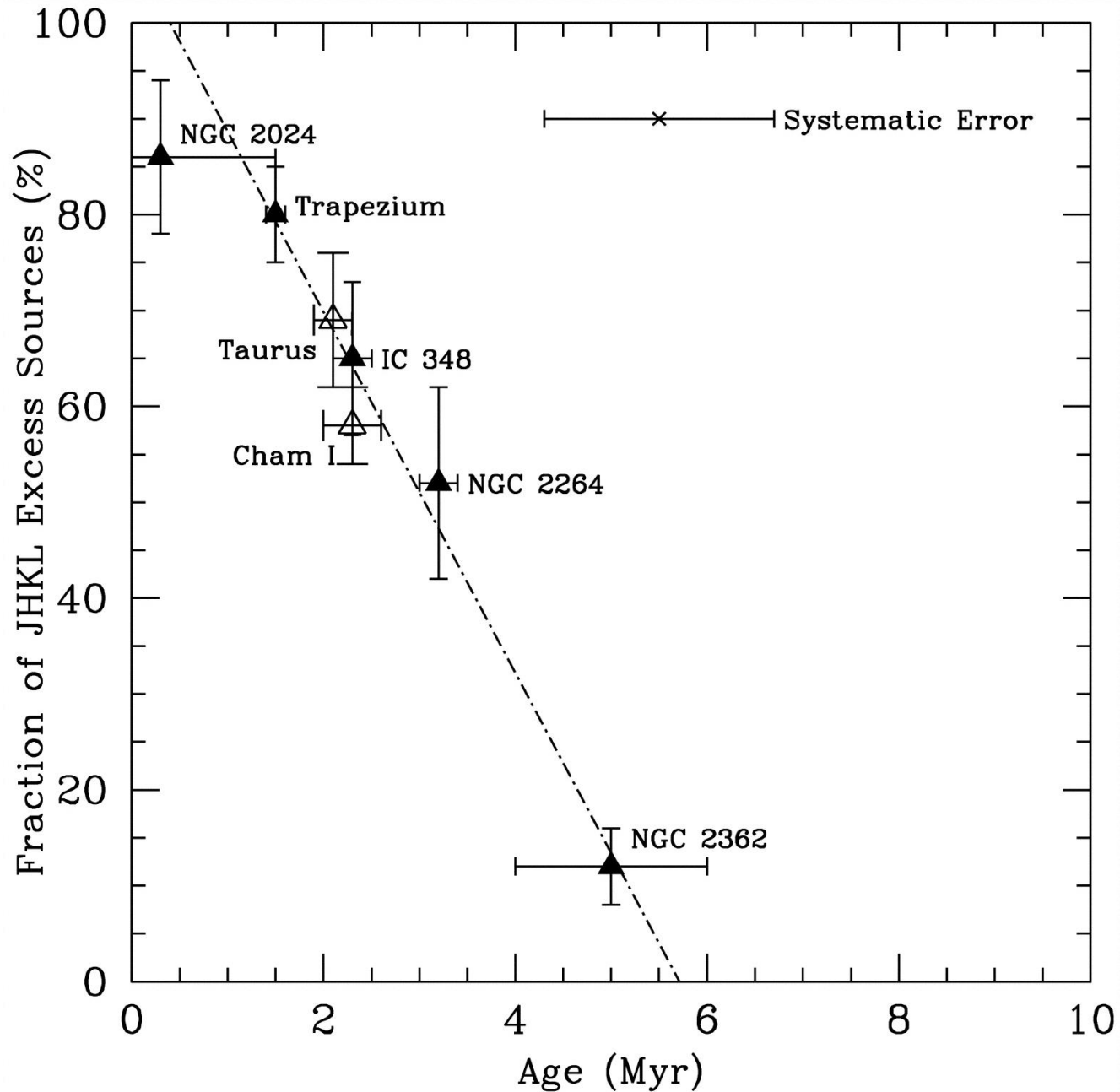


Fig. 3a–e. Evolutionary scenario: **a** embedded source (R CrA); **b** single dust disk causing near-IR and far-IR excess (HD 98922); **c** double dust disk (HD 144432); **d** single dust disk causing far-IR excess (β Pictoris); **e** more evolved dust disk (Vega)



One half of stars lose disks within 3 Myr

Disk disposed in ~6 Myr: planet formation timescale

Haisch+ 2001

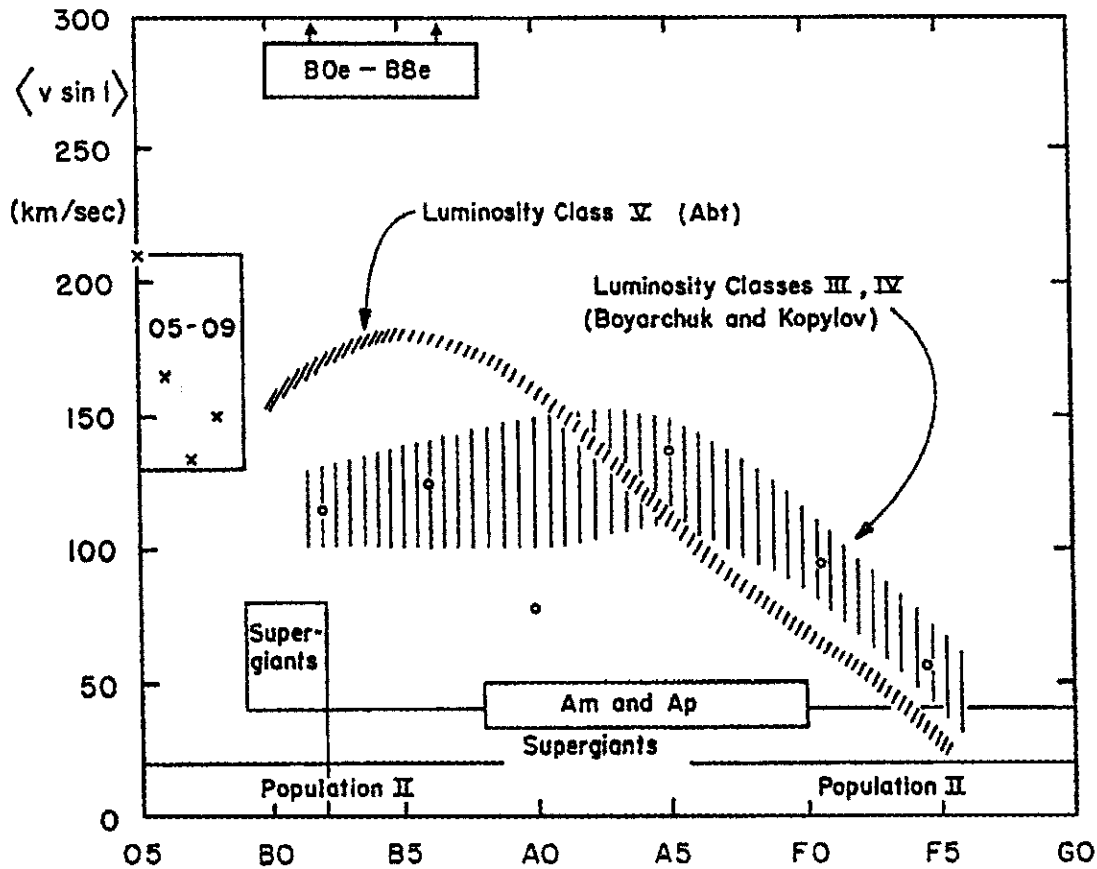


Fig. 3. Projected equatorial velocities, averaged over all possible inclinations, as a function of spectral type. On the main sequence (luminosity class V), early-type stars have rotational velocities that reach and even exceed 200 km/s; these velocities drop to a few km/s for late-type stars, such as the Sun (type G2) (Slettebak [20]; courtesy Gordon & Breach)

- Early-type stars are fast rotators
- Stars later than ~F5 rotate very slowly
- Disk/planet formation?

THE FU ORIONIS PHENOMENON¹

Lee Hartmann and Scott J. Kenyon

Harvard-Smithsonian Center for Astrophysics, 60 Garden Street, Cambridge, Massachusetts 01238

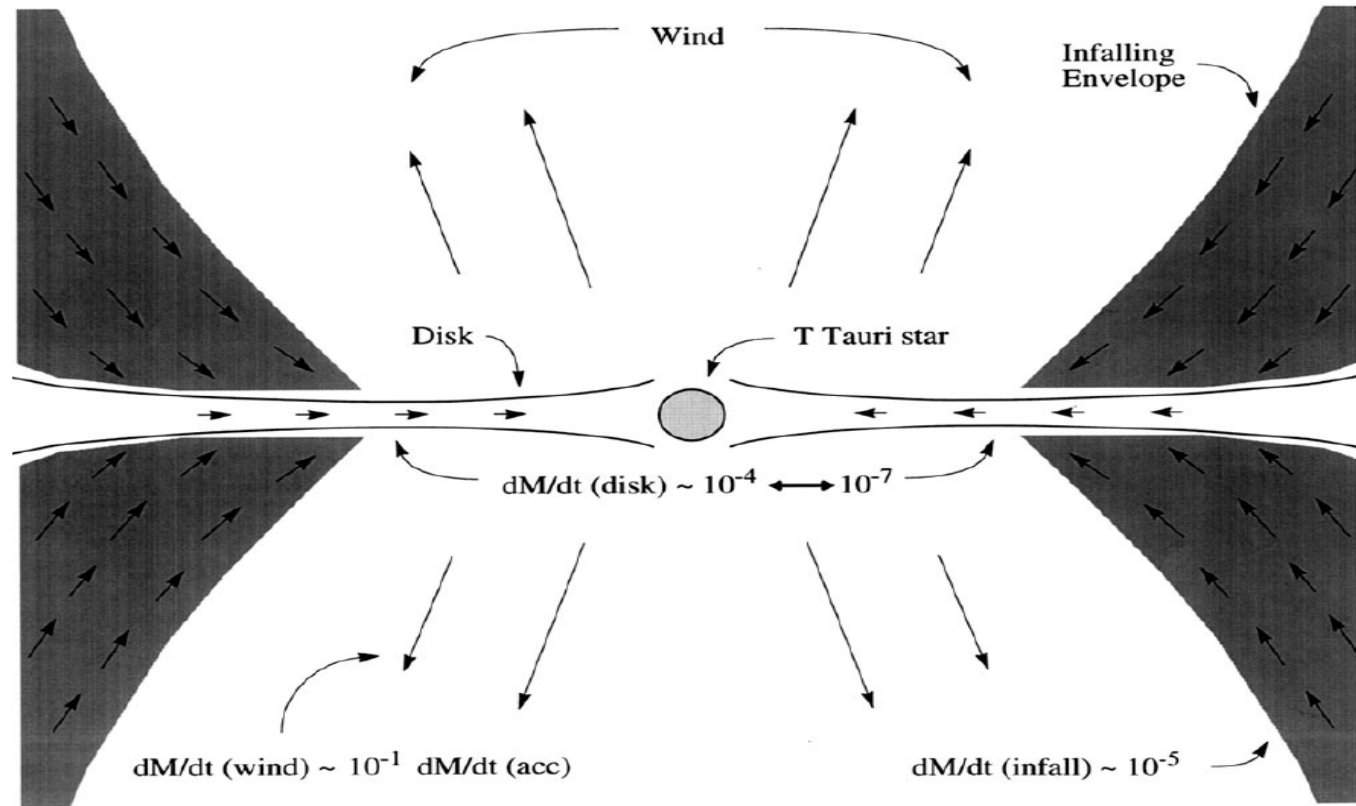


Figure 1 Schematic picture of FU Ori objects. FU Ori outbursts are caused by disk accretion increasing from $\sim 10^{-7} M_{\odot} \text{ yr}^{-1}$ to $\sim 10^{-4} M_{\odot} \text{ yr}^{-1}$, adding $\sim 10^{-2} M_{\odot}$ to the central T Tauri star during the event. Mass is fed into the disk by the remnant collapsing protostellar envelope with an infall rate $\lesssim 10^{-5} M_{\odot} \text{ yr}^{-1}$; the disk ejects roughly 10% of the accreted material in a high-velocity wind.

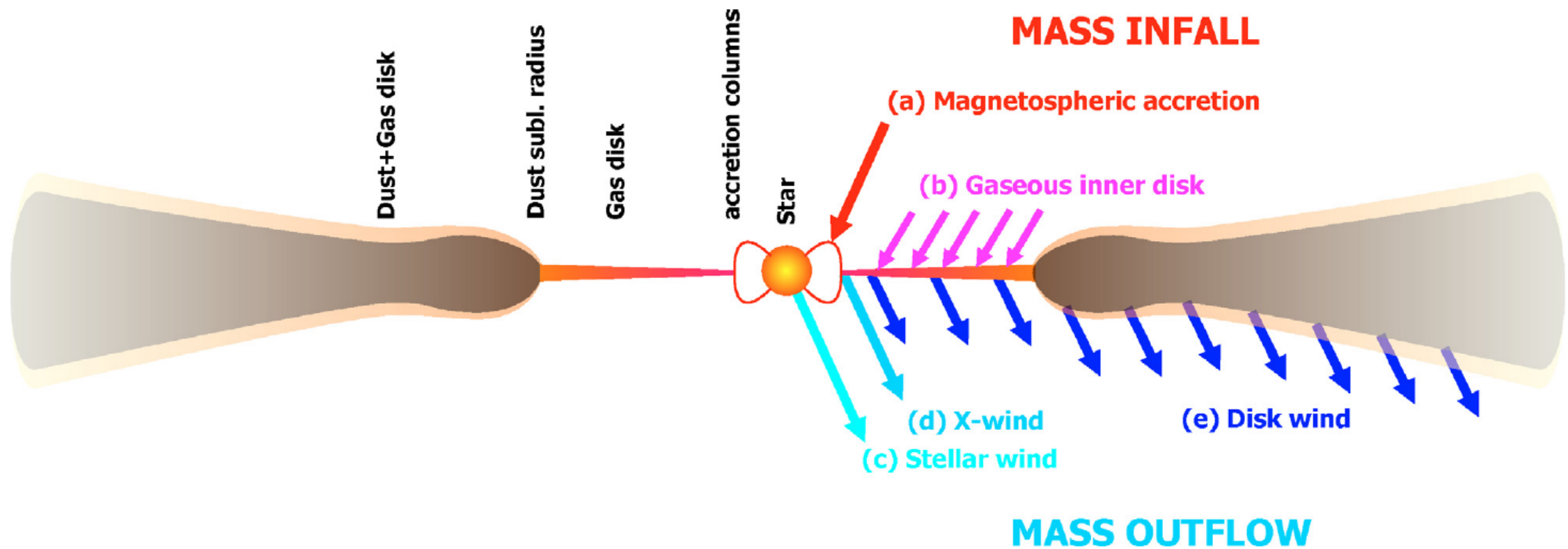
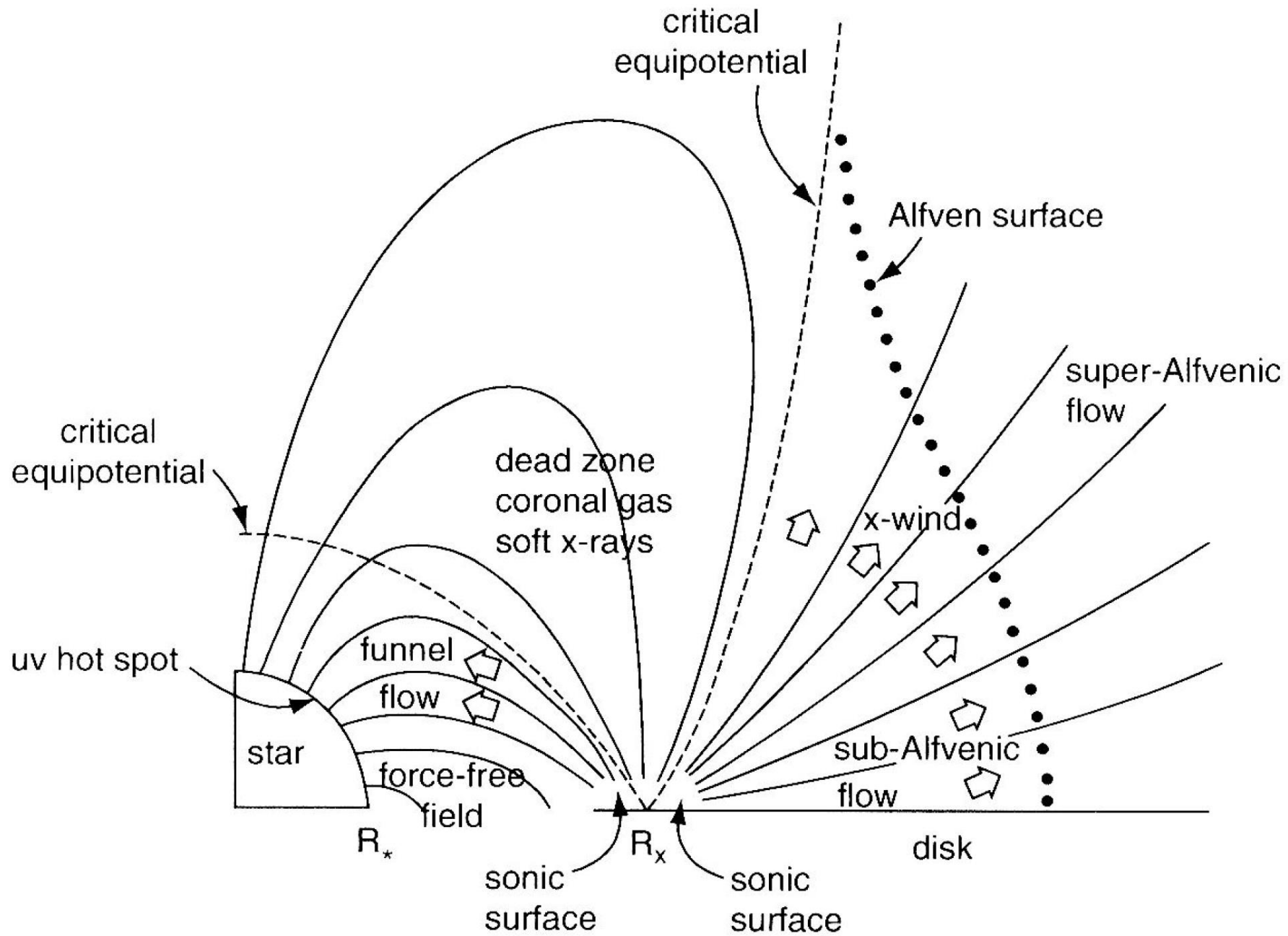


Fig. 1. Illustration of the regions which have been proposed as the origin of the permitted hydrogen recombination line emission observed towards HAeBe stars (this sketch is not to scale; read Sect. 1 for details about the individual mechanisms).



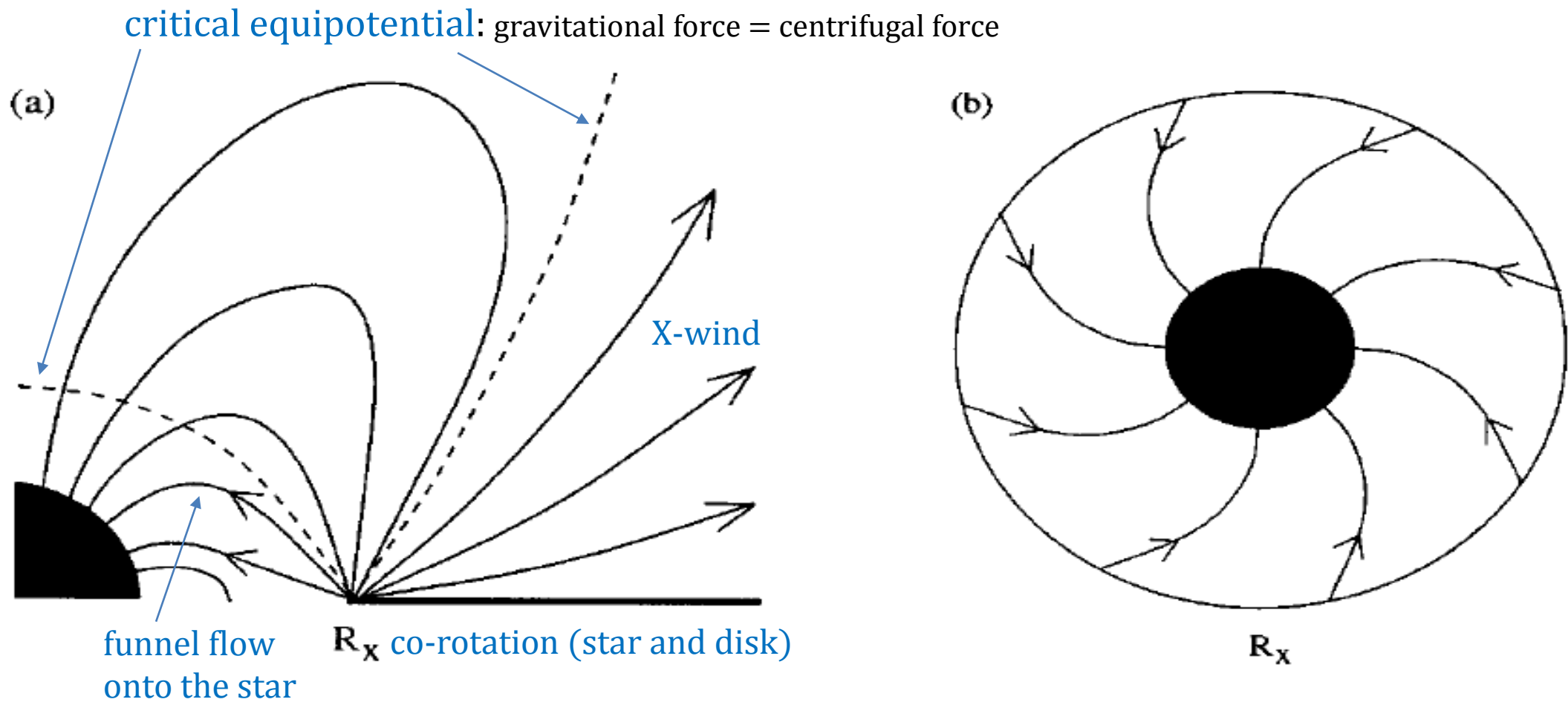


Figure 13 Schematic views of the (a) meridional plane and (b) equatorial plane of the configuration modeled by Shu et al (1994a,b) for the origin of bipolar outflows. The circumstellar disk is truncated at a distance R_X from the star. Both energetic outflows and funnel flows emerge from the disk truncation region. Gas accreting from the disk onto the star in a funnel flow drags the stellar field into a trailing spiral pattern. (From Najita 1995.)

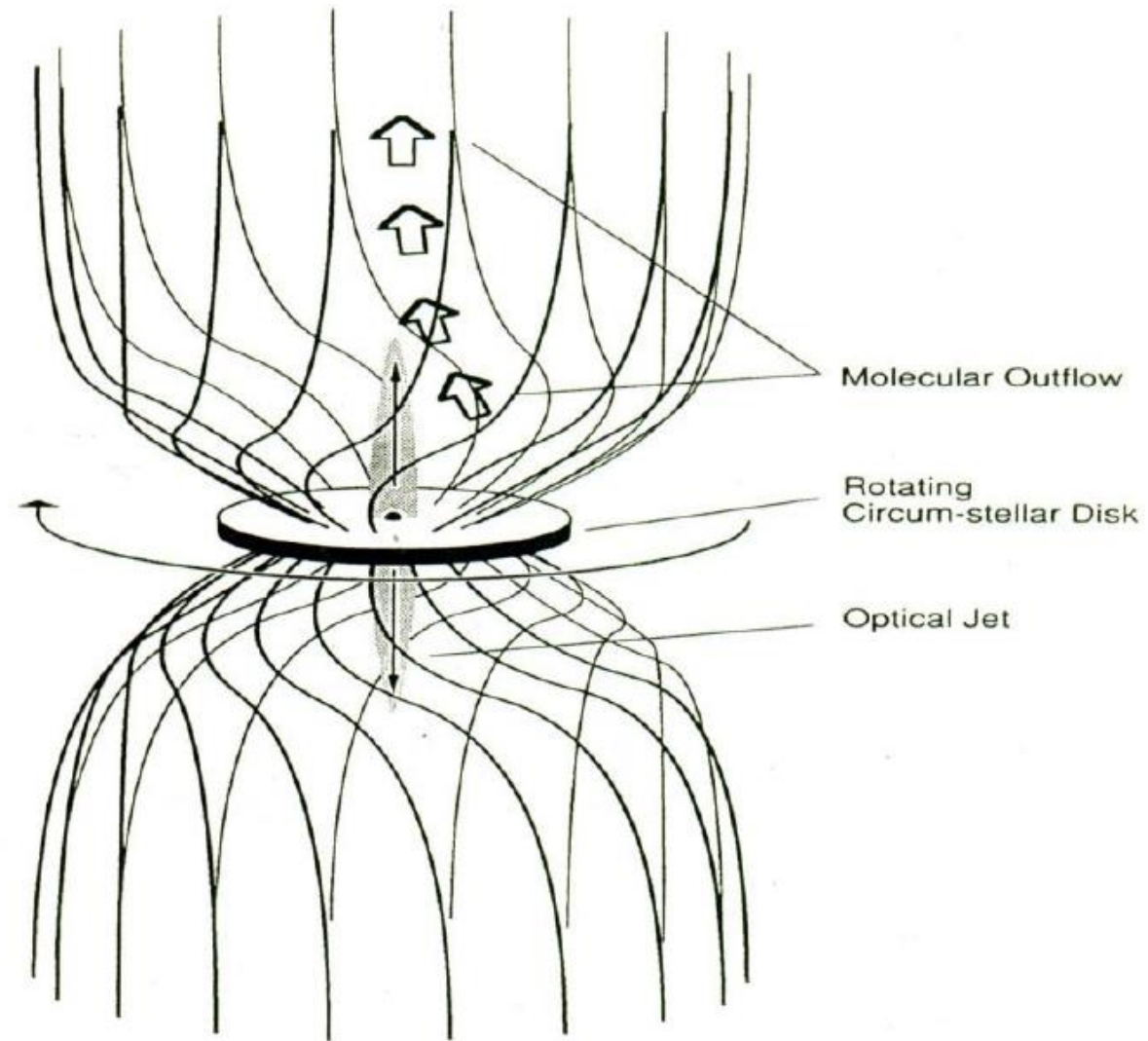


Figure 6. A schematic drawing of the magnetohydrodynamical model.

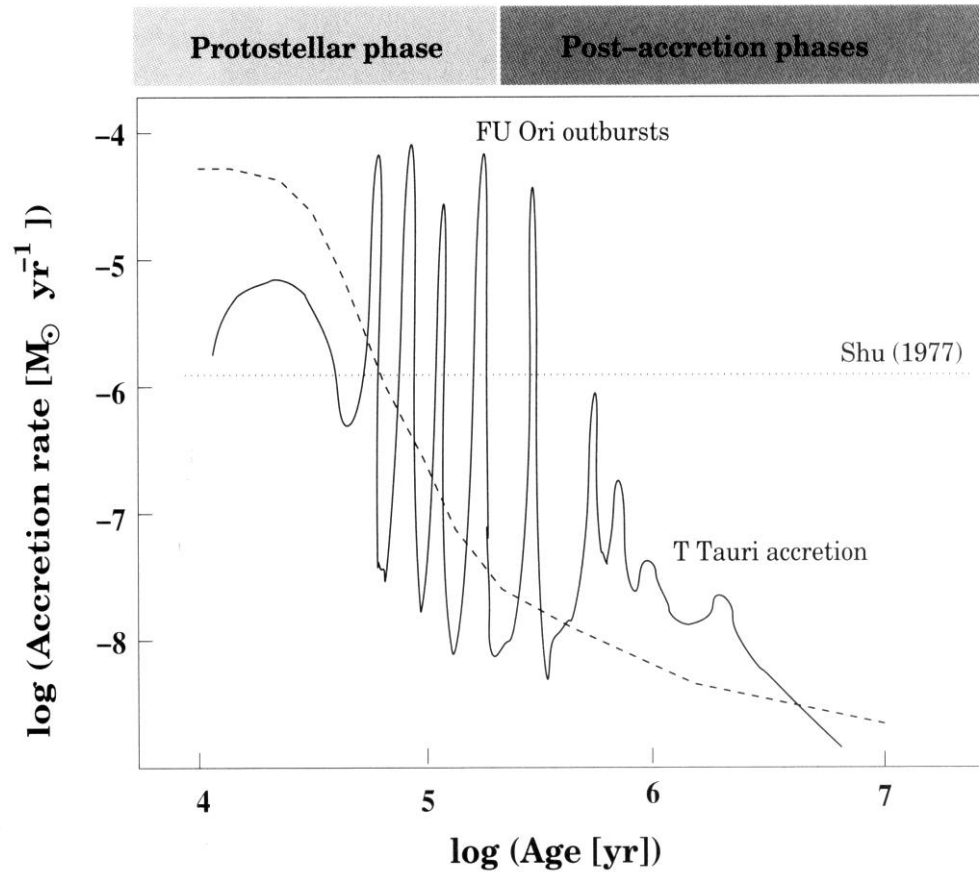
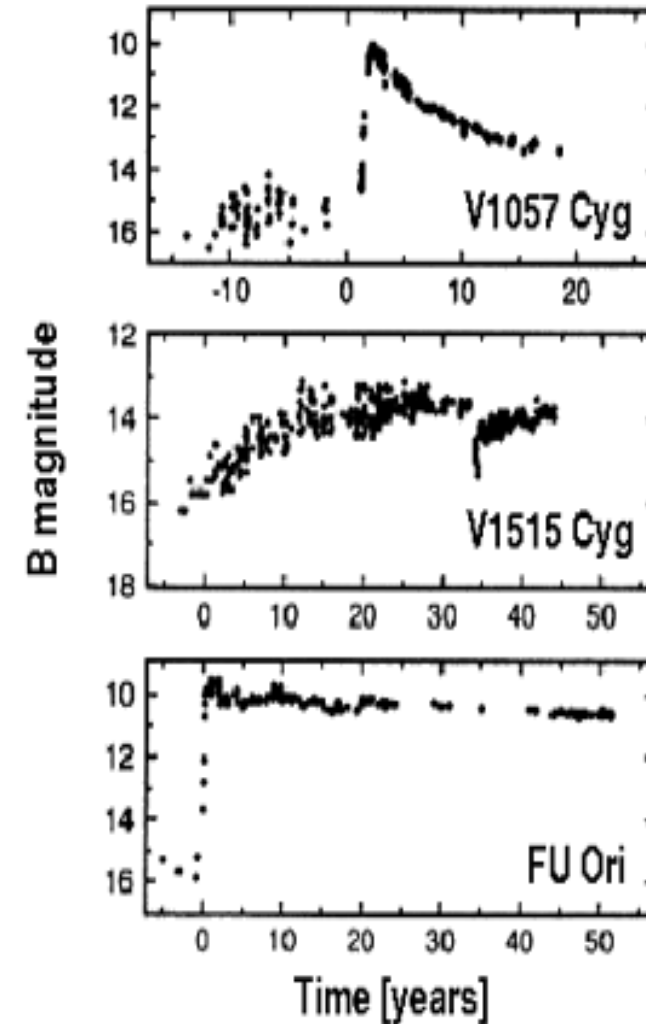


Fig. 6.1. The diagram schematically shows the time development of the accretion rates as they appear in various calculations and in relation to observed phenomena. The dotted straight line resembles the result from standard star formation [777], which does not depend on time and is based on infinitely large radius and mass and thus appears as a flat line throughout the entire time interval. The hatched curve represents an approximation to the results of the many more realistic calculations. The thick line was adapted from Hartmann [344] and shows additional features such as outbursts of FU Ori type protostars and T Tauri disk accretion. All rates apply for typical low-mass ($\sim M_{\odot}$) stars only.



Inside-out collapse (Shu 1977) isothermal sound speed \rightarrow constant accretion rate

Collision

Gas (hydrogen atoms) root-mean-squared speed

$$m_{\text{H}} \sqrt{\langle v^2 \rangle} = 3kT$$

For H I regions,

$$T \sim 100 \text{ K}, \langle v \rangle_{\text{HI}} \sim 1 \text{ km s}^{-1}$$

$$\text{For } e^-, \langle v \rangle_{e^-} \sim 50 \text{ km s}^{-1}$$

Cross sections σ

- Hard sphere OK for neutral atoms, i.e., ‘physical’ cross section



$$\sigma = \pi(a_1 + a_2)^2$$

$$\sigma_{\text{HI,HI}} \leftarrow a \sim 5.6 \times 10^{-9} \text{ cm}$$

$$\text{c.f., Bohr radius (first orbit)} = 5.3 \times 10^{-9} \text{ cm}$$

Cross sections σ

- For free e^- , p^+

$\sigma \gg \sigma_{\text{physical}}$ because of Coulomb force, need QM

$$a \sim \frac{2.5 \times 10^{-2}}{v^2} \text{ cm } (v \text{ in km})$$

If $v_{e^-} \sim 50 \text{ km s}^{-1}$, $a \sim 10^{-5} \text{ cm}$ for e^- - e^- collision

$$T = 3 \times 10^4 \text{ K}, \langle v \rangle \sim 10^3 \text{ km s}^{-1}$$

$$\longrightarrow a \sim 2.5 \times 10^{-8} \text{ cm}$$

c.f., classical electron radius $\sim 2.8 \times 10^{-13} \text{ cm}$

$$\frac{e^2}{r_0} = m c^2$$

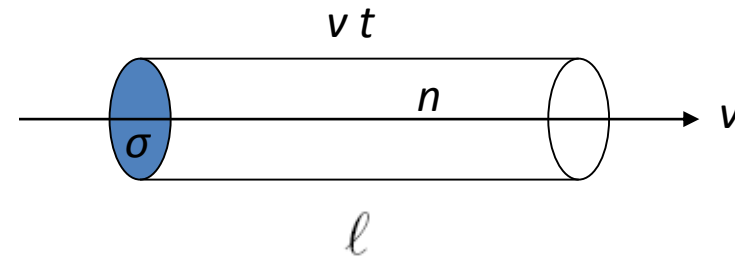
$$r_0 = \frac{e^2}{m c^2} \sim 2.8 \times 10^{-13} \text{ cm}$$

Conventional unit for cross section

$$1 \text{ barn} = 10^{-24} \text{ cm}^2$$

$$\sigma_{\text{HI,HI}} \sim 10^8 \text{ barns } (\sim 10^{-16} \text{ cm}^2)$$

Collision



of collisions = # of particles in the (moving) volume

$$N = n \sigma v t$$

of collisions per unit time = $N/t = n \sigma v$

Time (mean-free time) between 2

consecutive collisions ($N=1$) = $t_{\text{collision}} = \frac{1}{n \sigma v}$

Mean-free path $\ell = v t_{\text{col}}$, i.e., $\ell = \frac{1}{N \sigma}$

Ex 1 between hydrogen atoms in an H I region

$$n_{\text{HI}} \sim 10 \text{ cm}^{-3}; v_{\text{HI}} \sim 1 \text{ km s}^{-1}; \sigma_{\text{HI,HI}} \sim 10^{-16} \text{ cm}^2$$

$$t_{\text{HI,HI}} \sim 10^{10} \text{ s} \sim 300 \text{ years}$$

$$l \sim 10^{15} \text{ cm} \sim 100 \text{ AU}$$

∴ Collisions are indeed very rare.

Ex 2 between a hydrogen atom and an electron

$$\sigma_{e^-, \text{HI}} \sim 10^{-15} \text{ cm}^2 \text{ (polarization)}$$

$$t_{e^-, \text{HI}} \sim \frac{1}{10 \times 10^{-15} \times 10^5} \sim 30 \text{ years}$$

Ex 3 between electrons

$$\sigma_{e^-, e^-} \sim 10^{-12} \text{ cm}^2; n_e \sim 0.2 \text{ cm}^{-3}$$

$$t_{e^-, e^-} \sim \frac{1}{0.2 \times 10^{-12} \times 50 \times 10^5} \sim 10 \text{ days}$$